RECRYSTALLIZATION AND AGING EFFECTS ASSOCIATED WITH THE HIGH TEMPERATURE DEFORMATION OF WASPALOY AND INCONEL 718

by

© Adilson A. Guimaraes

A Thesis Submitted to the
Faculty of Graduate Studies and Research
in Partial Fulfilment of the Requirements for the
Degree of Master of Engineering

Department of Mining and Metallurgical Engineering
McGill University
Montreal, Canada
October 1980

ABSTRACT

Compression tests were carried out on cylindrical test pieces of Waspaloy and Inconel 718, using a computerized Instron testing machine. The test program covered strain rates from $5.0 \times 10^{-4} s^{-1}$ to $3.8 \times 10^{-1} s^{-1}$, temperatures ranging from 925°C to 1220°C and deformations up to strains of 0.7. Interrupted tests were also carried out to determine the nature of the static softening and hardening processes.

An increase in test temperature or a decrease in the strain rate produces a decrease in the flow stress of both materials. Dynamic recrystallization, partial or complete, was observed at temperatures above 950°C. At 950°C and below, dynamic recovery is the process controlling the deformation. The static softening processes were found to be static recovery and static recrystallization. Yield points were detected in Waspaloy under some conditions as well as in Inconel 718. This phenomenon was studied in greater detail in Inconel 718 and, although no single element was identified as responsible for its occurrence, the locking mechanism is believed to be short-range ordering. The stress-temperature curve for Waspaloy shows a bump or deviation from normal behavior in the vicinity of 1100°C. It is concluded that the deviation is related to the occurrence of the yield drop, and therefore to short-range ordering of the γ' forming elements.

RESUME

Des essais de compression ont été faits sur des échantillons cylindriques de Waspaloy et d'Inconel 718, à l'aide d'une machine d'essais Instron controlée par ordinateur. Les essais ont été faits à des vitesses de déformation comprises entre $5.0 \times 10^{-4} s^{-1}$ et $3.8 \times 10^{-1} s^{-1}$ à des températures variant entre 925°C et 1220°C et à des déformations allant jusqu'à 0.7. Des essais interrompus ont aussi été effectués pour déterminer la nature des processus de durcissement et d'adoucissement.

Quand la temperature de l'essai est augmentée ou la vitesse de déformation diminuée on remarque une baisse de la contrainte d'écoulement pour les deux matériaux. Une recristallisation dynamique, partielle ou complète, a été observée à des températures supérieures à 950°C. A 950°C et en dessous, la restauration dynamique contrôle la déformation. L'adoucissement statique s'effectue par restauration et recristallisation statique. Des décrochements de la contrainte ont été détectés sur le Waspaloy dans certaines conditions ainsi que sur l'Inconel 718. Ce phénomène a été étudié en détail pour l'Inconel 718 et, même si l'on n'a pu identifier l'élément responsable, le mécanisme d'immobilisation des dislocations semble dû à un ordre à parcours réduit. Les diagrammes contrainte-température dans le cas du Waspaloy, montrent un écart par rapport au comportement normal vers 1100°C. On en conclut que cette déviation est reliée au décrochement de la contrainte et donc à l'ordre à parcours réduit des éléments qui forment les précipités γ'.

RESUMO

Testes de compressão foram efetuados em amostras cilíndricas de Waspaloy e Inconel 718, com o auxílio de uma máquina de testar Instron computadorizada. Os testes foram feitos à velocidades de deformação entre $5.0 \times 10^{-4} s^{-1}$ e $3.8 \times 10^{-1} s^{-1}$, temperaturas entre 925 e 1220°C e deformações até 0.7. Testes interrompidos foram também efetuados com o objetivo de determinar a natureza dos processos de amolecimento e endurecimento estáticos.

Quando a temperatura de teste é aumentada ou a velocidade de deformação diminuida, um decréscimo na tensão de escoamento é observado para os dois materiais. Recristalização dinâmica, parcial ou completa, foi observada à temperaturas acima de 950°C. À 950°C e abaixo, a recuperação dinâmica é o processo que controla a deformação. Amolecimento estático se efetua através de recuperação e recristalização estáticas. Pontos (quedas) de escoamento foram detectados em Waspaloy para algumas condições particulares, bem como para Inconel 718. Este fenômeno foi estudado em detalhe para Inconel 718, e o mecanismo de bloqueio é deduzido como sendo ordenação à curto alcance, embora o elemento responsavel por esta ocorrência não tenha sido identificado. As curvas tensão-temperatura para Waspaloy mostram um afastamento do comportamento normal em tôrno de 1100°C. É concluido que este afastamento está relacionado com a ocorrência dos pontos de escoamento, e consequentemente com a ordenação a curto alcance dos elementos formadores do precipitado γ'.

To my parents
for their constant
support and confidence.

À meus pais,
pela confiança e apôio
constantes e irrestritos.

ACKNOWLEDGEMENTS

The author would like to express his most sincere thanks and appreciation to his thesis advisor, Dr. J.J. Jonas, for his guidance and encouragement. Particular thanks are also due to Dr. J-P.A. Immarigeon and Dr. I. Weiss, who contributed significantly through many stimulating discussions and suggestions.

The author is grateful to his fellow graduate students for their interest and support and for providing a pleasant atmosphere in which to work. Special thanks are owed to TRW Incorporated and the Special Metals Corporation, as well as to Dr. C.C. Chen of Wyman-Gordon Company for the provision of experimental materials.

The author would like to express his gratitude to the Canadian International Development Agency for the award of a Post-Graduate Fellowship and to Eletrometal Aços Finos S.A. of Campinas, Brazil, for providing the necessary leave period during which this work was carried out.

AGRADECIMENTOS

O autor agradece sincera e profundamente ao Professor J.J. Jonas, seu orientador, pelo interesse, comentários e estímulo com os quais ele contribuiu para este trabalho. É também enormente apreciada a colaboração prestada pelos Drs. J-P.A. Immarigeon e I. Weiss, através de várias discussões e sugestões.

O autor agradece também aos seus colegas de pós-graduação, pelo interesse, apoio e excelente ambiente de trabalho proporcionado, bem como às firmas TRW Incorporated, Special Metals Corporation e Wyman Gordon pela doação do material para as experiências.

Finalmente agradecimentos são extendidos à Canadian International Development Agency, pela bolsa de estudos concedida e à Eletrometal Aços Finos S.A. em Campinas, Brasil por proporcionar a oportunidade para a realização deste trabalho.

TABLE OF CONTENTS

LIST OF FIGURES

LIST OF TABLES

CHAPTER 1

INTRODUCTION

Nickel-base alloys comprise a broad range of compositions which find use in a variety of applications in the aerospace, gas turbine, chemical, petroleum and nuclear industries. The constant development of these alloys is due to their ability to work at very high temperatures with good creep, oxidation and corrosion resistance. Due to the fact that these alloys are designed to resist deformation at high temperatures, their deformation behavior is very complex. They are also very difficult to hot work; their ductility is limited, and their flow stresses are high.

A review of the literature concerning the hot working of nickel-base superalloys reveals that much of it is devoted either to practical improvements in processing or to detailed studies of their properties through observations of the worked microstructures. Information on the mechanisms of hot working is scanty and must be extracted from the kinds of practical publications mentioned above or from studies on pure metals, or single phase or experimental alloys. Even in the latter category, there are only a few papers in which the mechanisms of hot deformation are discussed in any detail.

The purpose of the present investigation was, therefore, to collect information on the mechanisms of hot working of the nickel-base superalloys. In particular, it was intended

to study, with the aid of the interrupted compression test, the softening processes that operate both during and after the deformation of Waspaloy and Inconel 718. After its inception the investigation was extended to obtain additional information concerning the yield drop which appeared while testing Inconel 718 at high temperatures.

CHAPTER 2

THE PHYSICAL METALLURGY OF NICKEL-BASE ALLOYS

The demand for more efficient power generation units, particularly gas turbine engines for military and civil applications, has accelerated the development of superalloys in the immediate past. The environment of a gas turbine is one of the most demanding and aggressive possible (1). In order to withstand these atmospheres at high temperatures, superalloys are strengthened by: i) solute elements such as Co, Fe, Cr, Mo, W, V, Ti and Al; ii) the precipitation of intermetallic compounds such as γ' and γ''; iii) the precipitation at grain boundaries of MC, M_7C_3, $M_{23}C_6$ and M_6C carbides and the boride M_3B_2. Here M may be Ti, Ta, Nb, V, Mo, W or Cr. In this chapter, the mechanisms of strengthening and hot working of these alloys will be reviewed.

2.1 Strengthening Mechanisms in Nickel-base Superalloys

2.1.1 Solid Solution Strengthening

Nickel-base superalloys always contain substantial substitutional solutes to provide strength, creep resistance and resistance to surface degradation. It is well known (2,3) that solubility of the elements added depends on: i) the atomic size difference with respect to Ni; ii) the relative positions of the solute and Ni in the periodic table*; iii) the lattice

*This includes the chemical affinity and relative valence factors of Hume-Rothery, as well as the effect of the electron hole number, Nv, which indicates the number of electron vacancies in the third shell of the first long period in Ni (4).

type of the solute (is it FCC like Ni?); and iv) the elastic modulus differences between Ni and the solute.

The high temperature oxidation resistance of superalloys is attributed to their tendency to form Cr_2O_3-rich protective scales having a low cation vacancy content, thereby reducing the diffusion rate of the metallic elements outward and of oxygen and sulphur inward (5). The excellent strength properties, on the other hand, arise from the high tolerance of nickel for alloying without phase instability due to its nearly filled 3d electron shell (5).

The effects of solutes on the yield strength via their lattice parameters and elastic moduli will now be discussed.

2.1.1.1 Lattice Parameter

Fig. 2.1 shows the elements which are important in the constitution of nickel-base alloys (6). It can be seen that these elements differ from nickel by 1 to 13% in atomic diameter and by 1 to 7% in Nv. With regard to the diameter difference, both solid solution hardening and precipitation hardening can be explained in terms of the internal strains generated by inserting either solute atoms or particles in an elastic matrix (7). For example, the yield stress for a dilute solid solution has been given by Mott and Nabarro (7) as:

$$\sigma = 2G\varepsilon c \qquad (2.1)$$

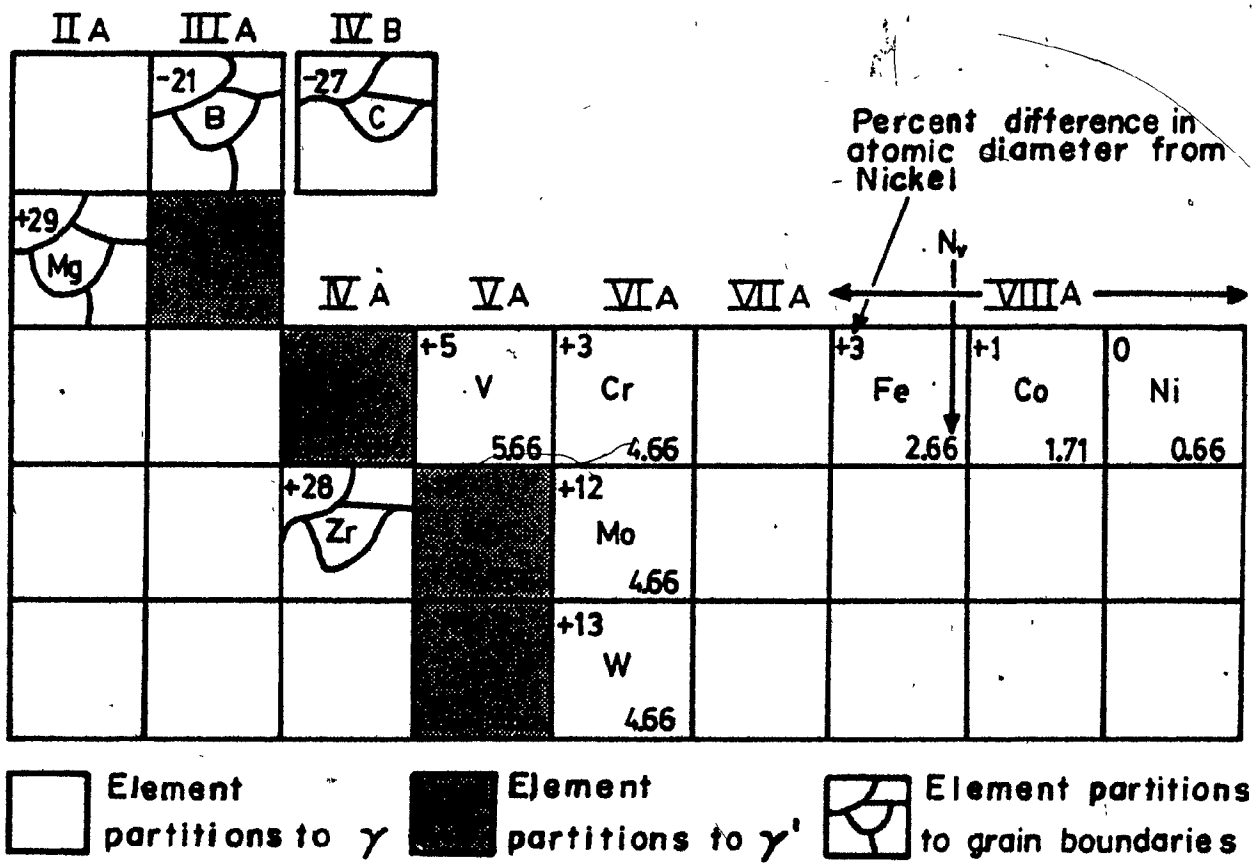

Atomic diameter of carbon, boron, zirconium, magnesium - Goldschmidt for CN 12 .

Atomic diameter of other elements from lattice parameter effect in nickel binary alloys .

FIGURE 2.1 Elements important in the constitution of nickel-base alloys (after Decker and Sims (6)).

where G is the shear modulus, ε is the misfit and c the concentration of solute atoms. The misfit is in turn specified by:

$$\varepsilon = \frac{\Delta a}{a_o} \cdot \frac{1}{c} \qquad (2.2)$$

where Δa is the difference between the lattice parameter a_o of the pure matrix and the lattice parameter a of the solute atom. A linear relationship between flow stress and lattice parameter change is obeyed for any single solute element in nickel - Fig. 2.2. We can see, however, that the change in flow stress of nickel for various solutes is not a single valued function of the lattice parameter, since Ti and Cr were expected to have smaller effects than Mo or W. The reason for this discrepancy is that the change in flow stress also depends on the number Nv (8,9). For the same lattice strains, the larger the valency difference between solvent and solute, the greater the hardening - Fig. 2.3. At least part of this effect may result from a lowering of stacking fault energy (6,8,9). According to Pelloux and Grant (10), solid solution hardening persists to 0.6 T_M. Above 0.6 T_M, the range of high temperature creep, γ strengthening is diffusion dependent. Thus the slowly diffusing elements, molybdenum and tungsten, would be expected to be the most potent hardeners. The amounts of Mo and W which can be added to the FCC γ matrix for strengthening is, however, generally limited by the instability of the alloy with respect to σ-phase formation.

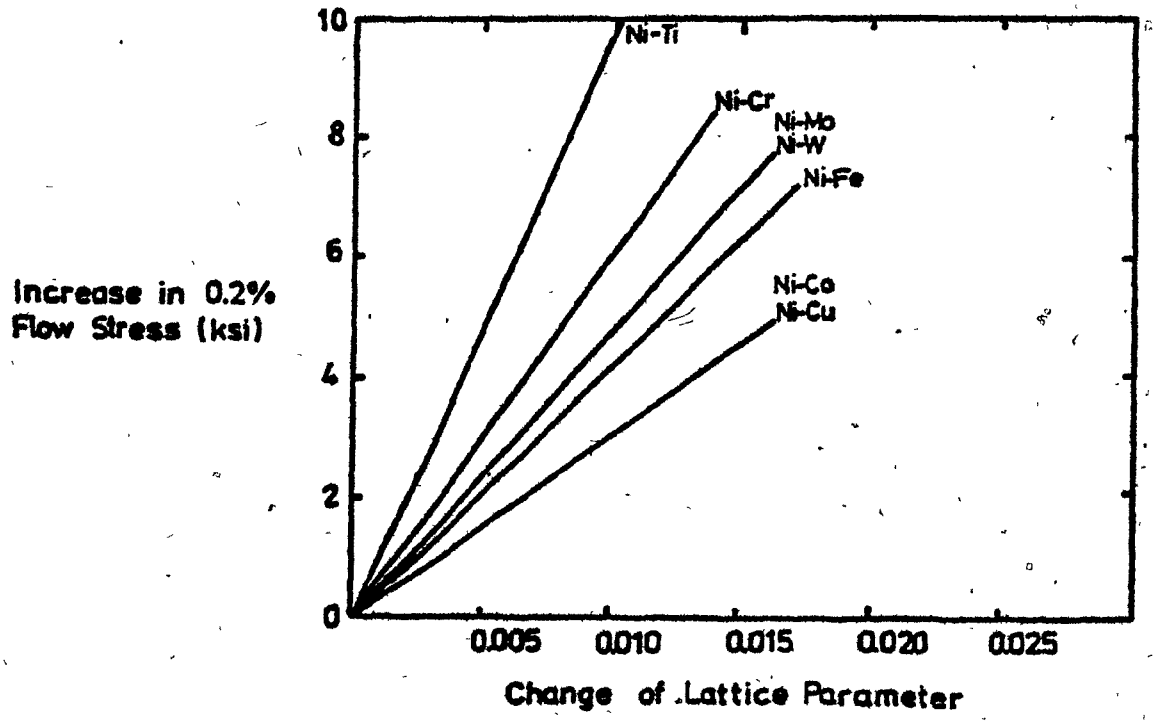

FIGURE 2.2 Effect of lattice parameter on flow stress of nickel alloys (after Decker and Sims (6)).

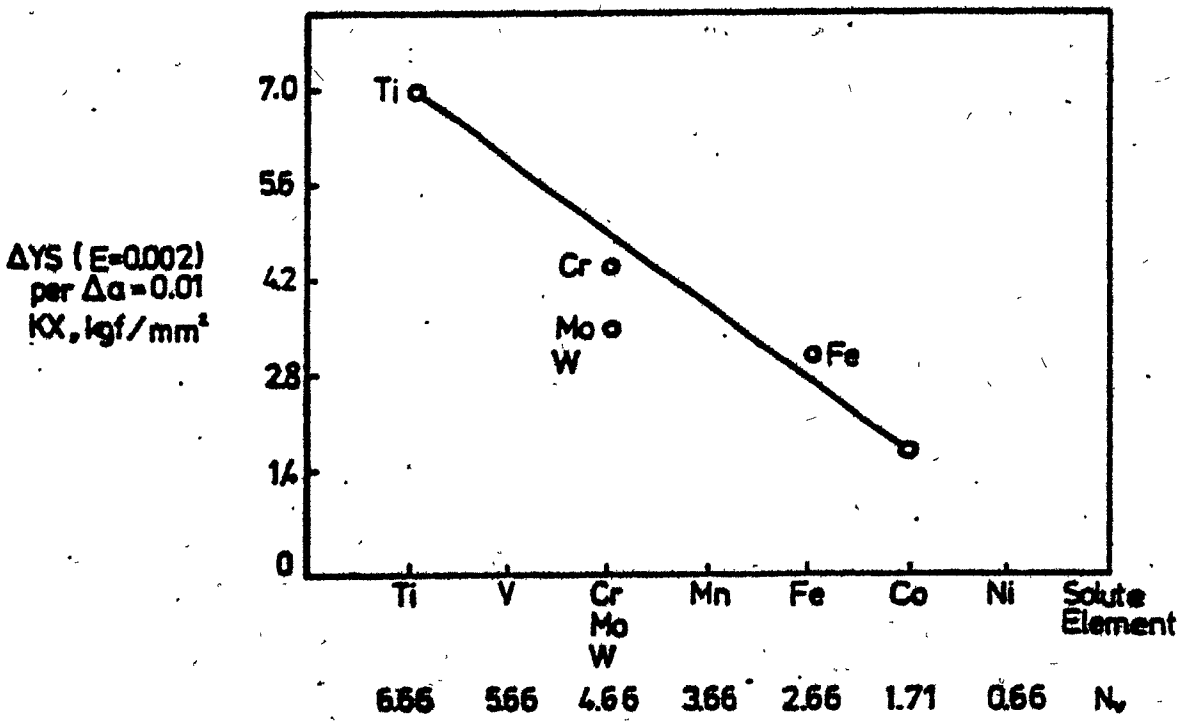

FIGURE 2.3 Effect of valency difference on hardening of nickel alloys (after Beeston et al. (8,9)).

2.1.1.2 Modulus

The role of the modulus difference between solute and solvent in the strengthening process is based on the extra work needed to force a dislocation through harder or softer regions in the matrix (11,12). The larger the difference between the shear moduli of solvent and solute, the greater is the expected increase in strength. To date, no detailed quantitative studies have been carried out for nickel alloys.

2.1.1.3 Short-range Order

Concentrated solid solutions are likely to exhibit appreciable short range order, particularly if dissimilar atoms are involved (13). The energy required to shear a short-range ordered crystal causes an increase in the flow stress of the alloy. The shear stress to move a dislocation through a short-range ordered zone is given by Flinn (14) as:

$$\tau = 16\sqrt{\frac{2}{3}}\,\frac{c(1-c)\nu a_s}{a^3} \qquad (2.3)$$

where c is the mole fraction of solute, ν is the interaction energy for the various atom pairs, a_s is the local order coefficient, and a is the lattice parameter in the short-range ordered region. Since all the terms in equation (2.3) are temperature independent, short-range order provides an athermal increment to the flow stress. However, the degree of short-range order decreases with increasing annealing temperature.

Consequently, the short-range order component of flow stress is sensitive to thermal history.

2.1.2 Precipitation Hardening

The major contribution to the strength of nickel-base superalloys is provided by the formation of stable, coherent intermetallic compounds such as γ' (ordered FCC-$L1_2$ structure, e.g. Ni_3 (Al,Ti)) and γ'' (ordered BCT-DO_{22} structure, e.g. Ni_3 (Nb,Al,Ti)). Fig.2.4 shows the unit cells for these two structures. Waspaloy and most nickel-base superalloys are strengthened by γ' and Inconel 718 by γ'' (15,16). The precipitation of carbides and borides provides additional strengthening mainly at moderate to high temperatures, at which significant improvements in creep behavior are observed (5).

2.1.2.1 The Mechanisms of Precipitation

Several studies extending over the past 20 years have considerably advanced our understanding of the nature of precipitation from supersaturated nickel-base alloys. In the early stages of precipitation, satellite reflections, indicative of periodic modulations in structure, are observed by X-ray diffraction. The occurrence of an aligned or modulated structure in the early stage of aging suggests that decomposition of the supersaturated solid solution may be taking place by spinodal decomposition (17). Ardell and Nicholson (18) have shown, however, that alignment can be the result of elastic interactions

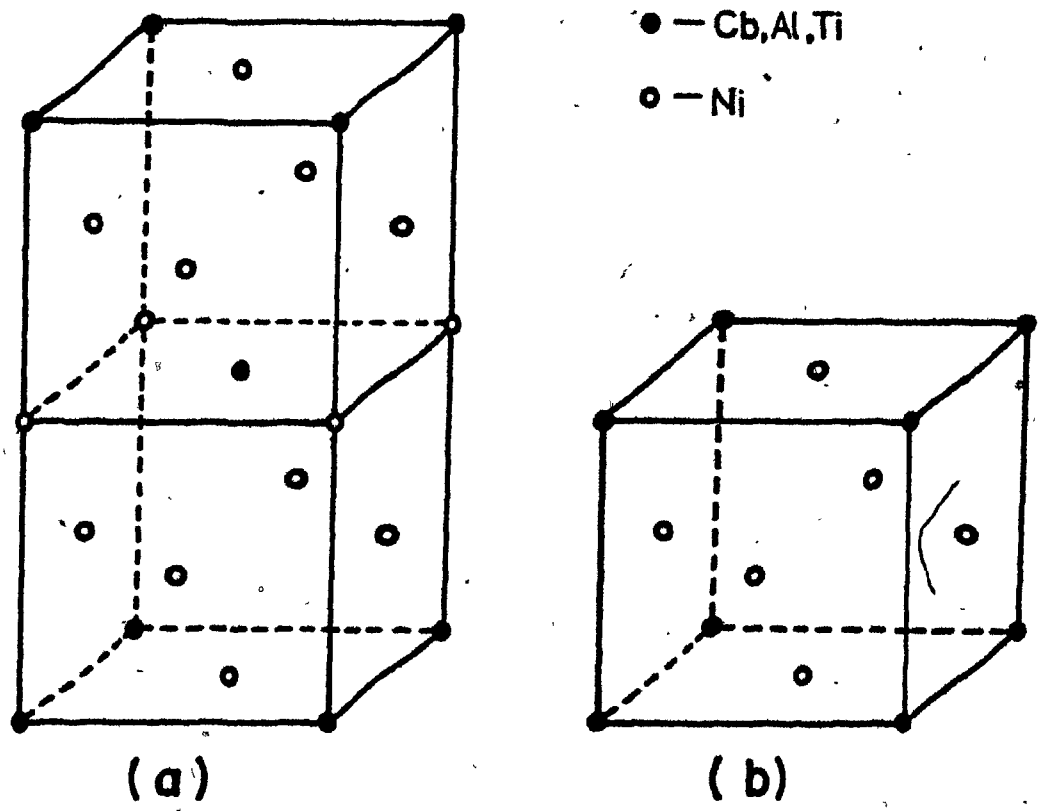

FIGURE 2.4 Unit cells showing ordering (a) BCT (DO_{22}) structure; (b) FCC ($L1_2$) structure (after Paulonis *et al*. (16)).

between γ' precipitates during coarsening. The general consensus today is that the nature of the precipitation process depends mainly on two factors: (a) the misfit between γ and γ' and (b) the degree of supersaturation.

At low supersaturations, the heterogeneous nucleation of coherent γ' occurs partially on dislocations, provided that the coherency strain is sufficiently large for a strong elastic interaction to exist (18-23). Homogeneous (continuous or classical) precipitation is the dominant mechanism for the near totality of γ-γ' systems (5,18,19,22-25). At high supersaturations, decomposition may occur spinodally, but there is to date, conflicting evidence to support this theory (18,26,27).

The electron microscopy of replicas has shown that the γ' phase forms coherently with the matrix and is oriented such that the cube faces are parallel to $(100)_{Ni}$. The elastic anisotropy of the matrix is influential in determining the orientation of the γ' (19).

2.1.2.2 Interaction between the Precipitate Particles and Dislocations

Several theories of strengthening by ordered precipitates have appeared in the literature recently (21,23,28-34). In all cases, the critical resolved shear stress (CRSS) is shown to be dependent on the volume fraction, size and strength of the precipitates. Among the factors that have been suggested as contributing to the particle hardening of nickel-base alloys are the following: i) the existence of order in the particles;

ii) the coherency strains mentioned above; iii) differences in SFE between particle and matrix; iv) the energy to create additional particle-matrix interface; and v) differences in elastic moduli between particle and matrix.

The methods used to treat hardening by solutes and by precipitates are basically similar. They depend on calculating the force of interaction between a moving dislocation and whatever obstacles are in its path. In order to move through a field of dispersed obstacles, a dislocation must bend to an angle, ϕ, dependent upon the obstacle strength, Fig. 2.5. For weak obstacles, $\phi \to \pi$; that is, very little bending is required for the dislocation to escape from the obstacle. For strong obstacles, $\phi \to 0$, as the dislocation is forced to almost double back on itself (23).

Brown and Ham (23) have shown that, for Ni-Al alloys, particles with radii (r) smaller than 3 Å have practically no effect on the flow stress, and when r is bigger than $\simeq$ 150 Å, the particles lose coherency and Orowan loops are observed around the particles. The maximum strengthening occurs for a particle radius of 40 Å (28). Davies and Stoloff (29) noted that ageing a Ni-14% Al alloy for 1 hr at 700°C after quenching produced an increment of flow stress in shear of 5.3 hbar. The value of r for their work was calculated by Brown and Ham (23), who found r = 18 Å. For a Ni-Cr-Al alloy, Gleiter and Hornbogen (30) reported an optimum size of r = 55 Å for maximum hardening. Several other values are available for different systems (31-39),

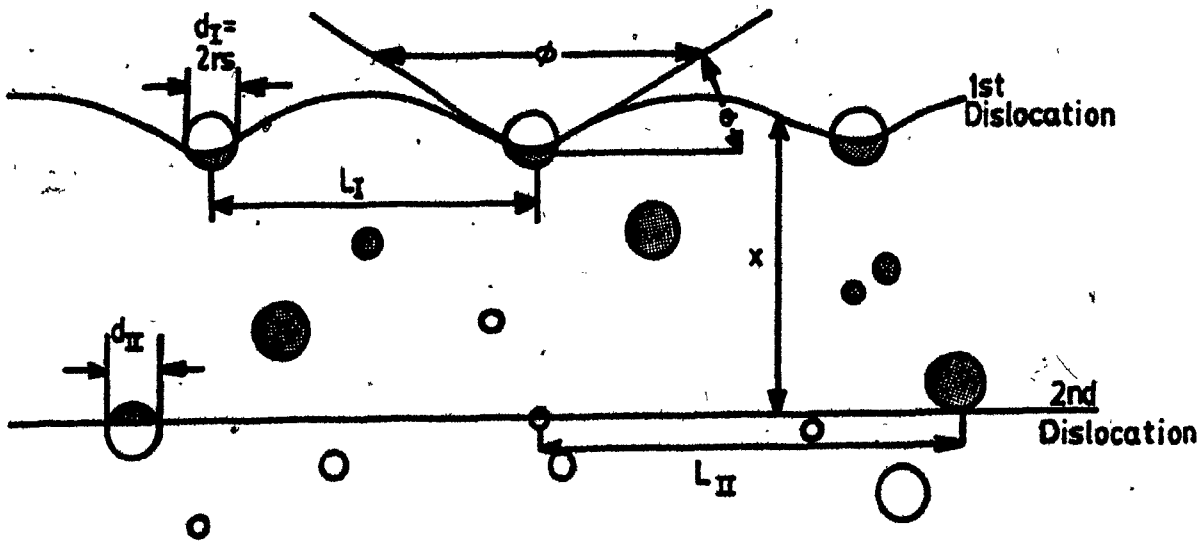

FIGURE 2.5 Dislocation pairs interacting with ordered particles, showing effect of bend angle ϕ on obstacle spacing. Shaded areas represent APB (after Stoloff (4)).

leading us to conclude that the optimum particle size for maximum flow stress (e.g., r = 35 Å), depends mainly on the volume fraction and γ-γ' mismatch (i.e. on the chemical composition). For each system, a curve like the one in Fig. 2.6 based on ref. 21 can be determined. For the ascending part of curve (A-B), the increase in CRSS ($\Delta\tau$) with increasing particle radius is a consequence of the bowing out of the dislocation between the particles. $\Delta\tau$ increases only until the dislocation has bowed out to a semi-circular shape. Further bowing out leads to the formation of Orowan rings or to prismatic cross-slip. This happens at point B. With increasing particle radius, the stress necessary to form an Orowan loop around the particle decreases very rapidly (B-C).

Of the various possible strengthening mechanisms listed above, there is now little doubt that the principal ones are: order strengthening and coherency hardening (39-45). Order strengthening arises when a dislocation passes through an ordered particle creating an antiphase boundary (APB). Under these conditions, the glide motion of the leading dislocation is impeded since it must do work to create an APB. In a like fashion, the motion of the trailing dislocation is assisted because it annihilates an APB. One outcome of this situation is that dislocations travel in pairs, the second removing the disorder created by the first. Coherency hardening arises through an elastic interaction between the strain fields of the dislocations and precipitates whenever there is a lattice parameter mismatch between the precipitate and matrix phases.

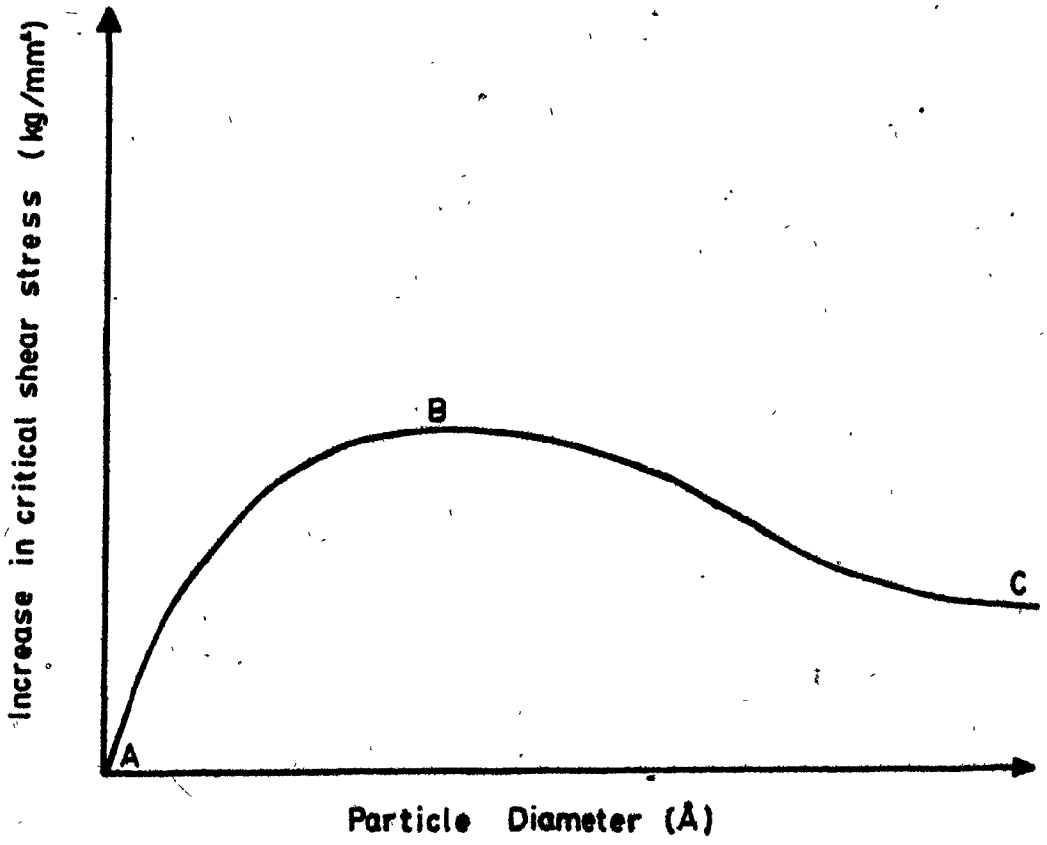

FIGURE 2.6 Dependence of the CRSS on particle diameter (after Gleiter and Hornbogen (21)).

It is of interest that various investigators in the literature have taken a broad (and conflicting) range of views regarding the relative roles of these two factors. For example, Brown and Ham (23) originally maintained that the contributions of order strengthening and coherency strengthening should be additive, each mechanism contributing to the yield stress the value it would contribute if it were acting alone. By contrast, Decker and Mihalisin (44) have concluded that strengthening is due primarily to coherency hardening. Taking still another view Raynor and Silcock (32) and Menjal and Ardell (42) have suggested that strengthening is due entirely to order hardening. Finally, Melander (45) has proposed that both mechanisms contribute, with coherency strengthening making a significant contribution only when the misfit is large enough. It should be added that Melander and Persson (39) consider that order contributes significantly when the alloys are underaged, but that coherency hardening has an important contribution when the alloys are in the peak-aged condition.

Enlightened by the more recent and detailed publications (39-43), we can conclude the following: i) There are very few γ/γ' alloys in which only one mechanism is likely to operate. ii) While there is fundamental disagreement on the contribution of coherency hardening to the increment in CRSS in underaged γ/γ' alloys, the same is not true of alloys aged to the peak condition. In the latter case, there is consistent experimental evidence to indicate that the contribution of coherency hardening is substantial. iii) In γ/γ'' alloys, e.g. Inconel 718, the

strength depends primarily upon coherency strengthening arising from the tetragonally distorted DO_{22} γ'' structure.

2.1.3 Strengthening Effects of Carbides and Other Minor Additions

The role of carbides in superalloys is complex and their contribution to the high temperature strength remains to be clarified. Nevertheless, some generalizations can be drawn, and these will be considered in turn. In nickel alloys, the carbides appear to prefer grain boundaries as location sites, while in cobalt and iron superalloys (and other alloy matrices of higher Nv), intragranular sites can be very popular.

Certain grain boundary carbides, depending on their morphology, can have detrimental effects on ductility (5,6). Accordingly, some investigators (46,47) have taken the logical step of reducing carbon to very low levels. However, further studies in this direction (6,46) uncovered sharply reduced creep life and ductility when the C level was decreased to less than 0.03% C. Clearly, carbides must be tolerated (and even encouraged) in superalloys, especially at the grain boundaries. It is, in addition, clear that the carbide morphology can influence the ductility (3,6), as well as the chemical stability of the matrix through the removal of essential, but reactive elements (3,6,48).

The common classes of carbide are MC, M_7C_3, $M_{23}C_6$ and M_6C and these can have somewhat differing effects. The MC carbides are the most refractory and stable, and are a major source of reserve carbon for later chemical interaction. M_7C_3,

in the form of Cr_7C_3, is not usually stable in most superalloys, generally transforming on aging to $M_{23}C_6$. $M_{23}C_6$ shows a marked tendency for grain boundary precipitation and is profuse in alloys with moderate to high chromium concentrations. These carbides promote significant improvements in rupture strength, apparently through the inhibition of grain boundary sliding (3). Finally, the carbide M_6C is similar to $M_{23}C_6$, but is most frequently found when the refractory metal content is high.

The most remarkable alloying effects in superalloys are due to minute additions of boron, zirconium, magnesium and hafnium. Boron is generally present to the extent of 50-500 ppm in superalloys and is an essential ingredient. It is located at grain boundaries where, at the triple points, it reduces the onset of grain boundary tearing under rupture loading conditions (3,6). Appropriate zirconium, magnesium and hafnium additions can supplement the effect of boron. It has been suggested (48) that boron and zirconium act like carbon and must be present during solidification to prevent injurious trace elements such as oxygen and sulphur from collecting at the grain boundaries and forming brittle films. Magnesium additions have been used in a similar way to improve the microfissure resistance of Inconel 718 during welding. Hafnium also has a high affinity for sulphur, hence it can be used as a getter to prevent grain boundary embrittlement by sulphur (48).

2.2 The Mechanisms of Hot Deformation.

The mechanisms through which superalloys are strengthened have been reviewed above, and it was seen that both solute additions and precipitates are factors responsible for the good high temperature properties of these alloys. It should now become evident that these same strengthening mechanisms will also lead to a loss in workability, to higher recrystallization temperatures and to a narrower temperature range of hot working. The manner in which this arises can be deduced from experiments on the microstructural changes occurring under hot working conditions, mostly performed on pure metals, single phase or experimental alloys (49-62). These investigations form the basis for the current theories on hot deformation mechanisms, and they will now be reviewed briefly.

During hot working, most metals and alloys initially undergo a period of work hardening, in which the dislocation density is continuously increasing. After this region, the behavior of the material being deformed will depend upon the mechanism of restoration (49,53). In metals with high stacking fault energies, the dislocations are fairly mobile, and are free to climb and cross slip out of their slip planes. The moving dislocations are continually breaking up and rebuilding the subboundaries, and as a net result maintain an equilibrium subgrain size, dislocation density and associated flow stress. This mechanism is known as dynamic recovery. When the metals and alloys being deformed have low stacking fault energies, the dis-

location mobility is diminished, and leaving the slip plane is more difficult. Under these conditions, the amount of recovery produced by the annihilation of individual dislocations is no longer sufficient to maintain a stable subgrain structure. The sub-boundaries will then, after a critical amount of deformation, attain a dislocation density high enough to transform them into mobile high angle boundaries. As they move, they eliminate the dislocations, leaving behind a dislocation-free, recrystallized structure. The grain boundary bulge theory, which accounts for the formation of the new grains, assumes that certain large-angle boundaries are already unstable and merely bow out in areas of locally higher stored energy. By bulging out in this manner, a new "nucleus" is produced (62). The new grains can also be created through the formation of high-angle boundaries by the accumulation of dislocations in certain sub-boundaries (also known as recrystallization in situ) (52). After deformation, further restoration may take place by static recovery and metadynamic and static recrystallization (49-53).

The hot workability of metals in industry is closely linked to the above mechanisms of restoration. They determine the flow stresses developed as well as the rate of crack propogation, consequently controlling the amount of deformation which can be applied in a single pass.

Luton *et al.* (56,57) tested pure Ni and Ni-Fe alloys in the hot working region, and concluded that the restoration mechanism was dynamic recrystallization. They established that

during deformation, cracks were formed at triple points and serrations on the grain boundaries. The growth of these cracks was impeded by the movement of the grain boundaries away from the cracks during dynamic recrystallization, resulting in improved ductility. Dynamic recrystallization was also found to be the restoration process in the hot working range during experiments on pure nickel by Sah et al. (58), and by Shapiro and Dieter on pure nickel (59) and Inconel 600 (60).

Using torsion testing, Fulop (63,64) studied the mechanisms of deformation and fracture in Waspaloy from room temperature to 1093°C, at strain rates between $3 \times 10^{-2} s^{-1}$ and $7.0\ s^{-1}$ and at strains of up to 45. Warm working behaviour was observed from 816°C to 899°C along with partial recovery. Recrystallization was initially observed at 954°C and in the range 1010°C to 1093°C the samples were completely recrystallized dynamically, recrystallization starting at the maximum of the flow curve and becoming complete at the end of the work softening stage. The effects of hot working on the structure and properties of Waspaloy were studied through rolling experiments by Bailey (65) at finishing temperatures ranging from 960°C to 1060°C with reductions from 18% to 49%. The new grains seen in the as-rolled microstructures are described as being dynamically recrystallized, but it may be argued that they were formed by static or post-dynamic recrystallization between passes and during cooling after deformation.

The hot workability of superalloys has also been studied through the use of a Gleeble testing machine which makes it possible to submit the specimen to a thermomechanical history experienced by a given bar or billet during deformation processing (66-68). Cremisio and McQueen (66) found that for Hasteloy X a ductility maximum at about 1120°C was due to dynamic recrystallization, provided that the samples were deformed sufficiently to store the energy required for recrystallization. For Inconel 718, they reported that the progress of dynamic recrystallization is retarded due to the pinning of the grain boundaries by γ" and other precipitates. Weiss et al. (67) testing Inconel 600, and Bailey (68), testing Unitemp HN, concluded that the recrystallized grains in the microstructure of the broken hot tensile specimens were the product of dynamic recrystallization.

Marsh and Oakes (69), describing forging practice for Waspaloy and Inconel 718, suggested that forging be initiated at a temperature at which dynamic recrystallization, and therefore, extensive restoration, occurs. Finish forging, by comparison, should be carried out at lower temperatures, to prevent undesirable grain growth in the final product.

Observations of γ' particle sizes and distributions before and after deformation indicate that the recrystallization process involves a local resolutioning of γ' ahead of the advancing recrystallized boundaries with discontinuous reprecipitation in the recrystallized grains (70,71). The kinetics

of recrystallization were said to be independant of the size of primary γ' precipitate for average sizes in the range 0.2-0.6 μm (71).

CHAPTER 3

EXPERIMENTAL MATERIALS AND PROCEDURE

3.1 Compression Testing

Hot compression is a suitable testing technique for hot working studies because the stress state is very close to those found in deformation processing (72). No basic instabilities such as necking arise (73,74), and testing can generally be carried out to strains of 0.7 without barrelling and even to as much as 1.2 with slight barrelling, if friction between the specimen and anvils is minimized (72,73). This can be accomplished by using smooth, hardened platens and by grooving the ends of the sample to retain the lubricant (75,76). The presence of such grooves does not affect the results significantly (77). Although the deformation in hot compression is usually homogeneous for most materials, flow localization can occur if there is appreciable flow softening (78). Such flow softening is generally associated with the presence of unstable microstructures. When the strain rate is high enough, due to adiabatic heating, the localization can become catastrophic leading to the formation of shear bands (79). More detailed descriptions of the characteristics, advantages and disadvantages of compression testing are available elsewhere (72-77).

3.2 Experimental Materials

The materials used in this investigation were: i) Waspaloy - a nickel-base superalloy supplied by TRW Inc., Metals Division, Minerva, Ohio, heat No. KW7208; and ii) Inconel 718 - a nickel-iron base superalloy supplied by Special Metals Corp., New Hartford, New York, heat No. 9-5630. Both materials were received in the heat treated condition (Table 3.1) for optimum high temperature creep and stress rupture properties. The chemical compositions of these materials are given in Table 3.2.

3.2.1 Specimen Preparation

The materials used in this study were initially in the form of rods, 12.7 mm in diameter. Compression samples were machined from the rods according to Fig. 3.1. The specimen dimensions were based on the load cell capacity and crosshead speed range of the Instron. The end faces of the specimens were grooved to retain the glass lubricant used in high temperature deformation. The groove design was patterned on previous investigations (80,81) which showed that the best results are obtained with flat-bottomed grooves, where the grooves are wider at their bases than are the ridges between them.

TABLE 3.1

Heat Treatment of the Experimental Materials

WASPALOY	Solutioning	1080°C	4 hours A.C.
	Intermediate (Stabilization) Aging	845°C	24 hours A.C.
	Final (Precipitation) Aging	760°C	16 hours A.C.
INCONEL 718	Solutioning	955°C	1 hour A.C.
	Intermediate (Stabilization) Aging	720°C	8 hours F.C. 62°C/hr to 620°C
	Final (Precipitation) Aging	620°C	8 hours A.C.

A.C.: air cooling

F.C.: furnace cooling

TABLE 3.2

Composition of the Materials Tested in Wt%

MATERIALS	WASPALOY	INCONEL 718
C	0.062	0.030
Mn	0.02	0.16
Si	0.10	0.11
Cr	19.35	18.10
Ni	Bal	Bal
Co	13.34	0.37
Mo	4.19	3.05
Nb + Ta	-	5.34
Ti	2.94	0.98
Al	1.30	0.49
B	0.005	0.003
S	0.006	0.002
P	0.015	0.010
Cu	0.02	0.10
Fe	0.82	18.26
Zr	0.062	-

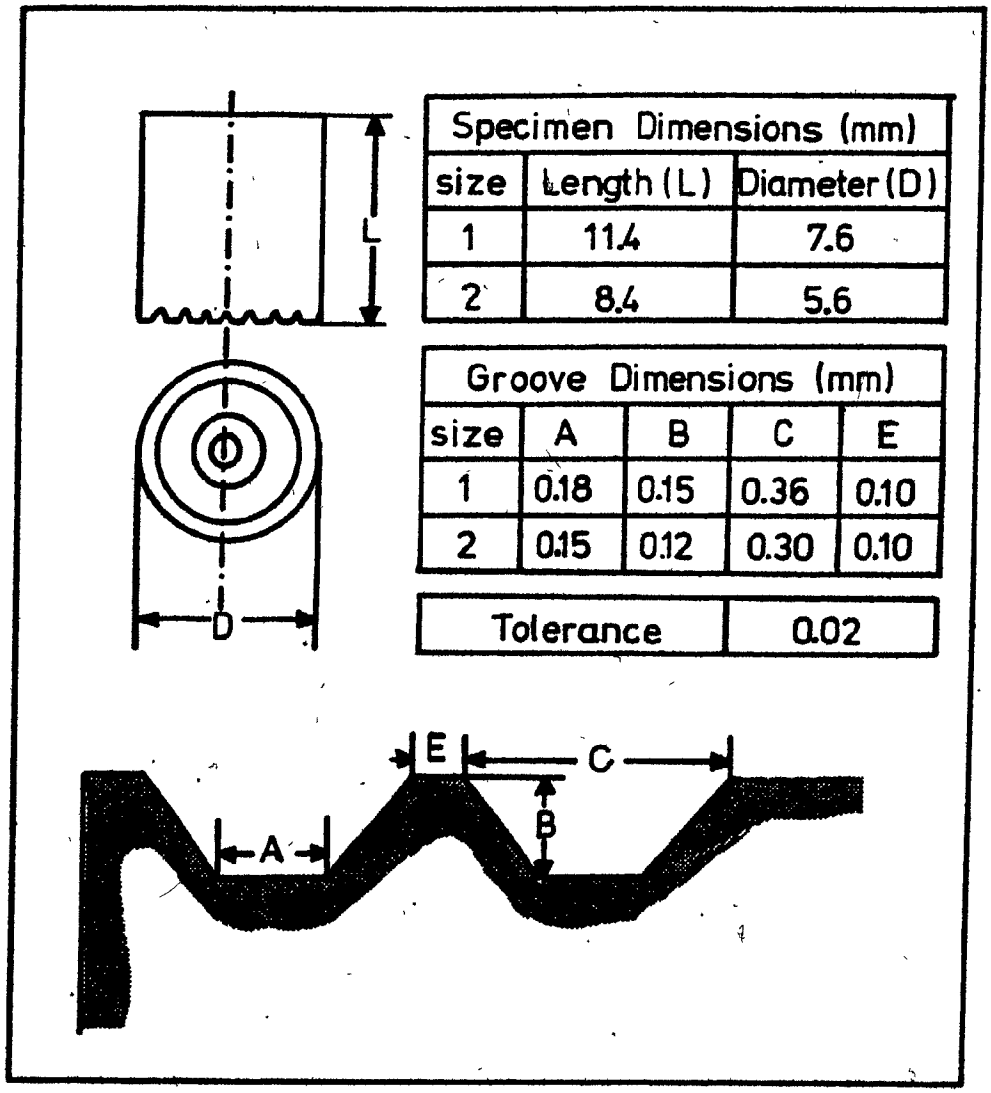

Specimen Dimensions (mm)		
size	Length (L)	Diameter (D)
1	11.4	7.6
2	8.4	5.6

Groove Dimensions (mm)				
size	A	B	C	E
1	0.18	0.15	0.36	0.10
2	0.15	0.12	0.30	0.10

Tolerance	0.02

FIGURE 3.1 Specimen geometry and groove design.

3.2.2 Lubricants

The glasses used were manufactured by the Corning Glass Co. Ltd. and Ferro Industrial Products Ltd. Table 3.3 shows the glasses used for the different test temperatures.

3.3 Experimental Equipment

The tests were carried out on a 10,000 Kg Instron testing frame (Model TT-D) that has been modified for high temperature, constant true strain rate compression. The essential features of the compression train are shown in Figure 3.2. The train consists of two loading members, the upper ram and lower anvil with anvil support. In this design, the water-cooled ram is connected to the crosshead, while the lower anvil rests on a water-cooled stainless steel base supported by a 2500 Kg load cell. The design of the lower anvil (Fig. 3.3) permits the test piece to be quenched within one to four seconds after the completion of a test.

A Satec three-zone platinum split furnace was used to maintain a constant temperature during the tests. The temperature of each zone was monitored by a Pt/Pt-13% Rh thermocouple. Each zone was adjusted so as to produce a uniform ($\pm$ 2°C) temperature region between the anvil ends. The specimen temperature was measured by means of a further Pt/Pt-13% Rh thermocouple that was attached to the lower anvil about two centimeters away from the specimen. The thermocouple was supplied covered with a superalloy sheath by Omega Ltd; its output was monitored

TABLE 3.3

Lubricants Used for the Mechanical Tests

Glass	Temperature Range
Corning 0010	900°C - 1000°C
Corning 7050	1000°C - 1100°C
Ferro 3124	1050°C - 1150°C
Corning 1720	1150°C - 1250°C

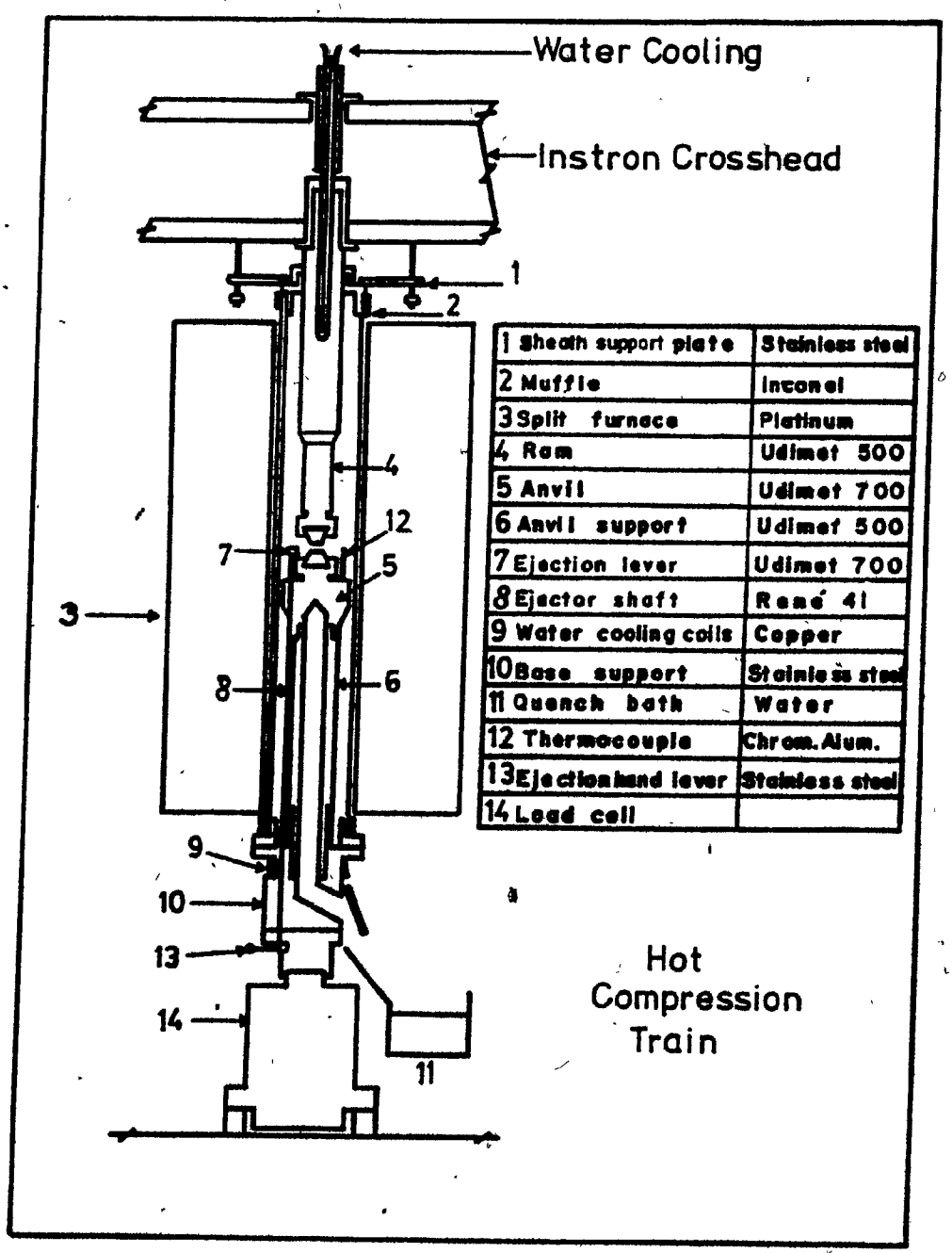

1 Sheath support plate	Stainless steel
2 Muffle	Inconel
3 Split furnace	Platinum
4 Ram	Udimet 500
5 Anvil	Udimet 700
6 Anvil support	Udimet 500
7 Ejection lever	Udimet 700
8 Ejector shaft	René 41
9 Water cooling coils	Copper
10 Base support	Stainless steel
11 Quench bath	Water
12 Thermocouple	Chrom. Alum.
13 Ejection hand lever	Stainless steel
14 Load cell	

FIGURE 3.2 Schematic diagram of the hot compression train (after Weiss (82)).

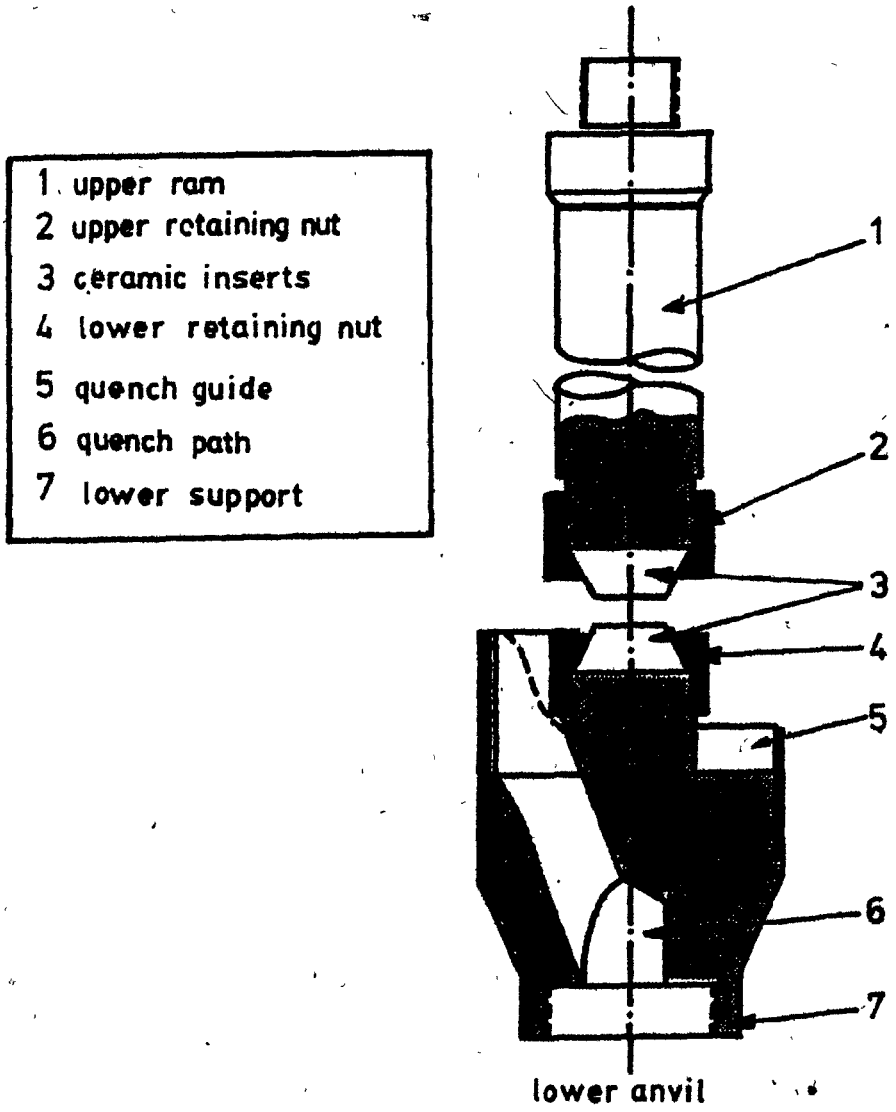

FIGURE 3.3 Schematic representation of the geometry of the ceramic inserts in the upper and lower anvils (after Weiss (82)).

by means of a digital thermometer. Oxidation of the samples was prevented by carrying out the tests in a protective high purity argon atmosphere.

A special device for providing constant true strain rates during testing was built by Luton et al. (83), and operates in conjunction with the Instron variable speed unit. The Instron controller is interfaced to a Canadian General Electric CGE/PAC 4020 process control computer. The interface consists of six relays which can be activated by the remote switches of the real time computer. In addition to this interface, the computer is also linked to the outputs of the load cell and displacement (DCDT) measuring devices (84).

The outputs from the load cell and DCDT pass through an interface consisting of a multiplexed analog-to-digital conversion system which is attached to a Vidar 600 low level scanner. The latter is in turn connected to a Vidar 521 integrating digital voltmeter. The data are converted into stress/strain curves by means of a plotting program.

The software which runs the Instron machine and produces the data acquisition includes three programs: i) the first runs regular compression tests; ii) the second operates interrupted compression tests; and iii) the third performs calibrations and handles data. The true stress-strain curves are produced by the data handling program. The displacement readings are corrected for the elastic distortion of the loading frame (85). The true stress-strain curves are plotted on an on-line Houston Instruments-DP8 (Complot) digital plotter.

For a more detailed description of the equipment, the reader is directed to references 82-86.

3.4 Test Procedure

Before starting an experiment, the furnace was heated up to the solution temperature and kept there for 30 minutes, before cooling to the testing temperature. Once the test temperature was achieved, 15 minutes were allowed before bringing the anvils together. With the anvils in contact, the reading of the DCDT was stored by the computer, and the constant strain rate device was calibrated. Recalibration of the strain rate equipment and the zero position of the DCDT was necessary when the sample size and/or test temperature was changed.

To conduct an actual test, the furnace and muffle were raised on the crosshead, and the sample placed on the lower anvil. The chamber was then closed and the system evacuated and purged with argon, before applying a constant flow of argon. The temperature was then raised to the solution temperature at a heating rate of 0.5°C/s, and after 30 minutes brought down to test temperature at a cooling rate of 10°C/min. The sample was kept at test temperature for 15 minutes, after which the calibration program was carried out and the test started. At the end of each experiment the deformed specimen was quenched.

CHAPTER 4

EXPERIMENTAL RESULTS

4.1 Experimental Conditions

The tests were conducted at constant true strain rates from $5.0 \times 10^{-4} s^{-1}$ to $3.8 \times 10^{-1} s^{-1}$ and in the temperature range 925°C to 1220°C. Specimens of diameter 11.4 mm (Fig. 3.1) were used for the testing of Inconel 718 and for the Waspaloy tests at temperatures above 1000°C. Reduced specimens of diameter 8.4 mm (Fig. 3.1) were used for the testing of Waspaloy at 950°C and 1000°C. Several types of experiments were performed; these had the following aims:

a) To determine the true stress/true strain curves at various constant strain rates and temperatures, both for Waspaloy (Table 4.1) and for Inconel 718 (Table 4.2).

b) To determine the static softening behaviour of Waspaloy through interrupted compression tests (Table 4.3). The strain rates were chosen so as to give similar flow curves for the two temperatures (equivalent structures and internal stresses).

c) To investigate the yield drop occurring in the flow curves for Inconel 718 (Table 4.4). In this case, the strain rates, were selected so as to give the highest possible yield drop for the three temperatures studied.

TABLE 4.1

Mechanical Tests for Waspaloy:
γ-γ' Solvus – 1015-1050°C (87-88)

Test Temperature °C	Strain Rate s^{-1}	Solution Temperature °C
950	5.0×10^{-4} to 3.8×10^{-1}	1200
1000	5.0×10^{-4} to 8.3×10^{-2}	1200
1000	5.0×10^{-4}	1150
1050	5.6×10^{-4} to 9.3×10^{-2}	1200
1100	1.9×10^{-3} to 9.3×10^{-2}	1200
1100	5.6×10^{-3}	1150
1150	5.6×10^{-3} to 9.3×10^{-2}	1200
1220	5.6×10^{-3} to 9.3×10^{-2}	1220

TABLE 4.2

Mechanical Tests for Inconel 718:
γ-γ'' Solvus - 925-955°C (87-88)

Test Temperature °C	Strain Rate s^{-1}	Solution Temperature °C
925	9.3×10^{-4} to 9.3×10^{-2}	1120
975	9.3×10^{-4} to 9.3×10^{-2}	1120
1030	5.6×10^{-3} to 9.3×10^{-2}	1120
1090	3.7×10^{-3} to 9.3×10^{-2}	1120

TABLE 4.3

Interrupted Mechanical Tests for Waspaloy

Test Temperature °C	Strain Rate s^{-1}	Solution Temperature °C	Interruption Strain	Holding Times s
1100	1.9×10^{-3}	1200	0.10	1 to 3.6×10^{3}
1150	5.6×10^{-3}	1200	0.10	1 to 3.6×10^{3}

TABLE 4.4

Testing Conditions for Studying the Yield Drop in Inconel 718

Test Temperature ^{o}C	Strain Rate s^{-1}	Solution Temperature ^{o}C	Annealing Time s
975	5.6×10^{-3}	1120	120 to 4.0×10^{5}
1030	5.6×10^{-3}	1120	60 to 4.0×10^{5}
1090	1.9×10^{-2}	1120	50 to 4.0×10^{5}

d) To study the influence of prior annealing time on the deformation behaviour of Waspaloy when tested at 950°C (Table 4.5).

4.2 The Flow Curves

The typical true stress/true strain curves in Figs. 4.1 to 4.8 show the effect of strain rate on the flow behaviour of Waspaloy at fixed temperatures ranging from 950 to 1220°C. Conversely, the effect of temperature on the flow curves is illustrated in Fig. 4.9 for the selected strain rate of 9.3×10^{-2} s^{-1}. The equivalent curves for Inconel 718 are presented in Figs. 4.10 to 4.14 (effect of strain rate in Figs. 4.10 to 4.13 and effect of temperature in Fig. 4.14). It can be seen that an increase in temperature or a decrease in strain rate leads to a lowering of the flow stress for both materials. Little work hardening was observed under conditions combining low strain rates and low temperatures; furthermore, the peak stresses were not well defined under these conditions. Increasing the strain rate or the temperature resulted in an increase in the amount of work hardening and in a better definition of the peak stress. For the conditions under which the peak stress was more easily defined, the strain to attain the peak stress increased with an increase in strain rate or a decrease in temperature. A steady state of flow was only achieved at higher temperatures for some of the lower strain rates. This is due to the relatively limited strain (0.7) imposed on the materials, which was not sufficient

TABLE 4.5

Tests for Investigating the Effect of Annealing Time on the Flow Stress of Waspaloy at 950°C

Annealing Time minutes	Strain Rate s^{-1}	Total Strain
15	-	0.0
45	-	0.0
180	-	0.0
15	3.8×10^{-1}	0.12
15	3.8×10^{-1}	0.40
15	3.8×10^{-1}	0.70
45	3.8×10^{-1}	0.30
45	3.8×10^{-1}	0.70
180	3.8×10^{-1}	0.70
15	5.0×10^{-4}	0.07
15	5.0×10^{-4}	0.20
15	5.0×10^{-4}	0.40
15	5.0×10^{-4}	0.70
45	5.0×10^{-4}	0.30
45	5.0×10^{-4}	0.70
180	5.0×10^{-4}	0.70

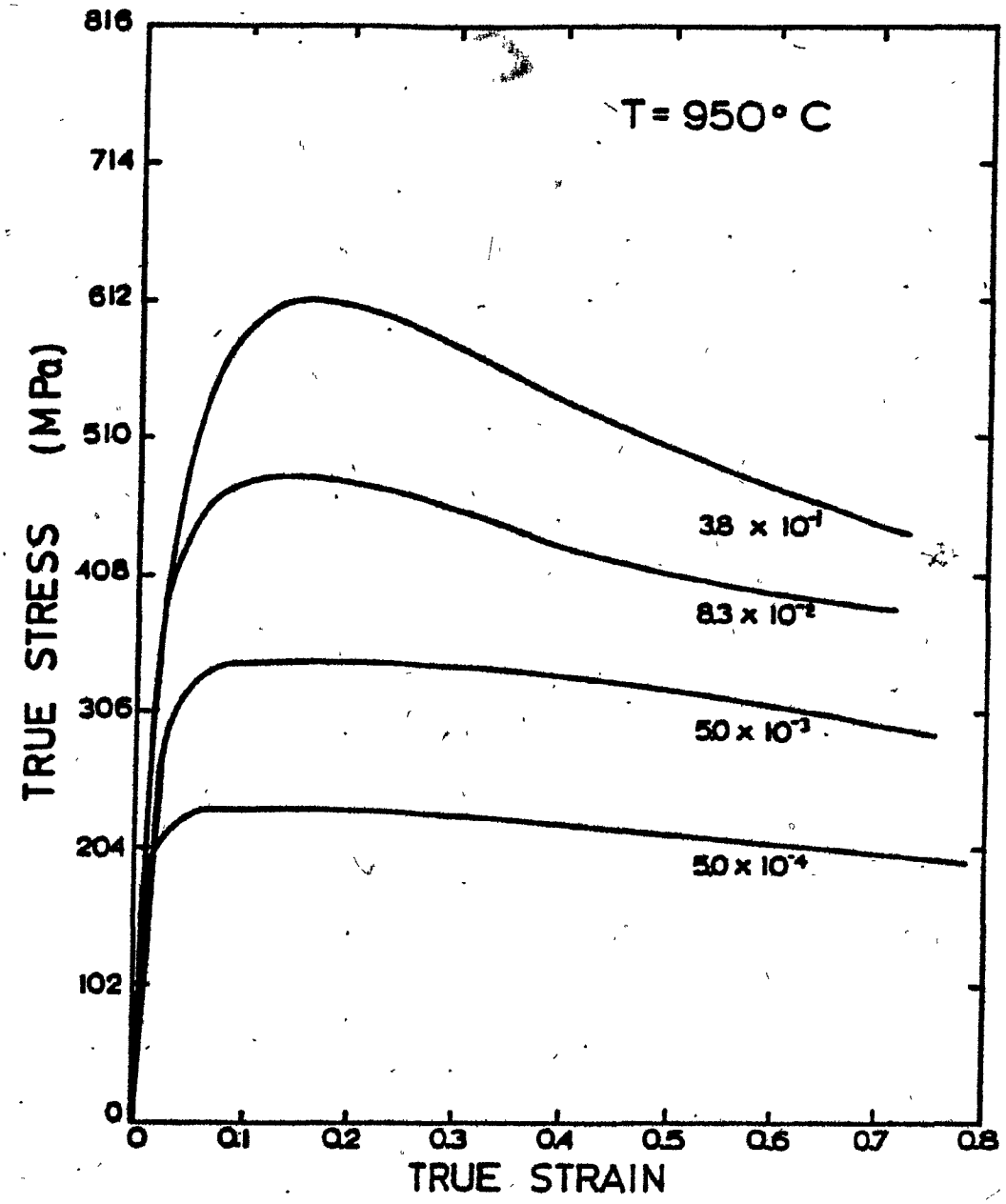

FIGURE 4.1 Strain rate dependence of the flow curve in Waspaloy tested at 950°C.

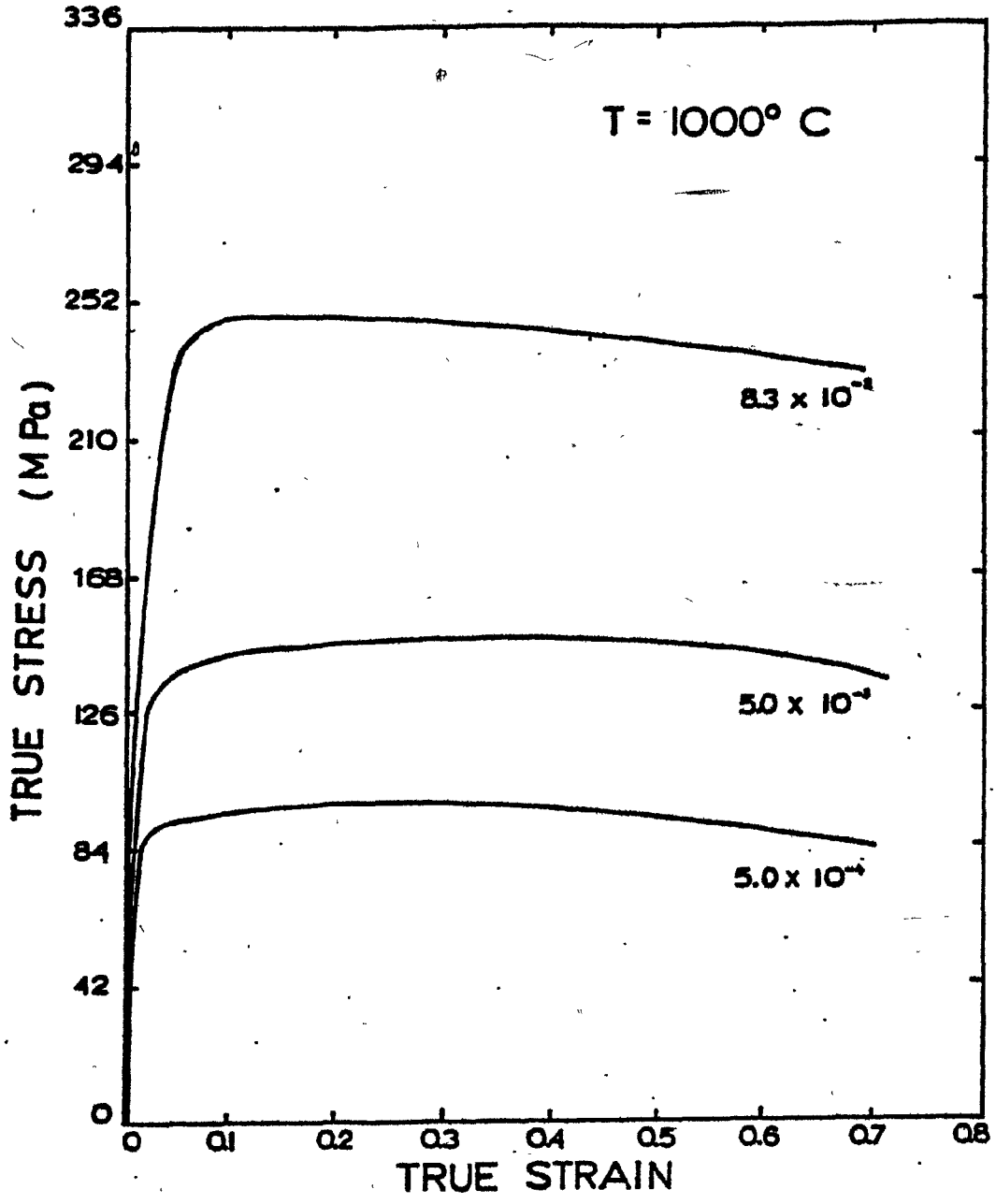

FIGURE 4.2 Strain rate dependence of the flow curve in Waspaloy tested at 1000°C.

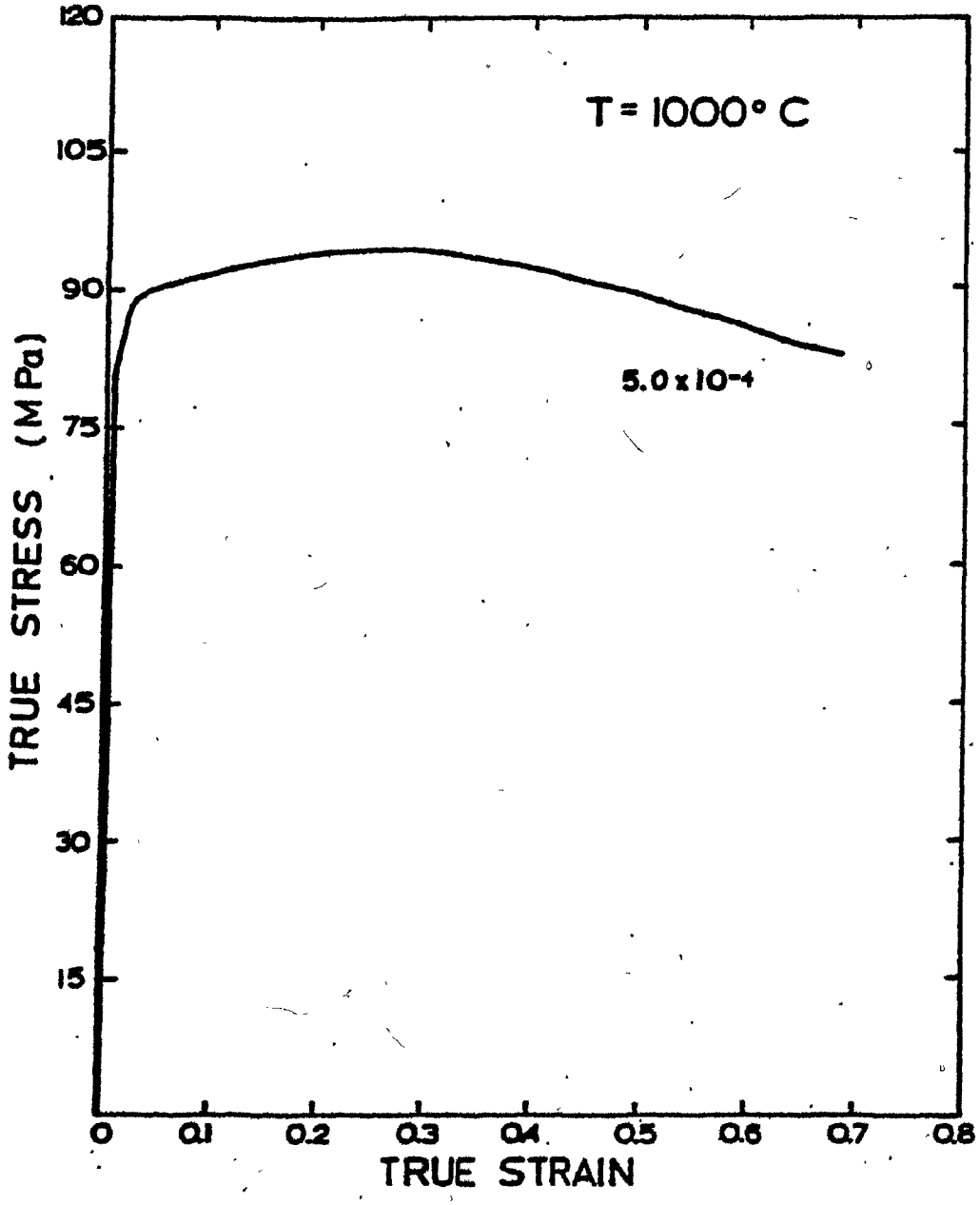

FIGURE 4.3 True stress-true strain curve for Waspaloy tested at 1000°C, strain rate $5.0 \times 10^{-4} s^{-1}$, pre-heated at 1150°C.

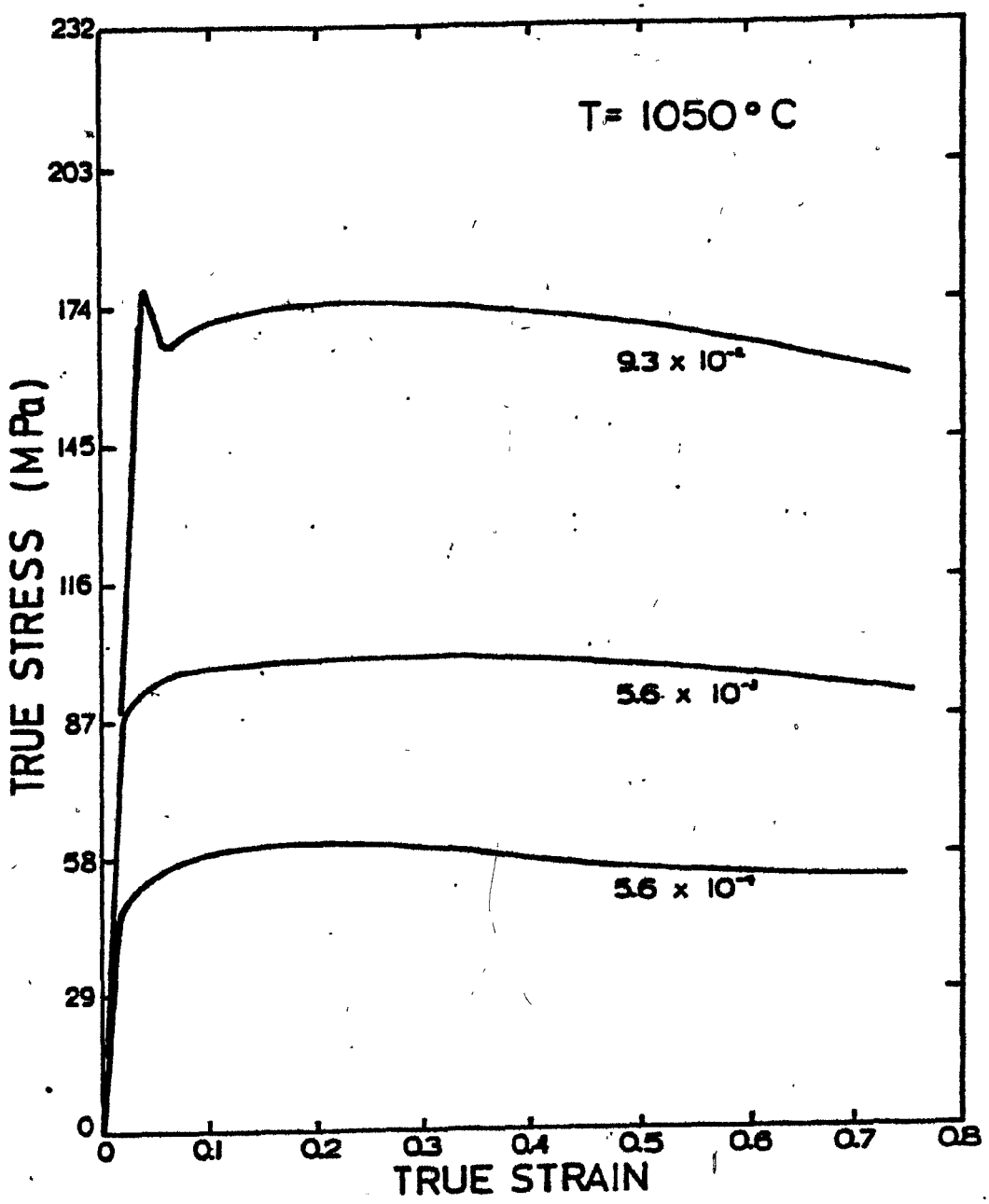

FIGURE 4.4 Strain rate dependence of the flow curve in Waspaloy tested at 1050°C.

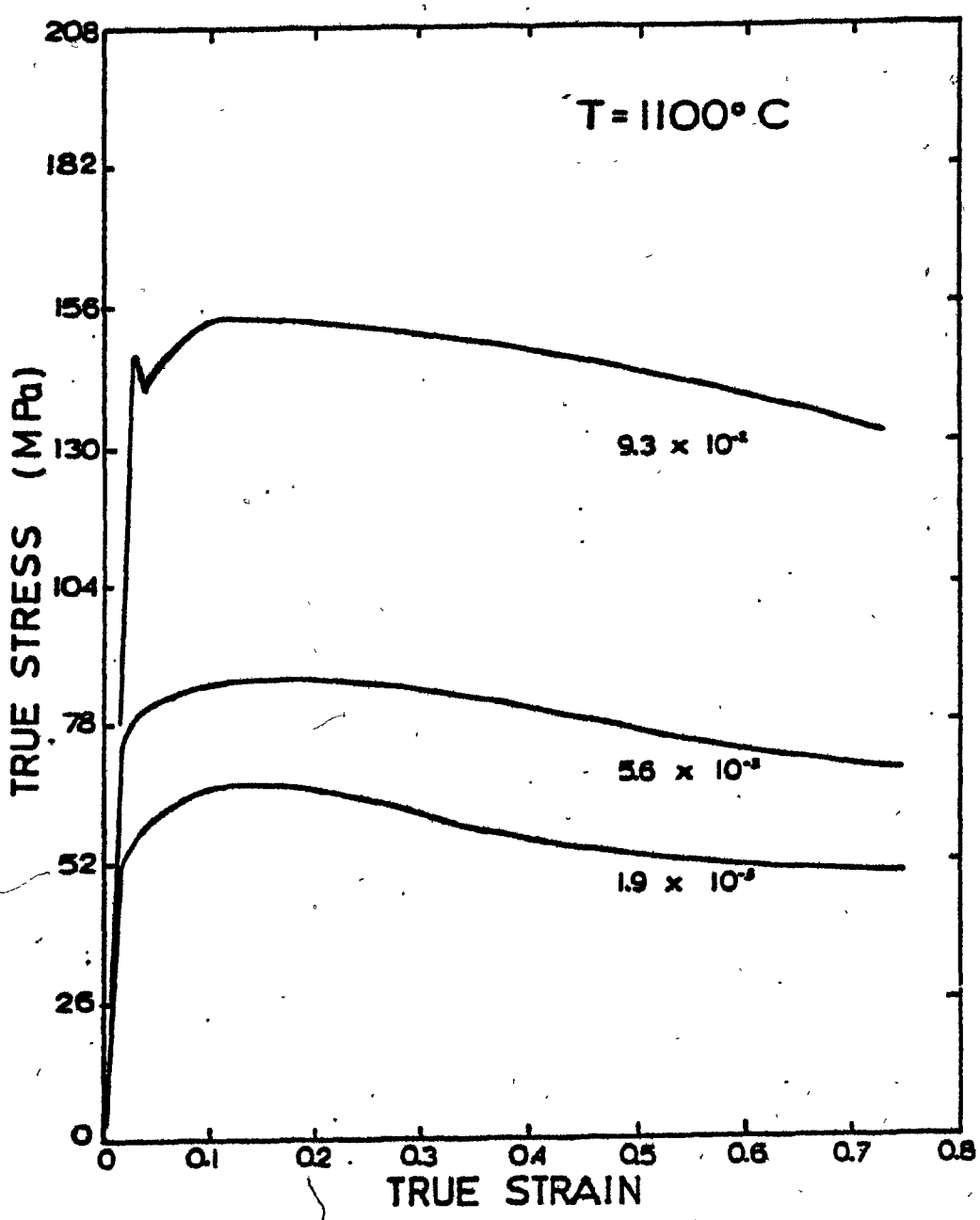

FIGURE 4.5 Strain rate dependence of the flow curve in Waspaloy tested at 1100°C.

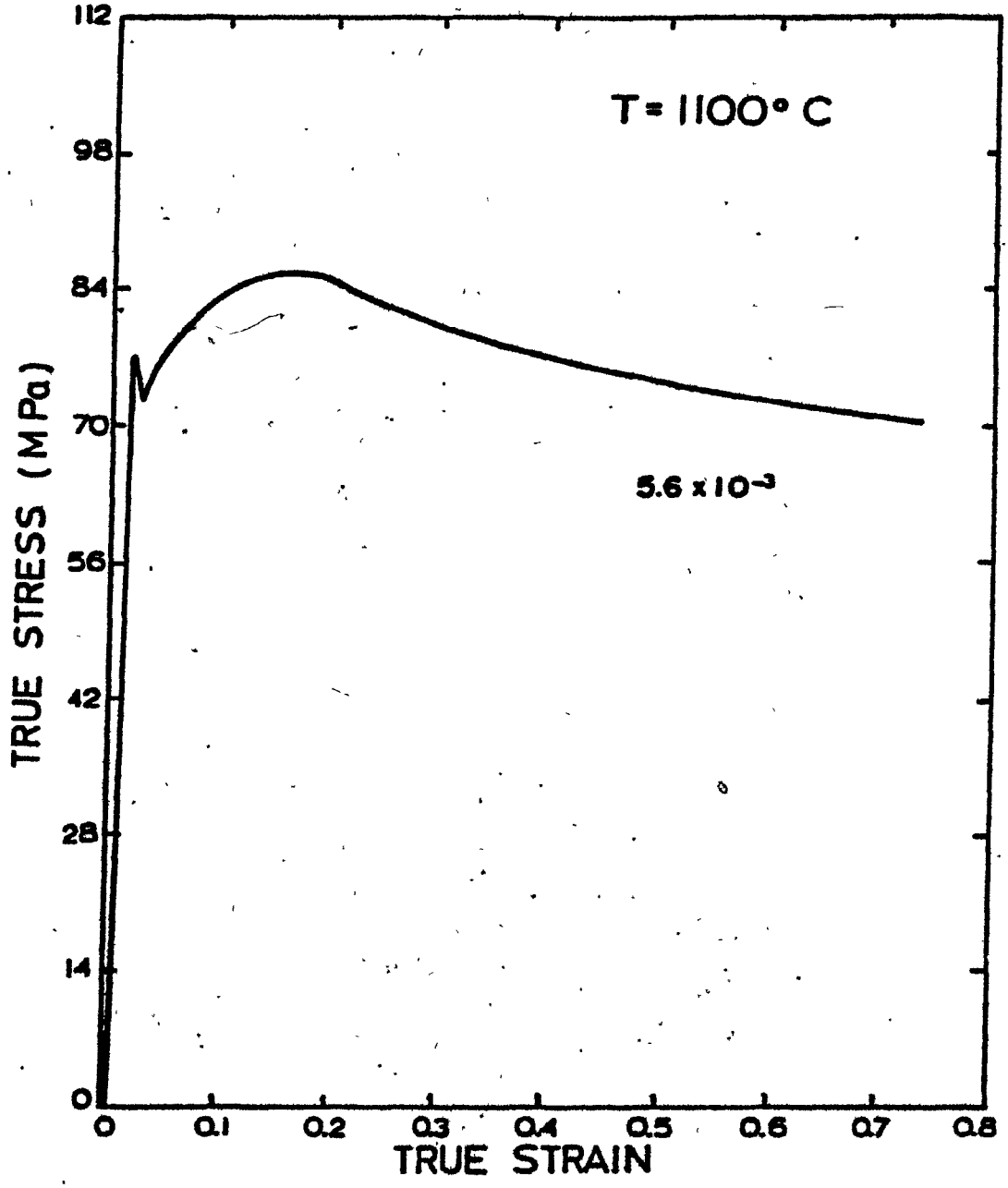

FIGURE 4.6 True stress-true strain curve for Waspaloy tested at 1100°C, strain rate $5.6 \times 10^{-3} s^{-1}$, preheated at 1150°C.

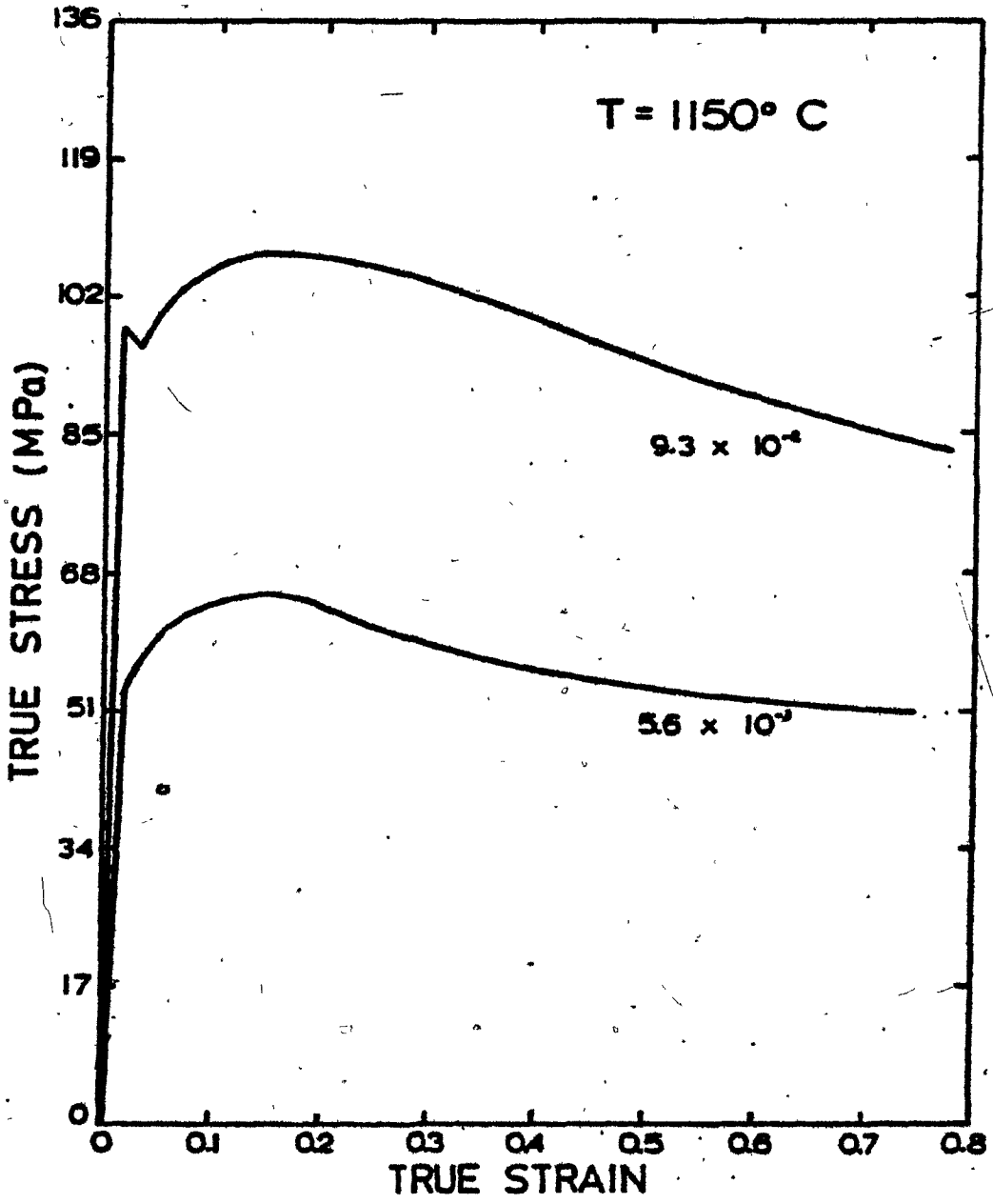

FIGURE 4.7 Strain rate dependence of the flow curve in Waspaloy tested at 1150°C.

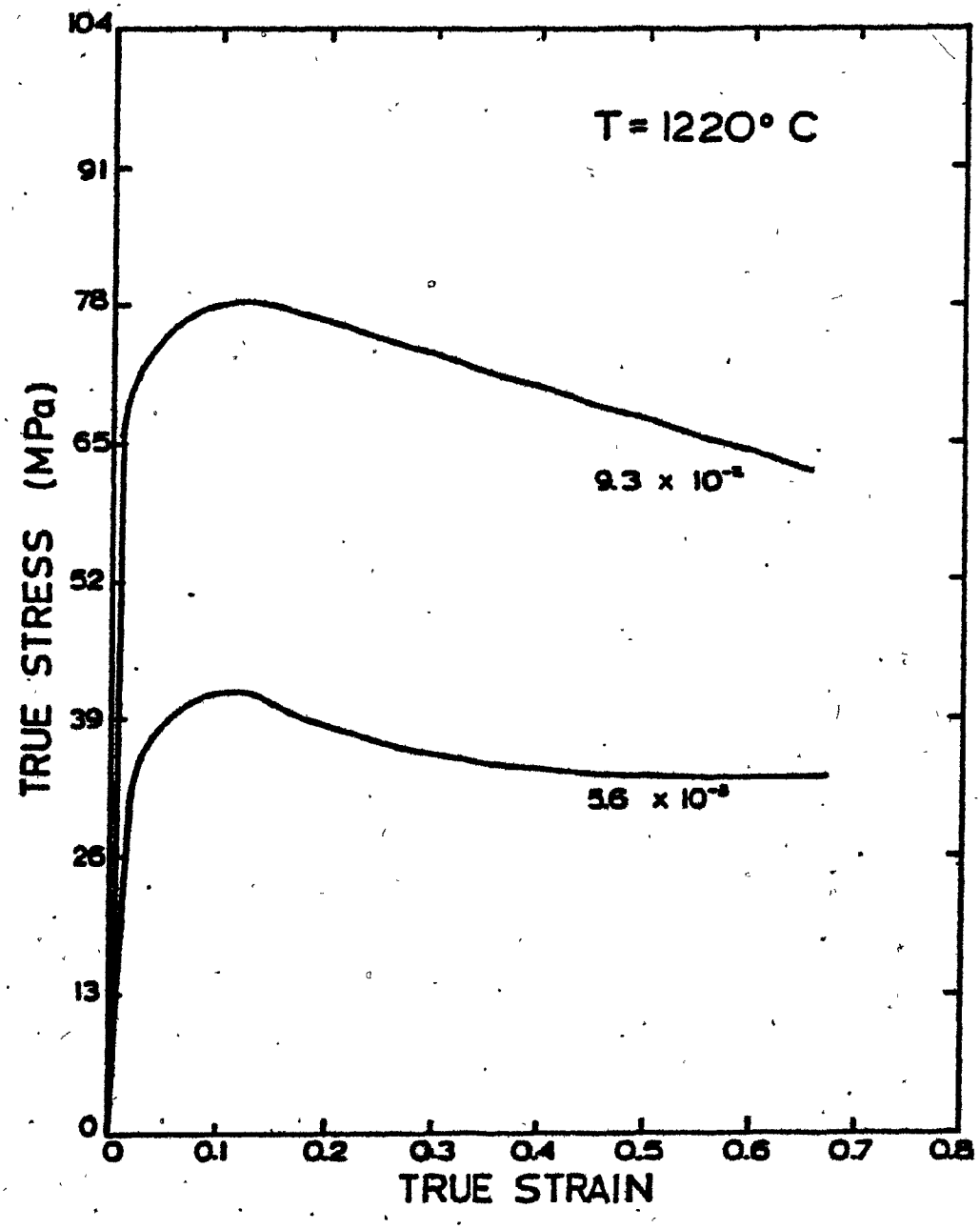

FIGURE 4.8 Strain rate dependence of the flow curve in Waspaloy tested at 1220°C.

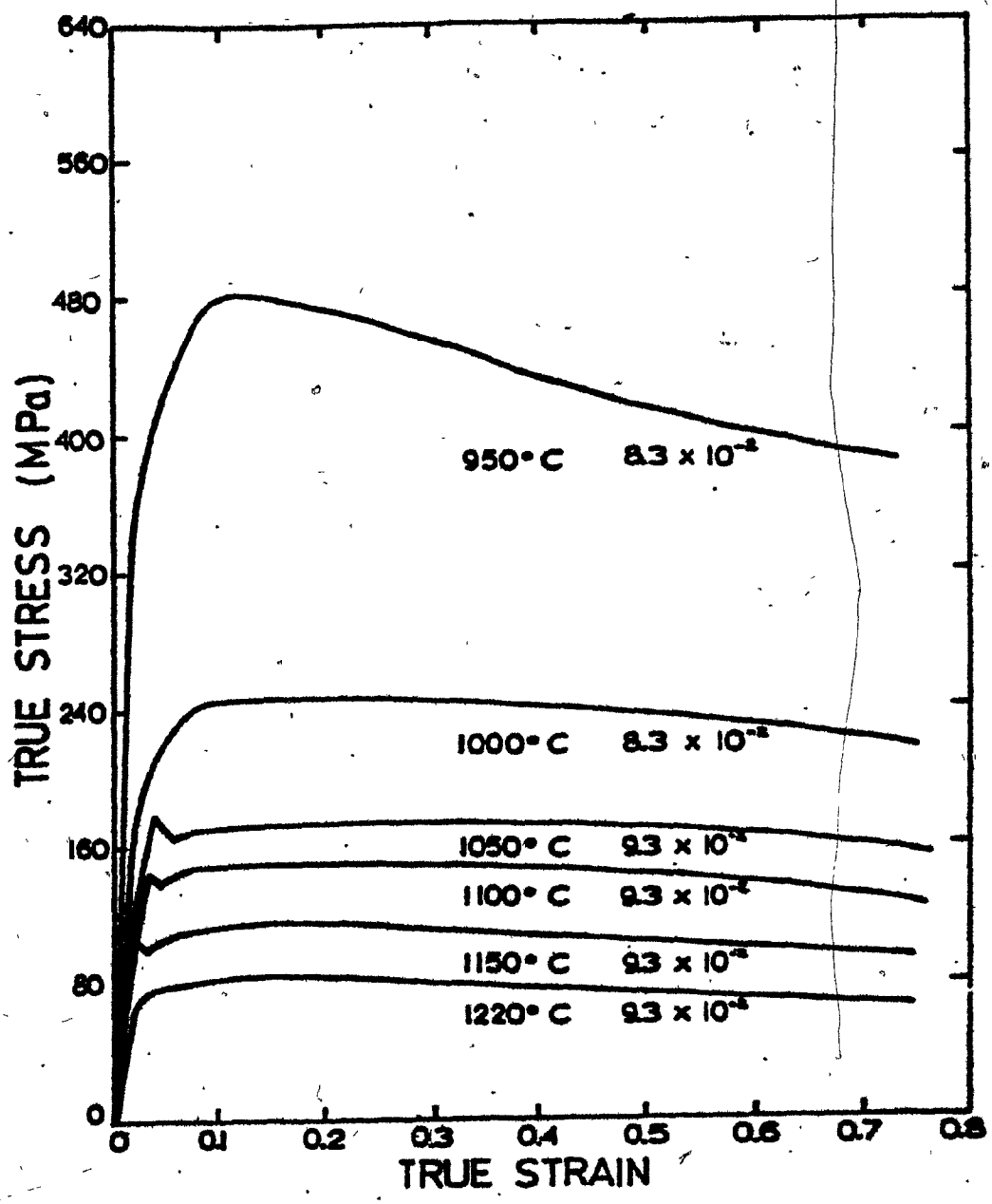

FIGURE 4.9 Temperature dependence of the flow curve in Waspaloy; strain rates: $9.3 \times 10^{-2} s^{-1}$ and $8.3 \times 10^{-2} s^{-1}$.

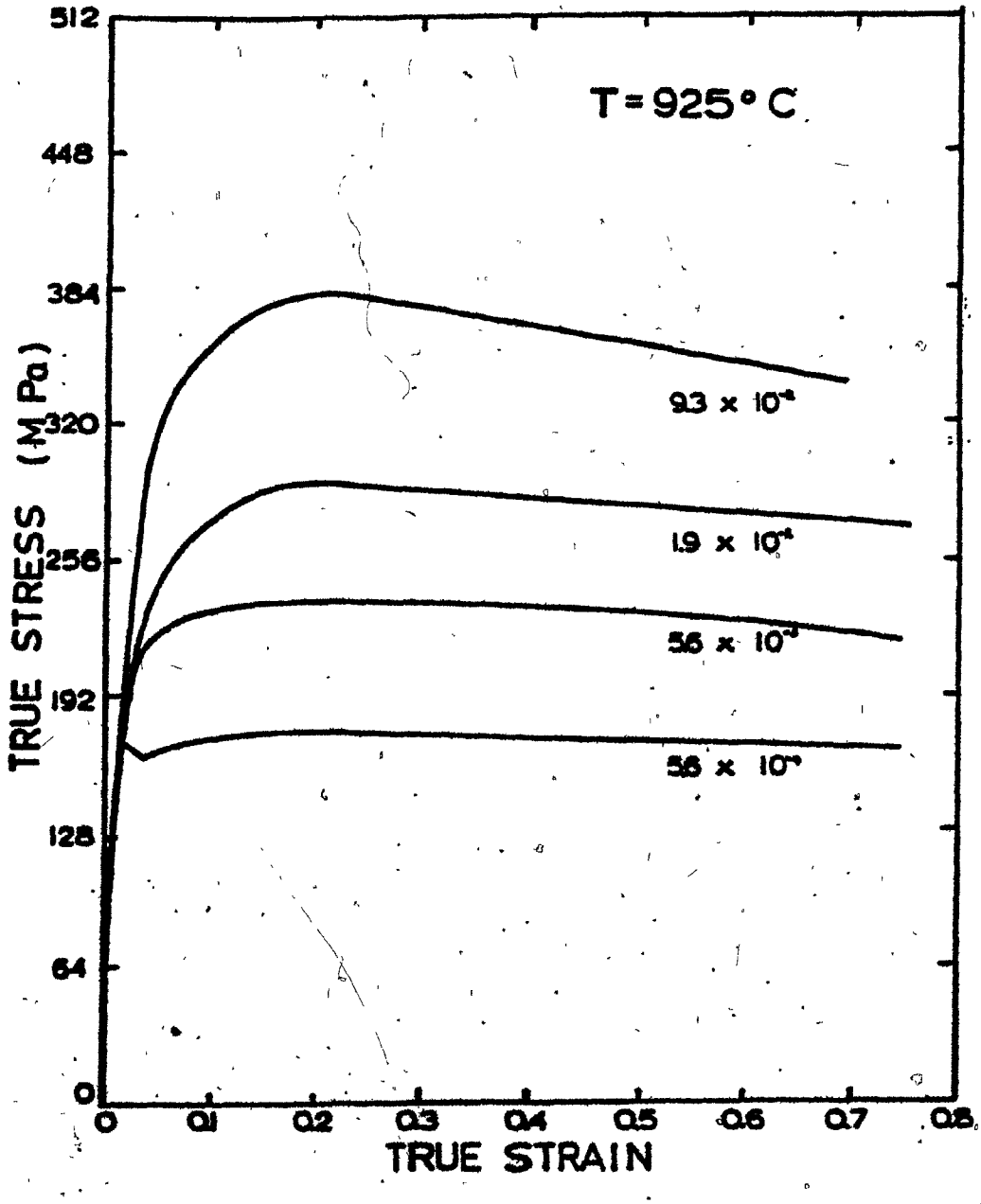

FIGURE 4.10 Strain rate dependence of the flow curve in Inconel 718 tested at 925°C.

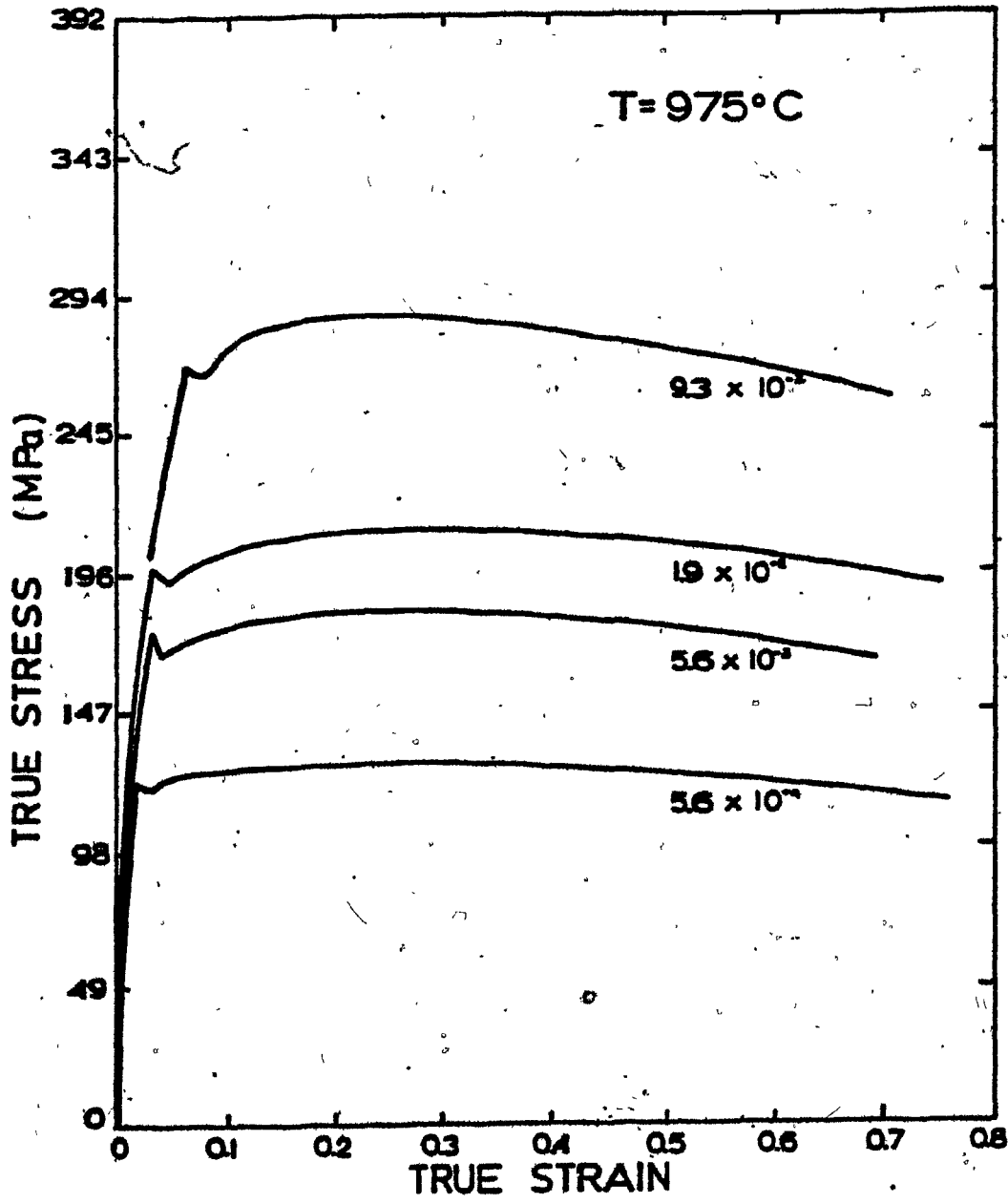

FIGURE 4.11 Strain rate dependence of the flow curve in Inconel 718 tested at 975°C.

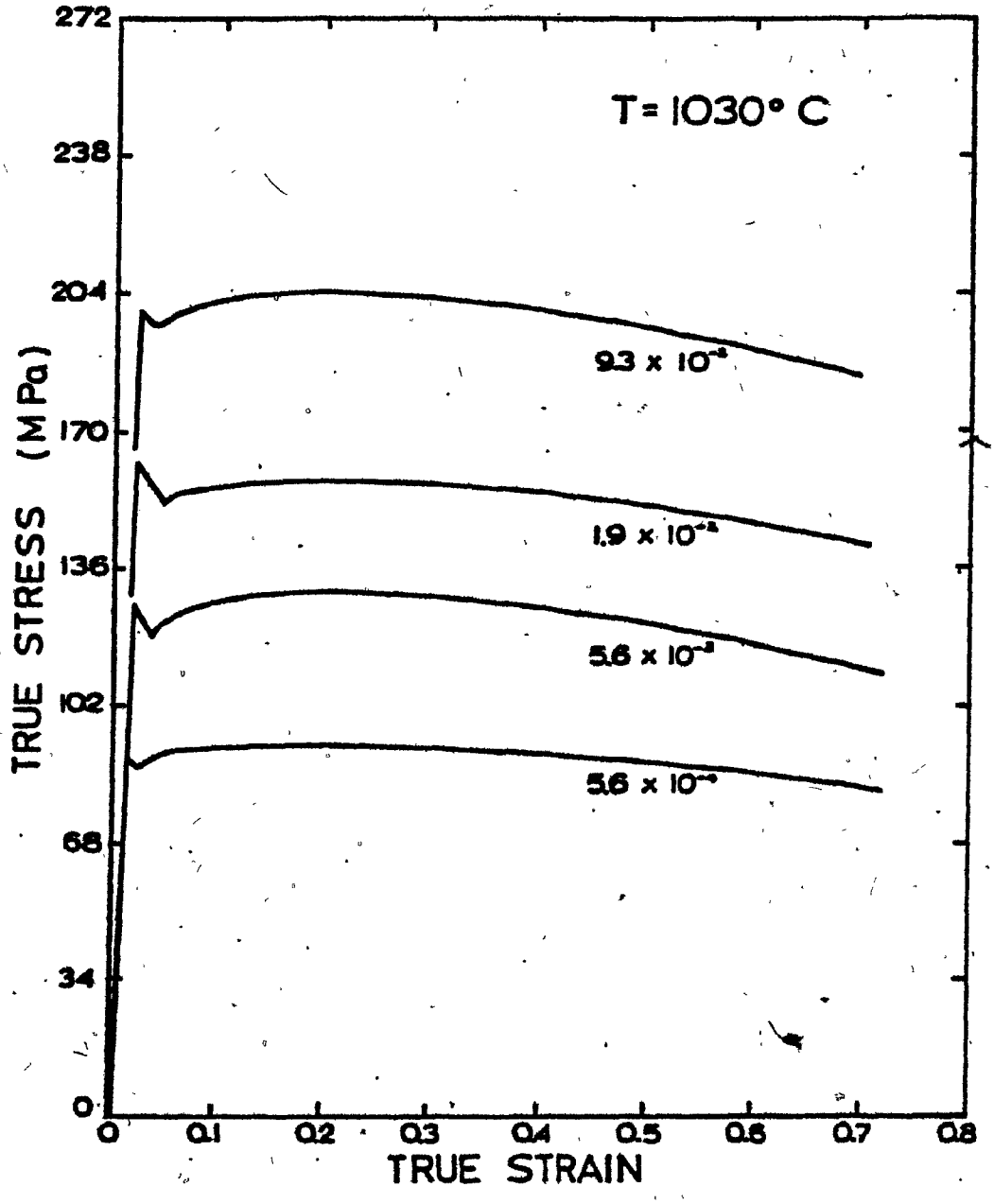

FIGURE 4.12 Strain rate dependence of the flow curve in Inconel 718 tested at 1030°C.

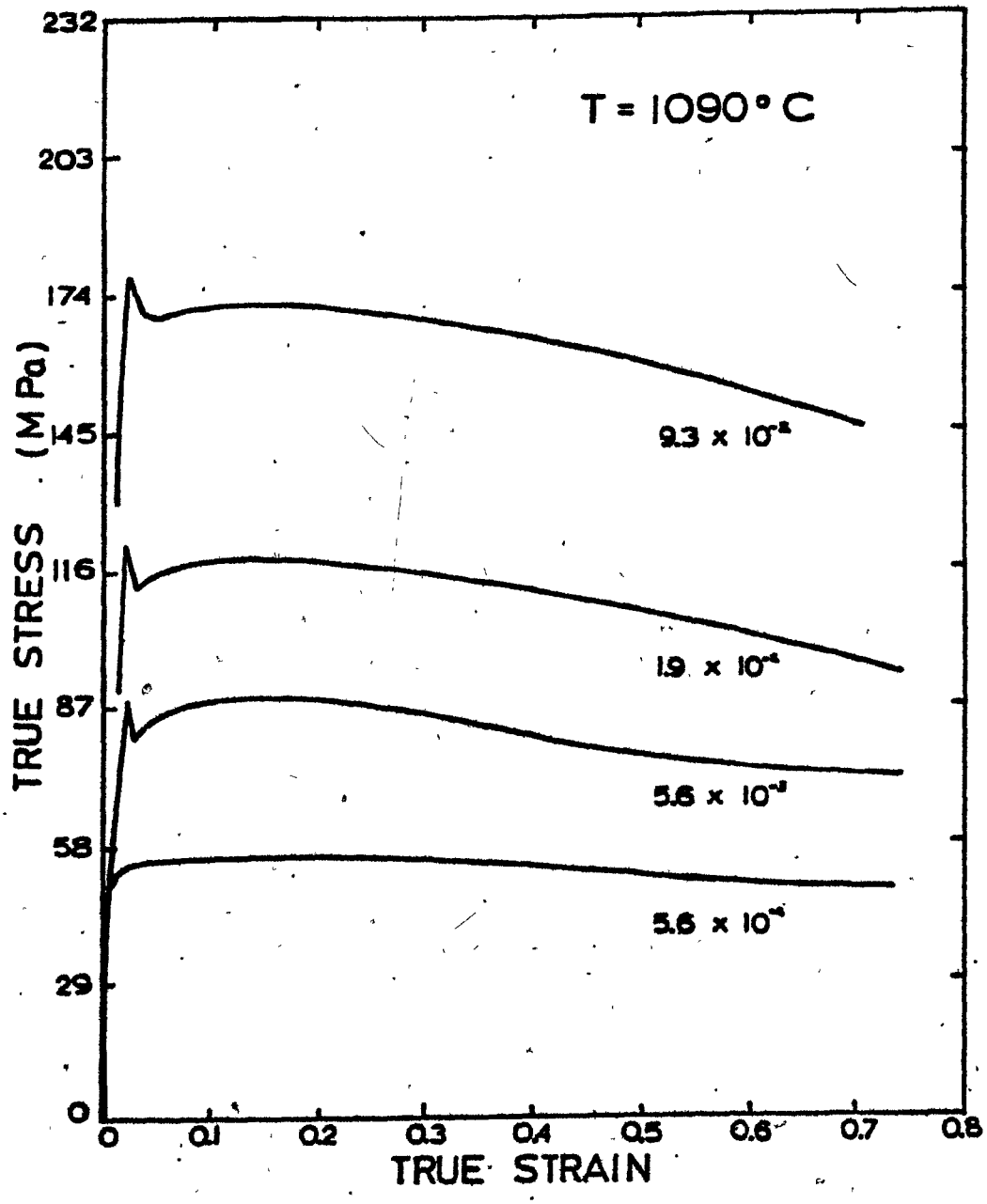

FIGURE 4.13 Strain rate dependence of the flow curve in Inconel 718 tested at 1090°C.

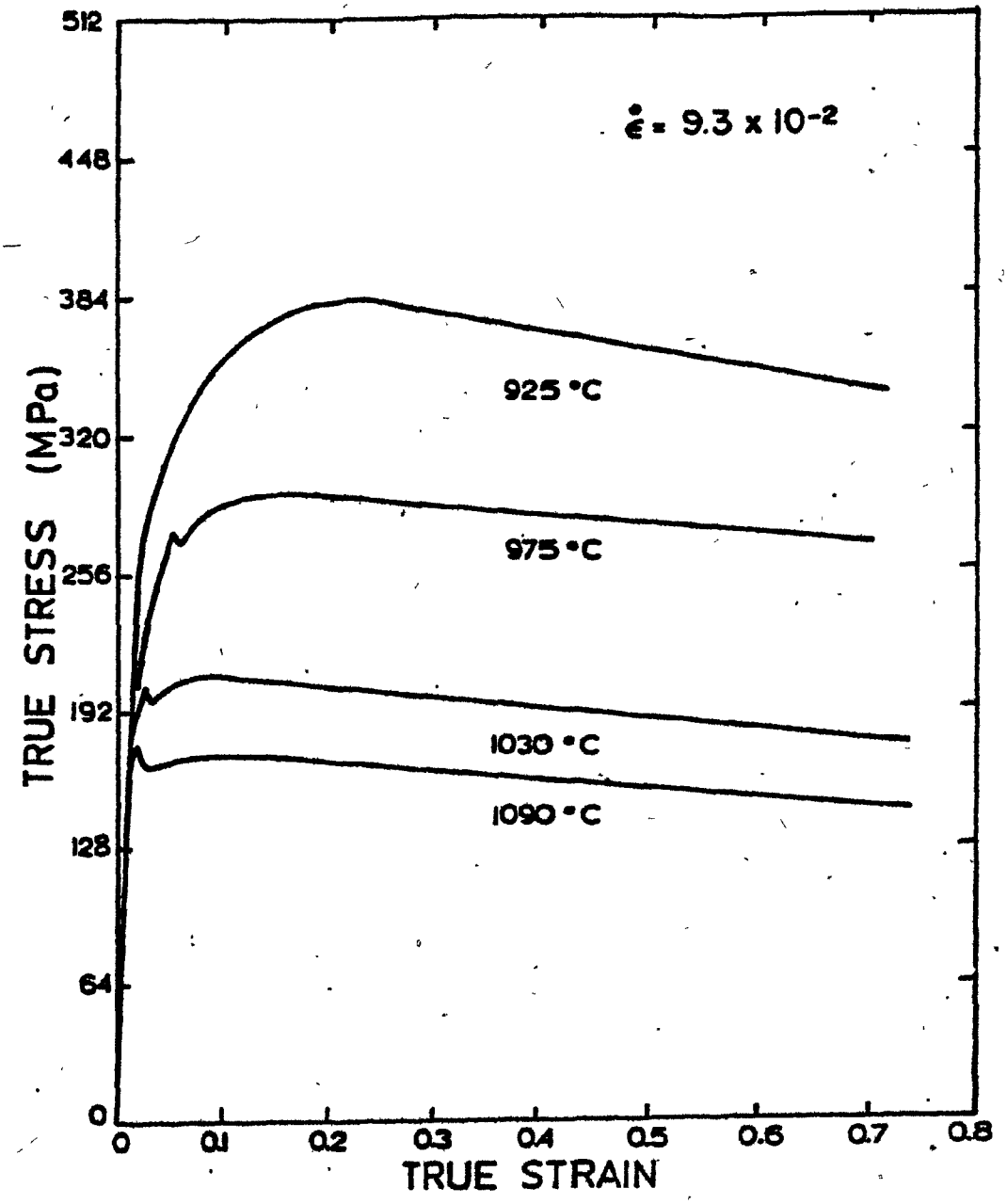

FIGURE 4.14 Temperature dependence of the flow curve in Inconel 718. Strain rate $9.3 \times 10^{-2} s^{-1}$.

for the steady state to be reached. The work of Fulop (64), on Waspaloy, is in agreement with the observations made so far; under conditions similar to those used in this work, Fulop achieved steady state flow only at an equivalent strain of 1.2. The flow softening observed at low temperatures is believed to be due to adiabatic heating and will be discussed later. For Waspaloy, when the solution heat treatment temperature was decreased from 1200 to 1150°C (Figs. 4.3 and 4.6), the flow stresses at a given test temperature remained unchanged, but a small yield drop appeared at 1100°C (i.e., above the γ' solution temperature). By contrast, in the test below the solution heat treatment temperature (Fig. 4.3), no yield drop is apparent. Yield drops also appeared while testing Waspaloy from 1050 to 1150°C at $9.3 \times 10^{-2} s^{-1}$, and while testing Inconel 718 from 925 to 1220°C. These yield drops will be discussed in greater detail below.

From the features exhibited by the curves, the determination of the kinds of softening mechanisms operating during deformation is not straightforward. Note that, for the conditions tested, no oscillations were observed on the curves at low strain rates. This would suggest that dynamic recrystallization was not occurring (56,64,65). We shall come back to this point after the presentation of the micrographs. In Figs. 4.15 and 4.16, the true stress/temperature curves for Waspaloy and Inconel 718, respectively, are shown. On the curves for Waspaloy, deviations are observed in the interval 1050 to 1150°C, i.e. just above the γ' solution temperature range. For Inconel

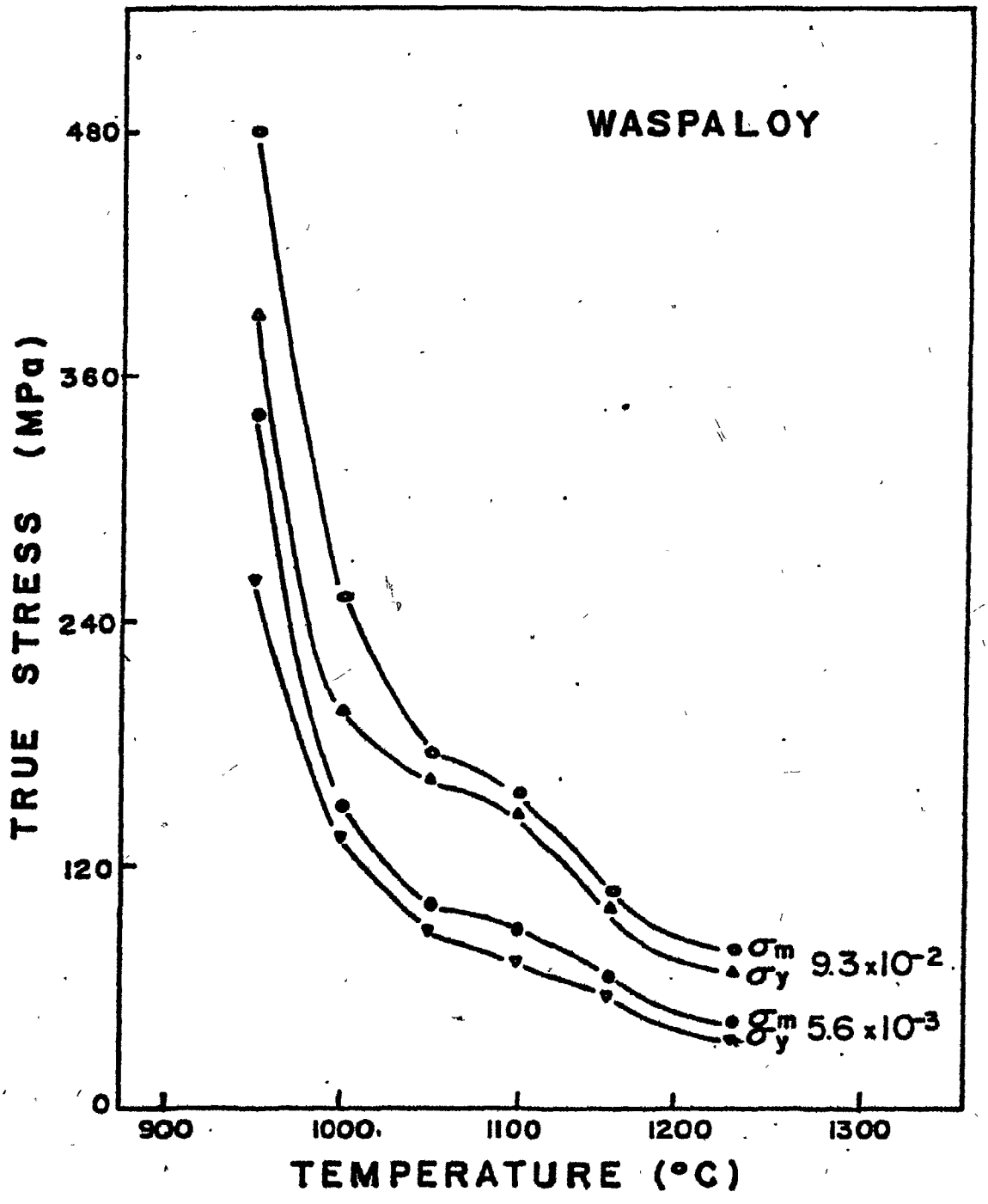

FIGURE 4.15 Temperature dependence of the flow stress in Waspaloy. Temperature range 950°C to 1220°C (σ_m – peak stress; σ_y – yield stress).

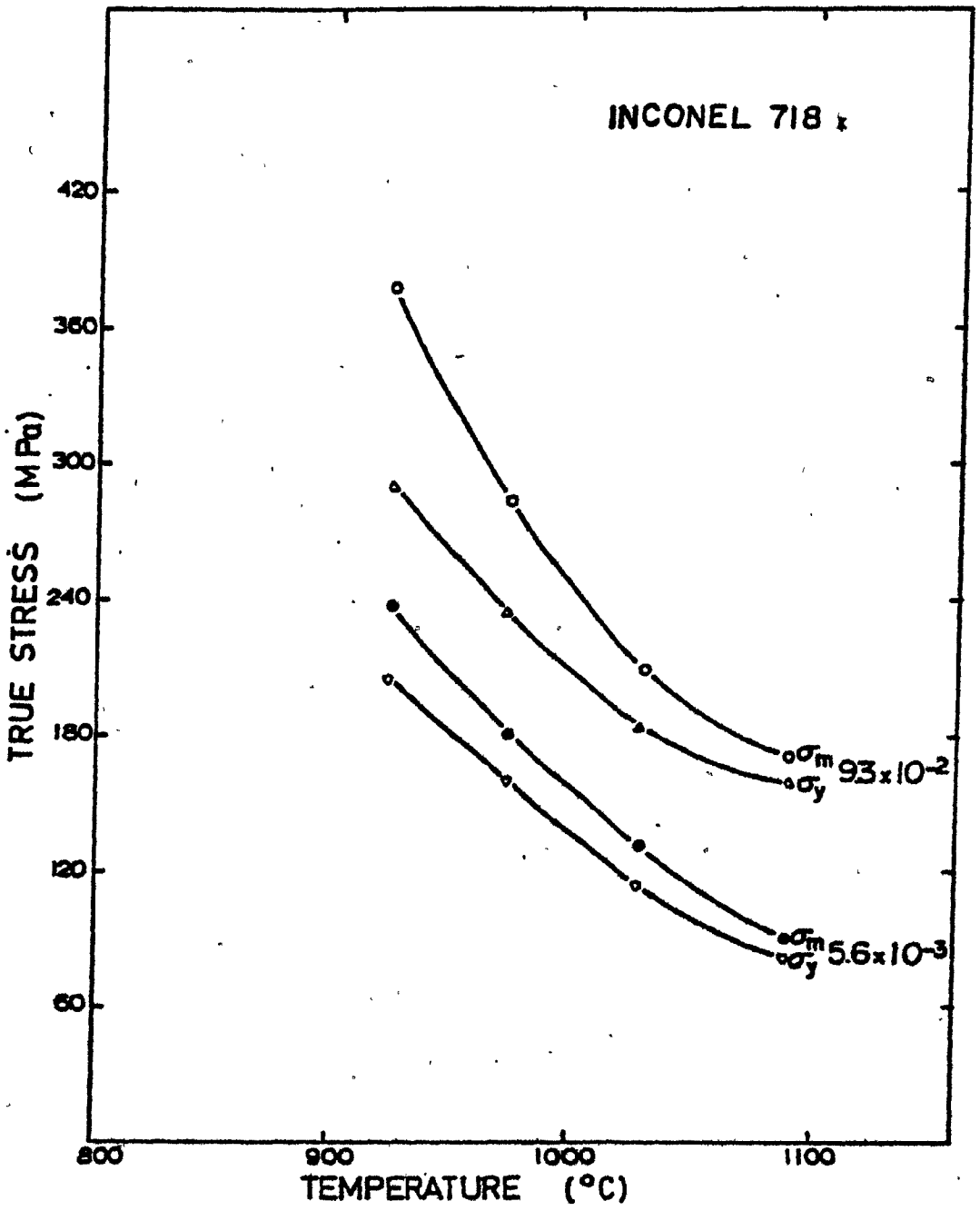

FIGURE 4.16 Temperature dependence of the flow stress in Inconel 718. Temperature range 925°C to 1090°C.

718 these 'bumps' were not detected. Instead a tendency towards increasing the difference $\sigma m - \sigma y$, i.e. the work hardening portion of the flow curves, with decreasing temperature is noted at a strain rate of $9.3 \times 10^{-2} s^{-1}$. This could be attributed to the fact that the yield drop is no longer present at the lower temperature, and therefore is unable to mask the work hardening behaviour.

4.3 The Interrupted Flow Curves

A technique developed by Petkovic et al. (53,85) for following the softening processes occurring between intervals of hot working, was employed to determine the softening processes that operate after the deformation of Waspaloy. The interruption strain was chosen to be before the peak stress, so that the material would be undergoing dynamic recovery only. This was done to facilitate the calculations and to increase the accuracy of the values for fractional softening. This is because, at the selected strain of 0.1, the difference between the flow stress immediately before unloading and the original yield stress is about as large as possible within the region in which dynamic recrystallization is not yet going on.*

---

*The critical strain ε_c for the start of dynamic recrystallization is said to be slightly less than the peak strain ε_p. According to Rossard (61), ε_c is given approximately by $^p\varepsilon_c = 0.83\ \varepsilon_p$. This is because, while the first nuclei are softening the material locally, the remaining material continues to get stronger, resulting in a positive slope for the flow stress curve.

After the interruption, the specimen was held at the test temperature for increasing times. After short holding times, the flow stress on reloading rises rapidly to a stress level comparable with the unloading stress (σ_m). After 180 s (1100°C) and 40 s (1150°C), yield drops began to be noticed on reloading. Increasing holding time beyond those times led to increasing yield drops, which later started to decrease. The occurrence of these yield points will be discussed in Chapter 5. After long holding times, the flow stress on reloading (σ_2) approaches that observed during the initial loading. This indicates that the work hardening introduced during initial straining is completely removed during the longer delays (Figs. 4.17-1100°C and 4.18-1150°C).

For the present purpose, the per cent softening (X) is defined as:

$$X = \frac{\sigma_m - \sigma_2}{\sigma_m - \sigma_1} \times 100 \qquad (4.1)$$

where σ_1 is the initial yield stress and σ_m and σ_2 are defined above. The fractional softening is plotted against the logarithm of the holding time in Figs. 4.19 and 4.20 for the conditions listed in Table 4.3. From these figures it can be seen that the softening is due to two different kinds of process (89): static recovery and static recrystallization. The plateau at approximately 40% softening has been attributed to static recovery (54,90). Recovery is seen to be complete after 30 s

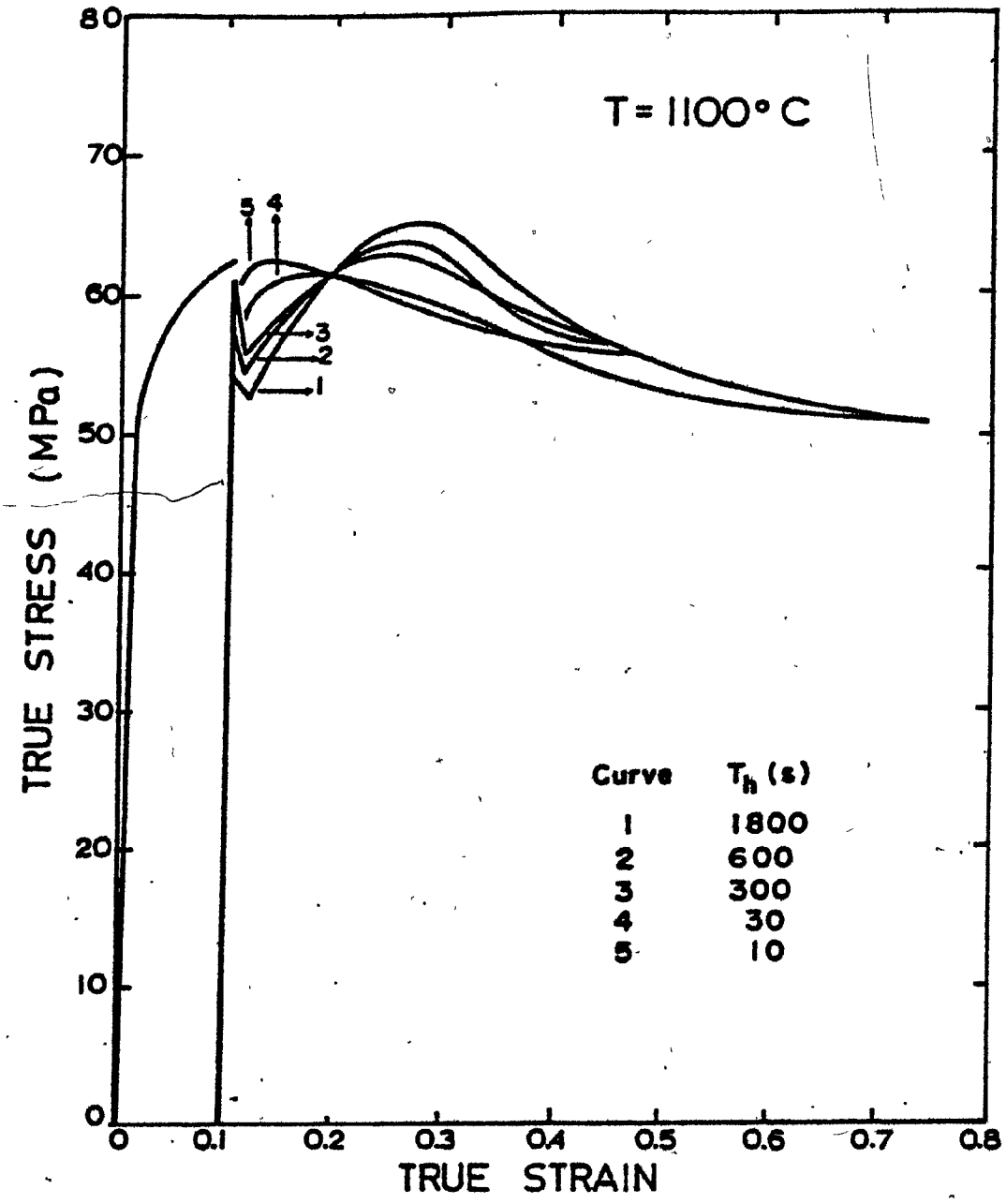

FIGURE 4.17 Flow curves for the interrupted tests in Waspaloy deformed at 1100°C. Strain rate $1.9 \times 10^{-3} s^{-1}$.

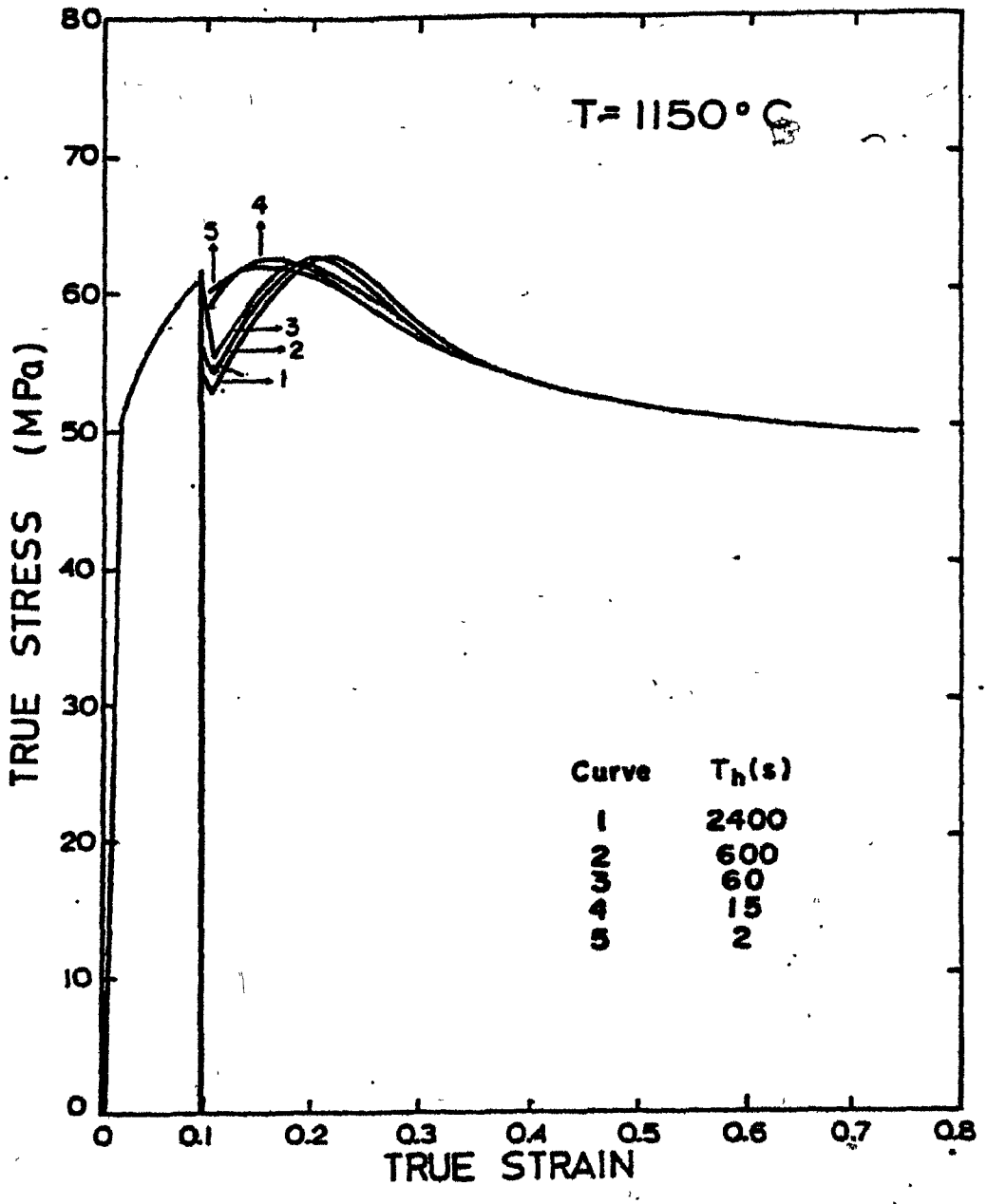

FIGURE 4.18 Flow curves for the interrupted tests in Waspaloy deformed at 1150°C. Strain rate $5.6 \times 10^{-3} s^{-1}$.

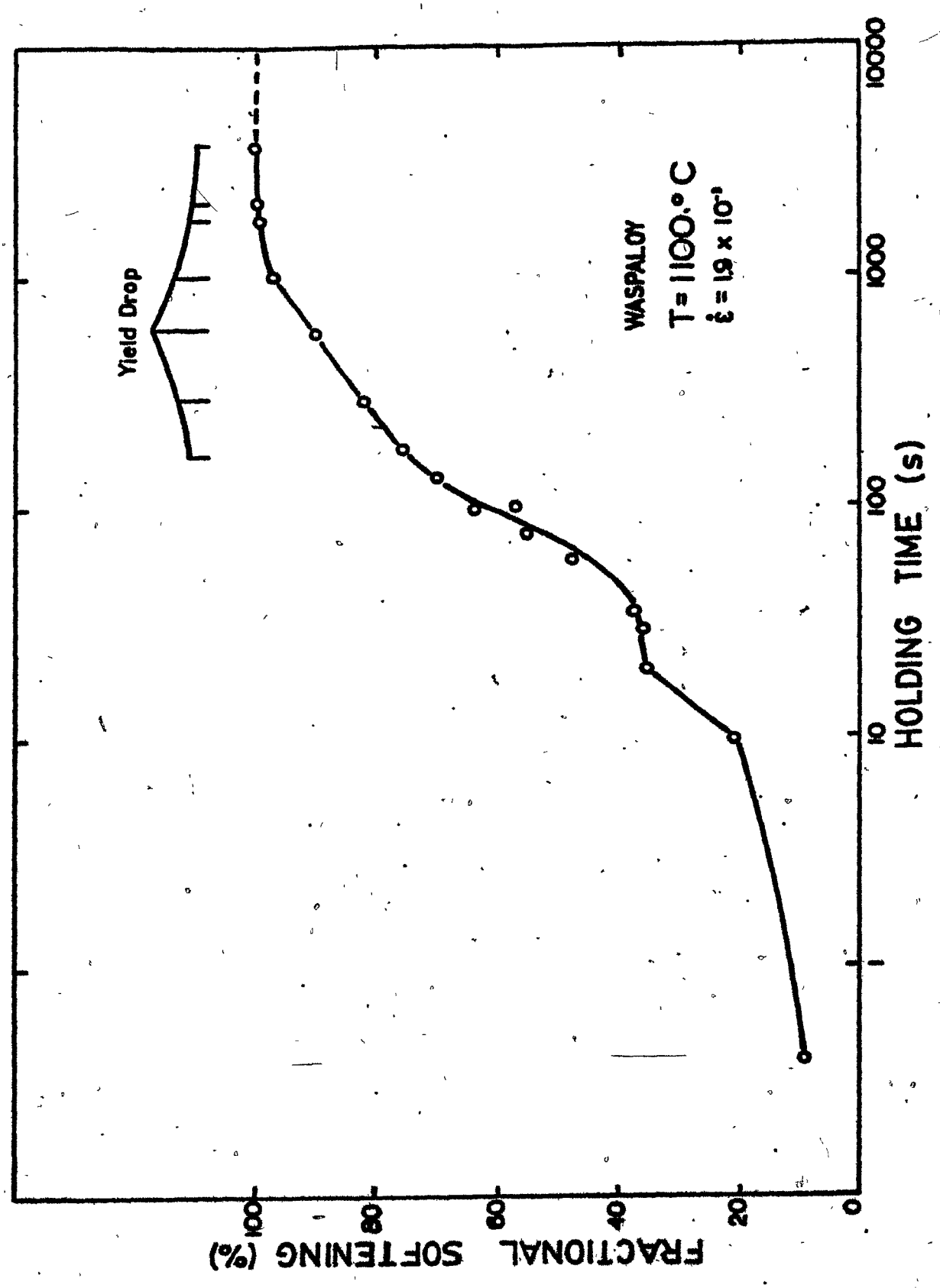

FIGURE 4.19 Effect of delay time on the softening behaviour of Waspaloy at 1100°C.

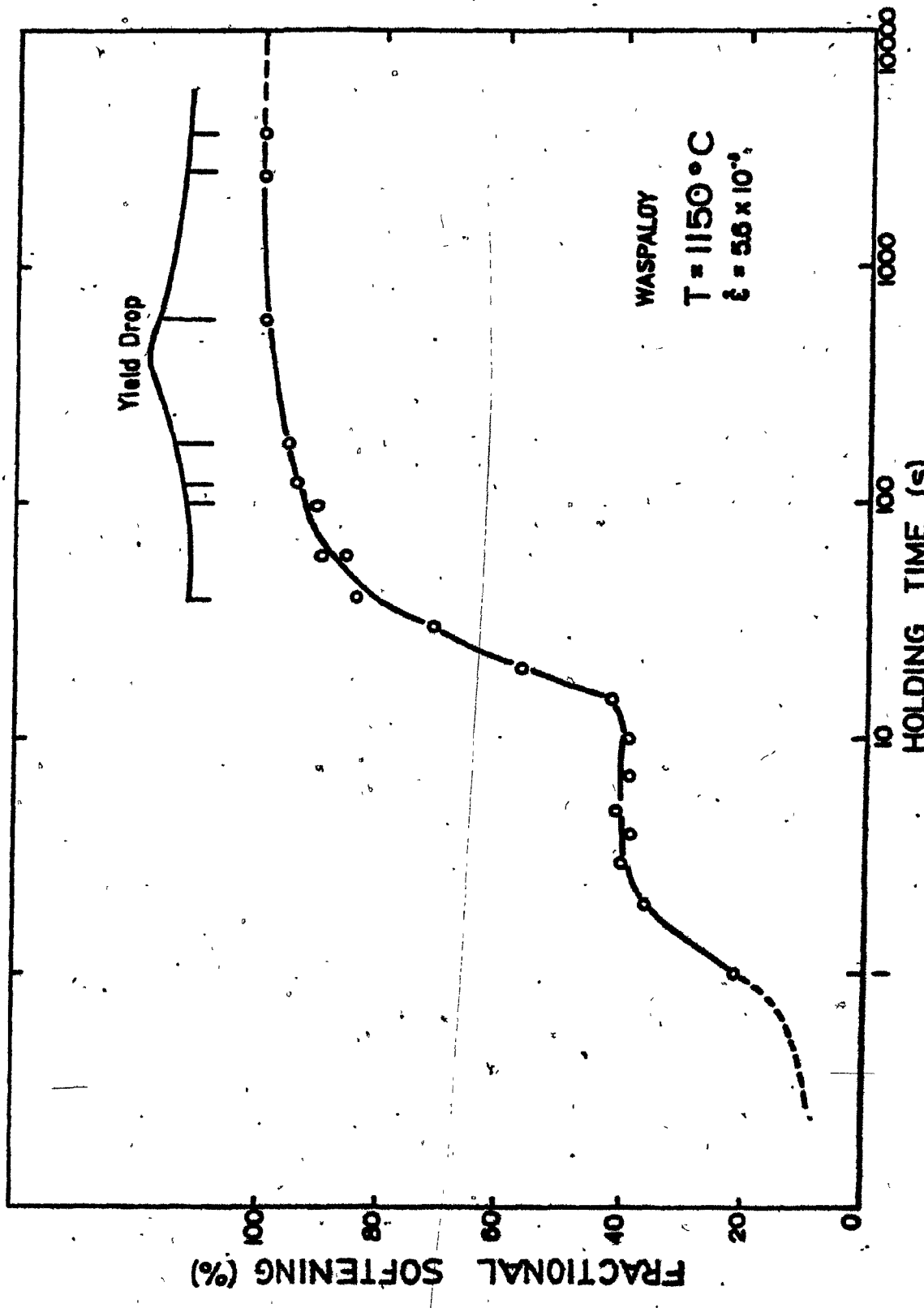

FIGURE 4.20 Effect of delay time on the softening behaviour of Waspaloy at 1150°C.

at 1100°C and after 4 s at 1150°C. By these times, 40% of the work hardening introduced during prestraining is removed. The length of the softening arrest or plateau is apparently temperature dependent, with the longer plateau evident at the higher temperature. The absolute time, however, i.e. the duration of the plateau in seconds, decreases with increasing temperature (35 s at 1100°C to 7 s at 1150°C); this is in agreement with the observations made by Petkovic (85), who attributed this fact to the higher activation energy associated with recrystallization than with recovery. The remainder of the softening can be ascribed to static recrystallization. The metallographic results to be described below will be seen to support this statement.

4.4 The Occurrence of the Yield Point in Inconel 718

As mentioned in Section 4.2, and illustrated in Figs. 4.1 to 4.14, yield drops occurred while testing Waspaloy in the temperature range 1050 to 1150°C and while testing Inconel 718 in the range 925°C to 1090°C (these temperatures extend from near the γ/γ' or γ/γ'' solvus temperature to 100-150°C above it). Because the yield points were observed over a wider range of strain rate and temperature for Inconel 718, and also because the material available was limited in the case of the Waspaloy, further studies on the appearance of yield drops were carried out only on Inconel 718.

For a constant strain rate, the relative magnitude of the yield drop initially increases and then decreases with increasing temperature. In a similar fashion, for a constant temperature, the magnitude of the yield drop initially increases and then decreases with increasing strain rate. The true existence of the yield drop should depend only on the annealing conditions and not on the testing conditions (i.e. strain rate). It is possible that the 'ordering' (or whatever the locking mechanism responsible for the yield drop) always occurs during annealing at, say 1090°C; but that its presence is not detected at certain strain rates. The reason is related to the elastic behaviour of the machine and sample as well as to the 'short transient' behaviour of the sample (91). This would explain the fact that at 1090°C, the yield drop was not detected for the strain rate of $5.6 \times 10^{-4} s^{-1}$. The apparent effect of testing temperature and strain rate on the appearance of the yield drop was just discussed above. A further effect (which is by contrast a real one) can be investigated by holding constant the temperature and strain rate of testing and by varying instead the holding time prior to testing. The magnitude of the yield drop is then measured and related to the annealing time. For this purpose, a variable called Relative Yield Drop (RYD) was defined as follows:

$$RYD = \frac{\sigma_U - \sigma_L}{\sigma_L} \times 100 \qquad (4.2)$$

Here σ_U is the upper yield and σ_L is the lower yield stress. The lower yield stress was taken as the point of intersection of the initial loading line with the back extrapolation of the work hardening curve after the yield drop. The RYD is plotted against the logarithm of holding time in Fig. 4.21 for the conditions listed in Table 4.4. It can be seen that the relative yield drop starts to increase, goes to a peak and then decreases with increasing annealing time. Furthermore, the time to the peak in RYD increases with decreasing temperature in the manner normally observed for thermally activated processes. At 1090°C and 1030°C, the RYD, after having decreased, starts to increase again, attaining a second peak before decreasing once more. The second peak is probably present at 975°C as well, but was not detected in the present experiments due to the very long times required to determine its presence.

For the 925°C temperature, the yield drop appeared only for the strain rate of $5.6 \times 10^{-4} s^{-1}$. At this temperature, yield drops can be expected to appear, according to Fig. 4.21 after a holding time of about 1000 s. The normal holding time employed prior to each continuous test is 15 minutes (see Section 3.4). For the test mentioned above (i.e. the one carried out at a strain rate of $5.6 \times 10^{-4} s^{-1}$), the data acquisition computer was not available at the planned time for the test to begin, which resulted in a delay of 2 minutes. This delay, along with the extra heating time introduced as a result of the slow strain rate being used, led to a holding time longer

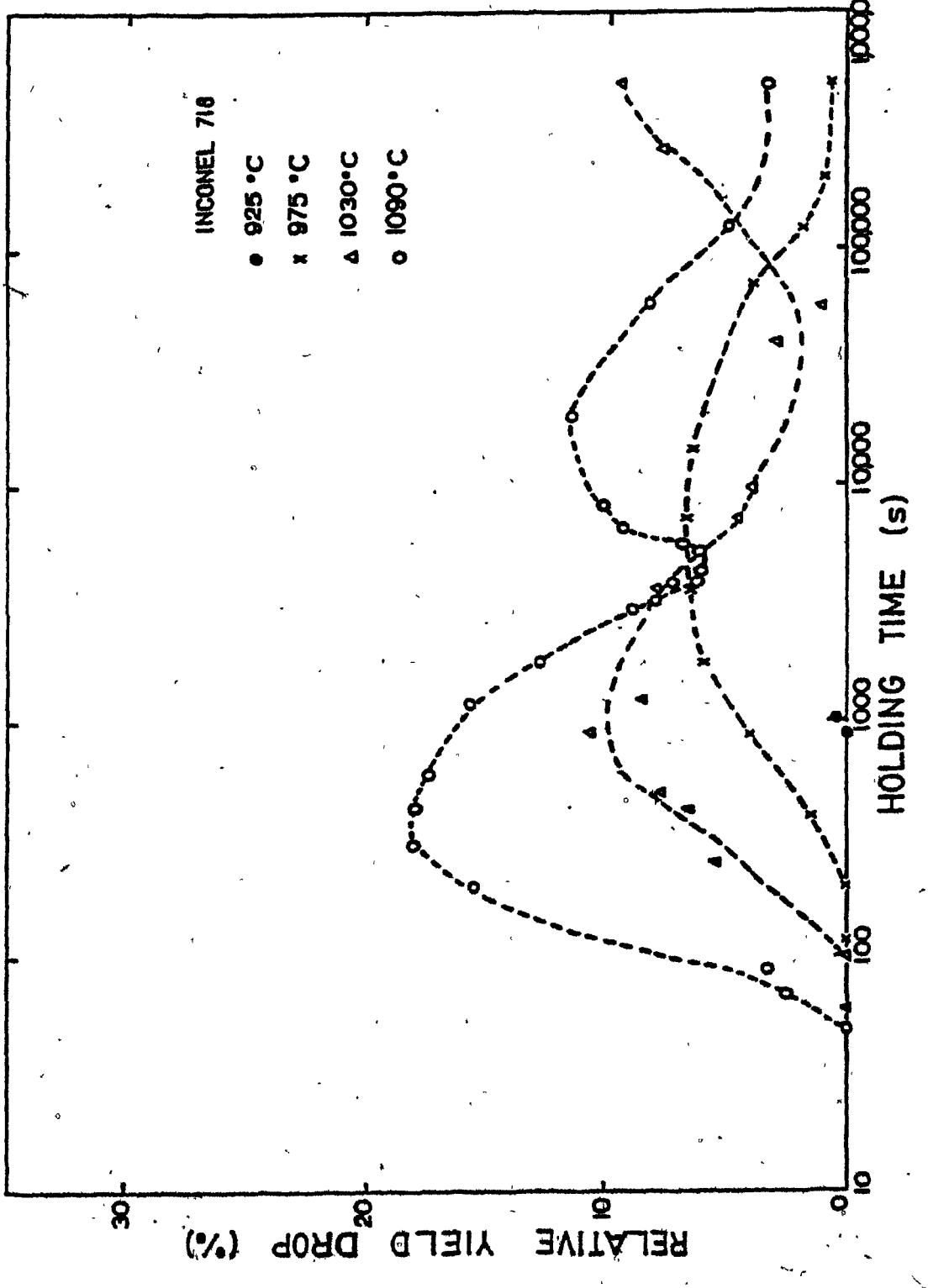

FIGURE 4.21 Dependence of the relative yield drop on annealing temperature and time for the Inconel 718.

by 150 s than the standard time of 900 s. This extra time may have provoked the appearance of the small yield drop noticeable in Fig. 4.10.

4.5 Influence of Annealing Time on the Working Behaviour of Waspaloy at 950°C

The purpose of this experiment was to investigate the influence of annealing time on the characteristics of the flow curves. Two strain rates were selected: $5.0 \times 10^{-4} s^{-1}$ and $3.8 \times 10^{-1} s^{-1}$, and the annealing time prior to testing was increased from 15 to 180 minutes. No significant changes in the flow curves were observed for the different annealing times. The specimens, prepared as specified in Table 4.5, were used to study metallographically the progress of the deformation.

4.6 Metallography

In order to investigate the change in structure with deformation, the test pieces were cut transversally for metallographic examination. The samples were ground on carborumdum papers and mechanically polished with 15,6 and 1 micron diamond paste. The specimens were then etched using Kalling's reagent* for Waspaloy and glyceregia** for the case of Inconel 718. The micrographs are presented in Figs. 4.22 to 4.42.

---

* Kalling's reagent - 2 g $CuCl_2$, 40 ml HCl, 60 ml methanol.

** Glyceregia - 15 ml HCl, 10 ml glycerol, 5 ml HNO_3.

4.6.1 Waspaloy

Fig. 4.22 shows the microstructure of Waspaloy after the standard solution heat treatment (30 minutes at 1200°C, furnace cool to test temperature, see Chapter 3). After this treatment, the ASTM grain size number was found to be 2.3 ($\bar{d}$ = 160 μm). The particles present in this sample, seen at a magnification of 75X in Fig. 4.22a, are probably MC carbides. The γ' can be seen at a magnification of 900X, as in Fig. 4.22b. Here the presence of γ' is hinted at by the textured appearance of the twin in the upper left hand corner of the micrograph.

Figs. 4.23 to 4.29 illustrate the microstructure of Waspaloy deformed at 950°C. In Fig. 4.23 and Fig. 4.24 is displayed a sequence of micrographs for increasing strains imposed at a strain rate of $5.0 \times 10^{-4} s^{-1}$ after annealing at testing temperatures for 15 minutes. At 0.4 strain, offsets at the grain boundaries at twin intersections can be observed. Some pores are also beginning to appear at triple points. At 0.7 strain, 'grain' boundary sliding is clearly evident along twin boundaries, and the pores at the triple points have grown bigger. The grain size appears to be increasing slightly, but this is probably due to the sectioning procedure, through which transverse specimen sections were examined. Similar observations apply to the samples deformed after 45 and 180 minutes of annealing time. With the aid solely of the optical microscope, it was not possible to detect any appreciable difference in the microstructures of the samples annealed for different periods. A more detailed

study including the use of a transmission electron microscope could clarify this point. When straining was carried out at $3.8 \times 10^{-1} s^{-1}$, the samples displayed the same features (Figs. 4.27 to 4.29), as those produced at a strain rate of $5.0 \times 10^{-4} s^{-1}$. Again the use of a transmission electron microscope would be required to detect any possible differences in the microstructures.

Figs. 4.30 to 4.32 illustrate the microstructures produced during deformation at 1000°C. As is evident from Fig. 4.30, dynamic recrystallization has begun by the time a strain of 0.4 is attained. At 0.7 strain, the proportion of these new dynamically recrystallized grains has increased, and the carbides which were present in the original grain boundaries can still be seen (Fig. 4.31) among the new small grains.

It is apparent from Figs. 4.33 to 4.36 that dynamic recrystallization is occurring. The mean grain size of the dynamically recrystallized grains determined from these micrographs is plotted against deformation temperature in Fig. 4.37, from which it is clear that the dynamically recrystallized grain size increases with working temperature. Above 1150°C, the structure is completely recrystallized dynamically, so that the grain size should not vary with increasing strain beyond 0.7 (i.e., once the steady state has been attained). This is in agreement with the flow curves presented in Section 4.2.

In Fig. 4.38, the micrographs are presented for the samples which were deformed 10%, and then held for 2100 s at

1100°C and 2400 s at 1150°C respectively. As can be seen, the samples are completely recrystallized to a new grain size, which confirms what was said in Section 4.3, i.e. that static recrystallization is the mechanism responsible for the second part of the softening curves (the part beyond 40% fractional softening). The statically recrystallized grain sizes are ASTM number 4.8 and 4.3 for the temperatures of 1100°C and 1150°C respectively.

4.6.2 Inconel 718

The micrographs for Inconel 718 after the standard solution heat treatment are presented in Fig. 4.39. In this case, the ASTM grain size was found to be number 2.7 ($\bar{d}$ = 140 μm). As already noted for Waspaloy, MC carbides can be observed at 75X (Fig. 4.39a) and γ" particles at 900X magnification. The latter are more clearly defined within the twins and are more readily observable than was γ' in the case of Waspaloy.

It is apparent from Figs. 4.40 to 4.42 that dynamic recrystallization begins at 975°C under the testing conditions employed and that at a strain of 0.7 at 1090°C, it is complete. These data can be compared with a minimum temperature of 1000°C for the initiation of dynamic recrystallization in Waspaloy, and a temperature and strain of 1220°C and 0.7 respectively for complete recrystallization.

The progress of dynamic recrystallization in Inconel 718 is seen to be retarded at 1030°C and 0.7 deformation (Fig. 4.41b) in comparison with Waspaloy at 1000°C and 0.7 strain (Fig. 4.31); that is, there is only partial dynamic recrystallization in the Inconel 718 as opposed to nearly complete recrystallization in the Waspaloy. This observation is in agreement with that of Cremisio and McQueen (66), who attributed the retardation of recrystallization to the pinning of the grain boundaries by precipitates. (In the present case, as the temperature is above the γ" solvus, the precipitates are likely to be carbides or possibly the inter-metallic Ni_3Cb.)

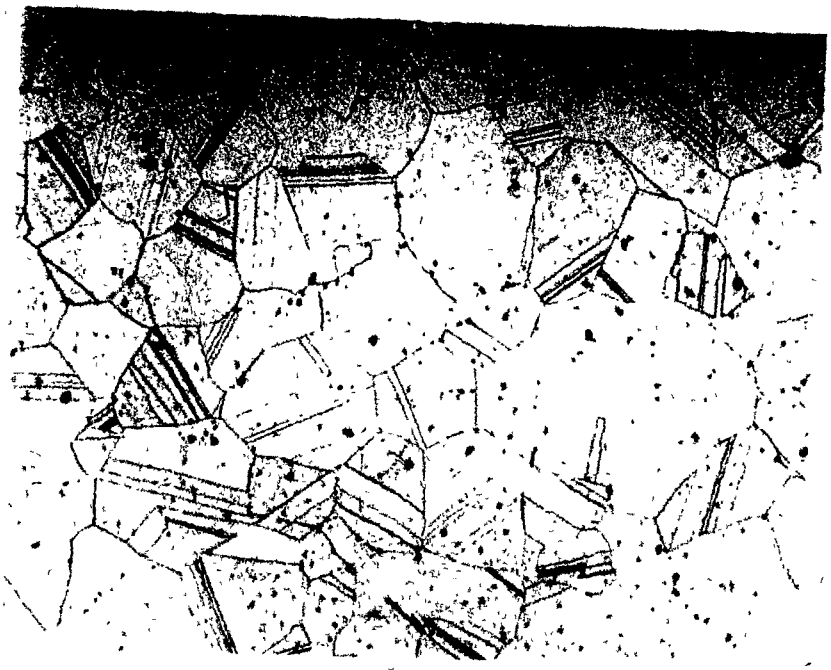

(a)

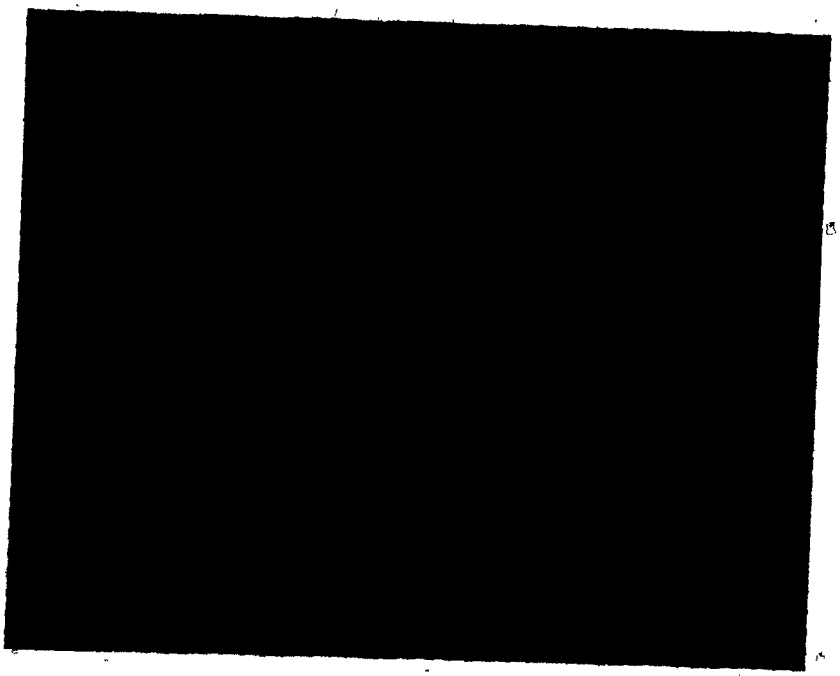

(b)

FIGURE 4.22 Microstructure of Waspaloy, aged at 1200°C for 30 minutes, quenched, no deformation. (a) X75; (b) X900.

(a)

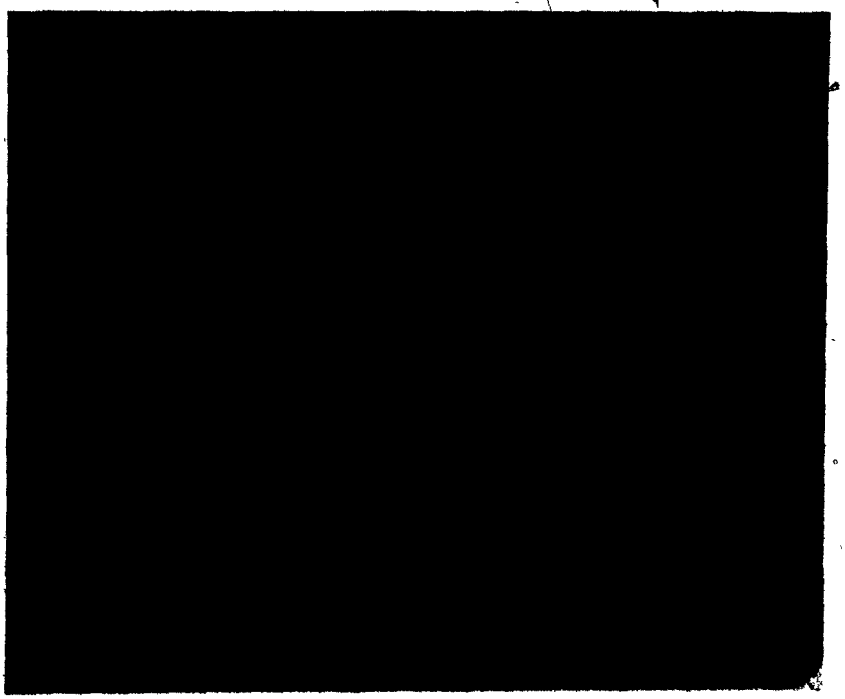

(b)

FIGURE 4.23 Microstructure of Waspaloy deformed at 950°C at $5.0 \times 10^{-4} s^{-1}$. Annealing time at 950°C, 15 minutes X75. (a) strain 0.07, (b) strain 0.2

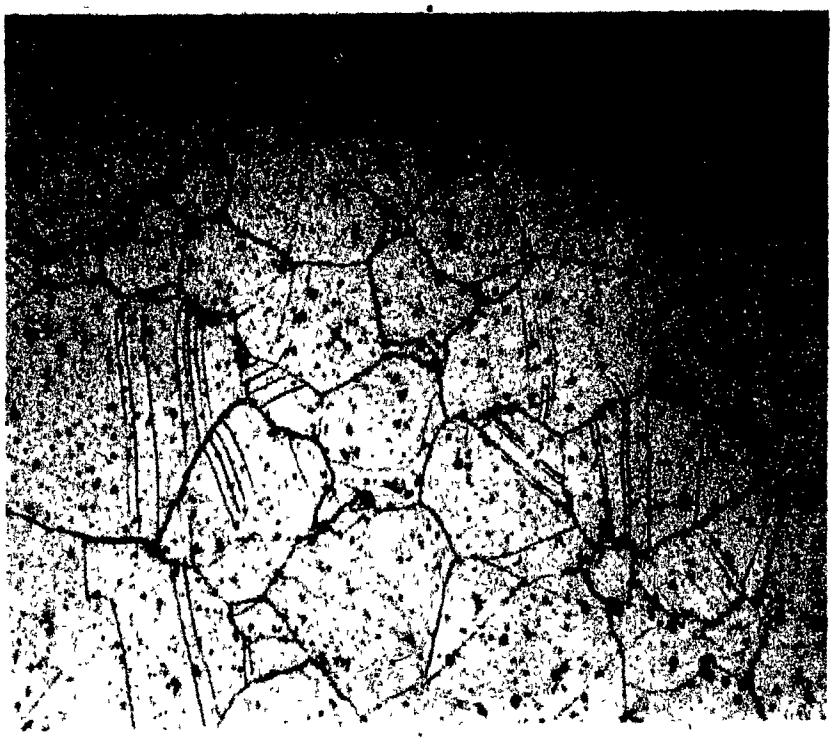

(a)

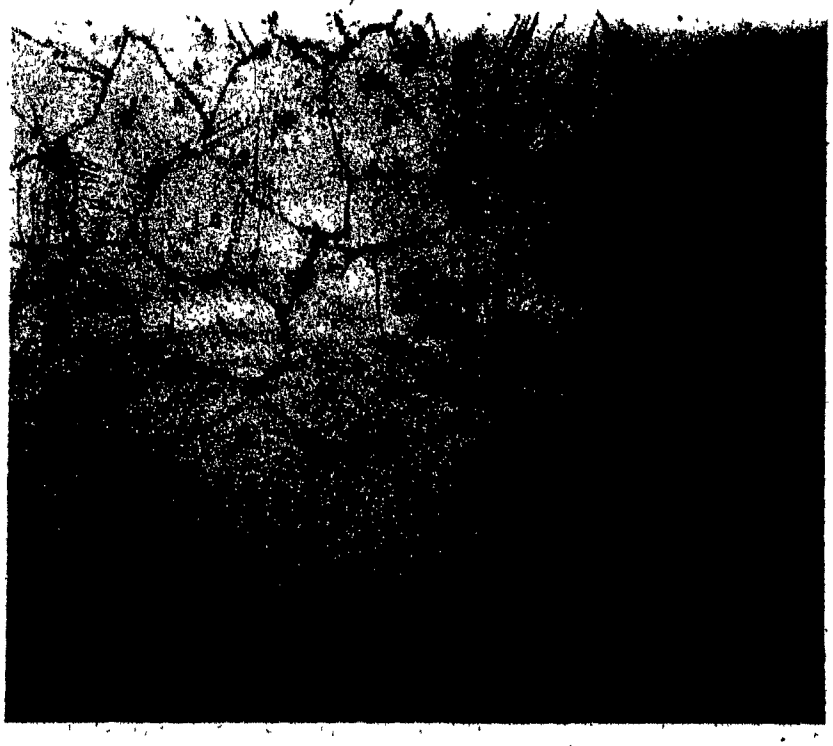

(b)

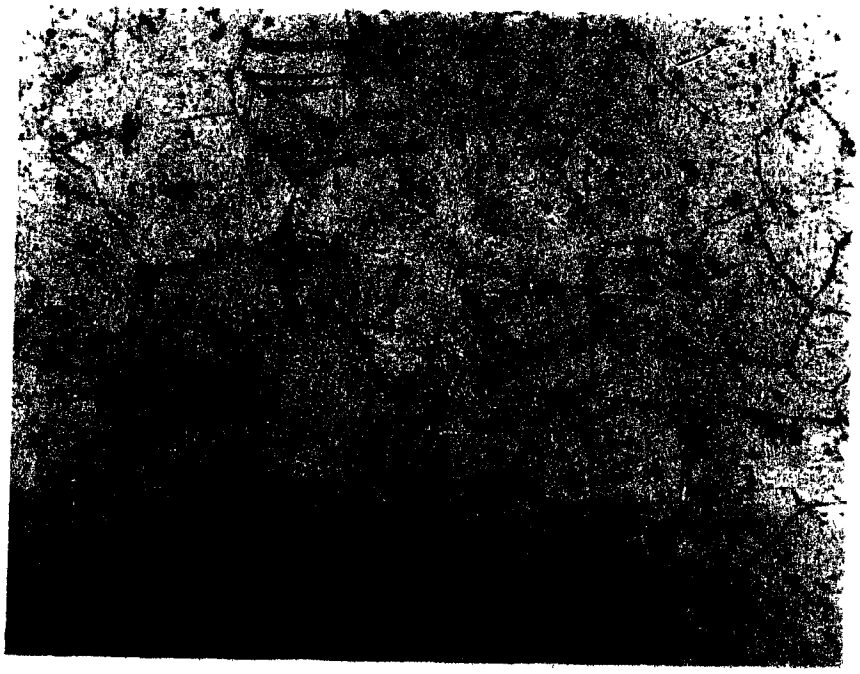

(a)

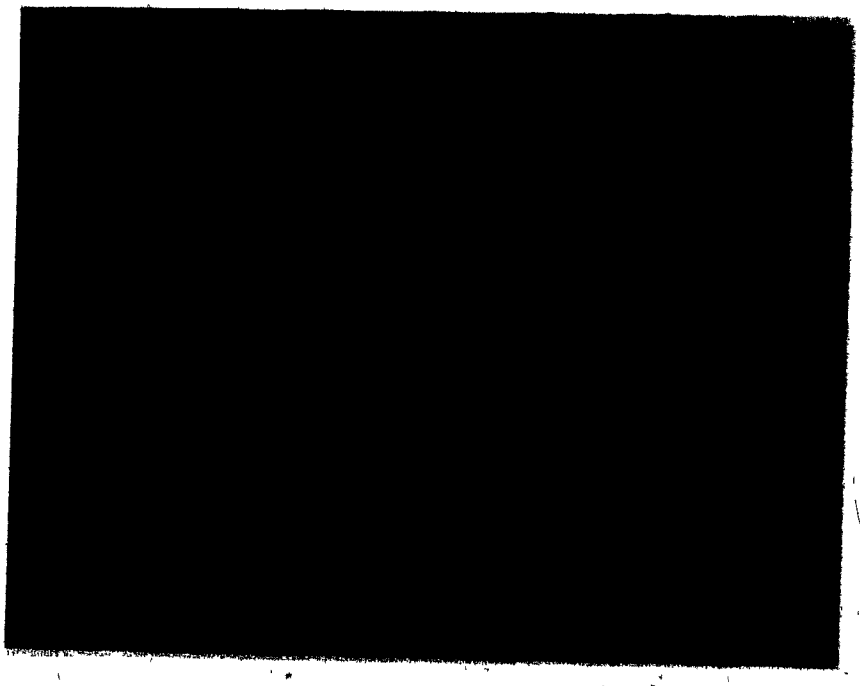

(b)

FIGURE 4.25 Microstructure of Waspaloy deformed at 950°C, at $5.0 \times 10^{-4} s^{-1}$. Annealing time at 950°C, 45 minutes. X75 (a) strain 0.3; (b) strain 0.7.

FIGURE 4.26 : Microstructure of Waspaloy deformed to a strain of 0.7 at 950°C and strain rate of $5.0 \times 10^{-4} s^{-1}$. Annealing time 180 minutes. X75

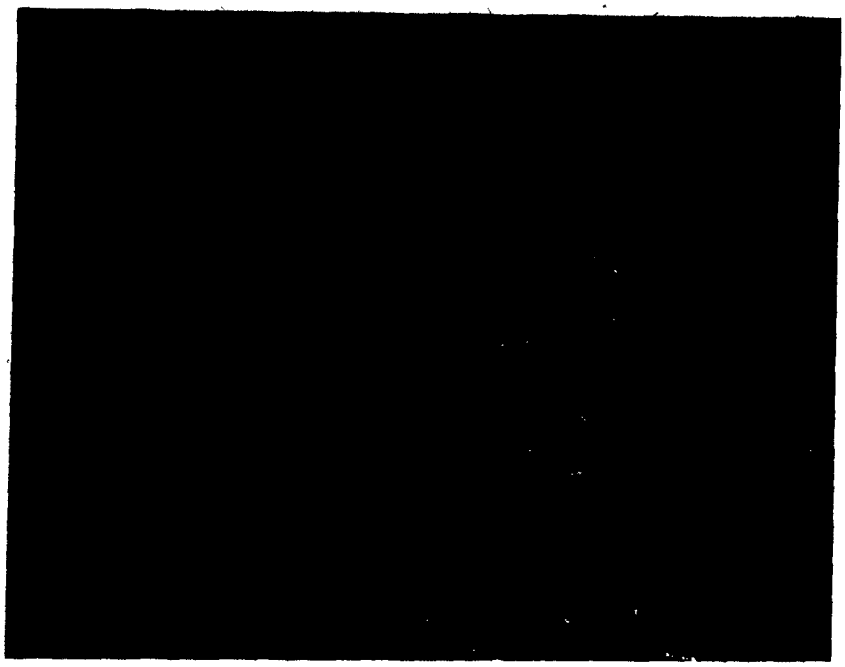

(a)

(b)

FIGURE 4.27 Microstructure of Waspaloy deformed at 950°C at $3.8 \times 10^{-1} s^{-1}$. Annealing time 15 minutes. X75 (a) strain 0.12; (b) strain 0.4

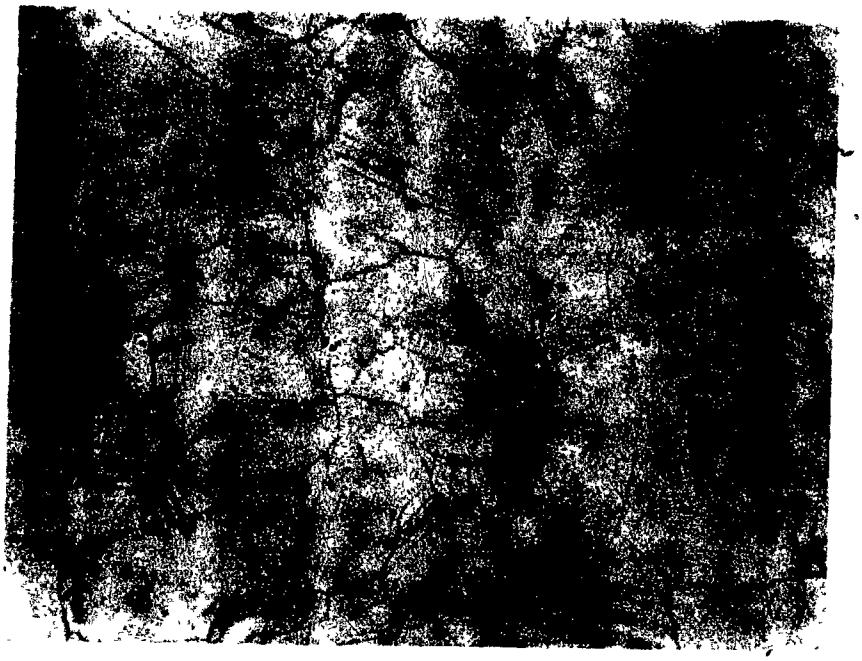

(a)

(b)

FIGURE 4.28 Microstructure of Waspaloy deformed at 950°C at $3.8 \times 10^{-1} s^{-1}$ X75. (a) strain of 0.7, annealing time 15 minutes; (b) strain of 0.3, annealing time 45 minutes.

(a)

(b)

FIGURE 4.29 Microstructure of Waspaloy deformed to a strain of 0.7 at 950°C and strain rate of $3.8 \times 10^{-1} s^{-1}$ X75. (a) annealing time 45 minutes; (b) annealing time 180 minutes.

(a)

(b)

FIGURE 4.30 Microstructure of Waspaloy deformed to a strain of 0.4 at 1000°C and strain rate of $5.0 \times 10^{-4} s^{-1}$ (a) X75; (b) X400.

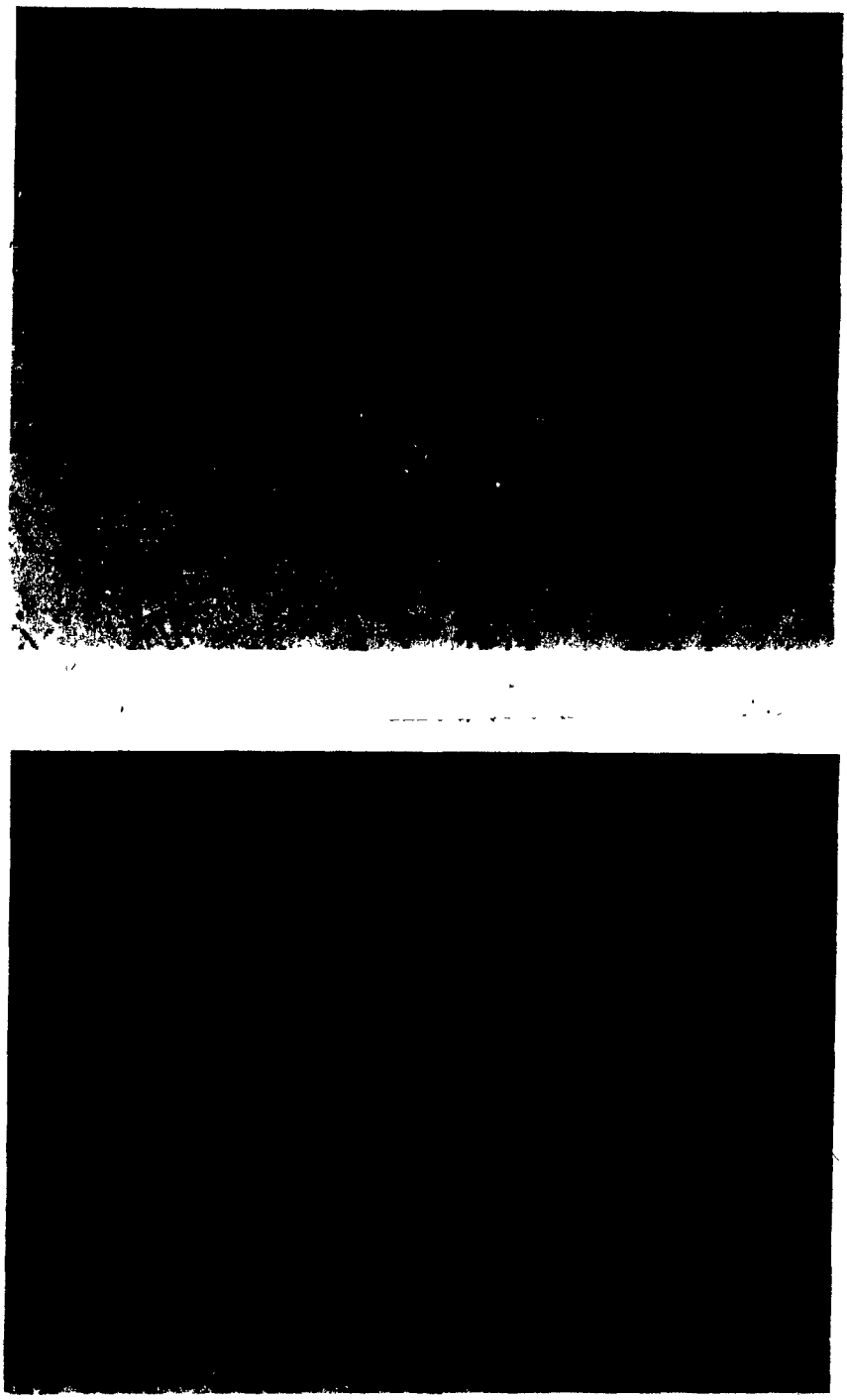

FIGURE 4.31 Two selected microstructures of Waspaloy deformed to a strain of 0.7 at 1000°C and a strain rate of $5.0 \times 10^{-4} s^{-1}$ X75.

(a)

(b)

FIGURE 4.32 Microstructure of Waspaloy deformed to a strain of 0.7 at 1000°C and strain rate of $9.3 \times 10^{-2} s^{-1}$ (a) X75; (b) X400.

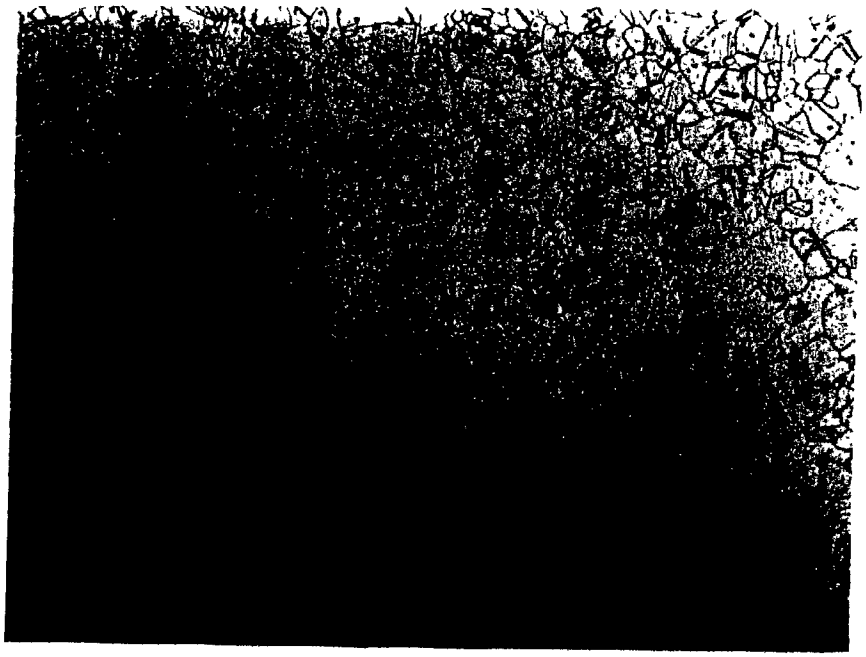

FIGURE 4.33 Microstructure of Waspaloy deformed to a strain of 0.7 at 1050°C and strain rate of $9.3 \times 10^{-2} s^{-1}$ X75.

FIGURE 4.34 Microstructure of Waspaloy deformed to a strain of 0.7 at 1100°C and strain rate of $1.9 \times 10^{-3} s^{-1}$ X75.

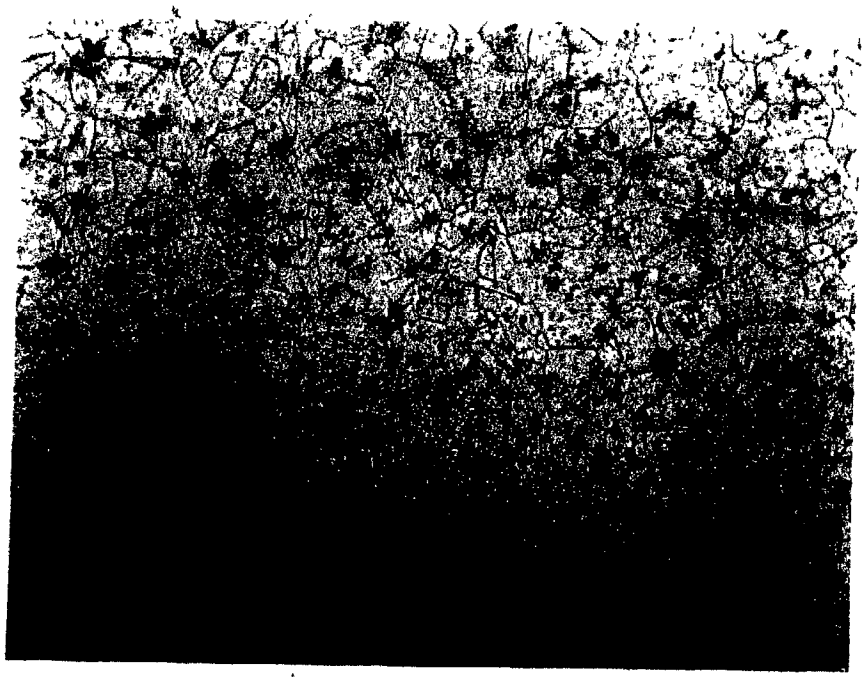

FIGURE 4.35 Microstructure of Waspaloy deformed to a strain of 0.7 at 1150°C and strain rate of $9.3 \times 10^{-2} s^{-1}$ X75.

FIGURE 4.36 Microstructure of Waspaloy deformed to a strain of 0.7 at 1220°C and strain rate of $5.6 \times 10^{-3} s^{-1}$ X75.

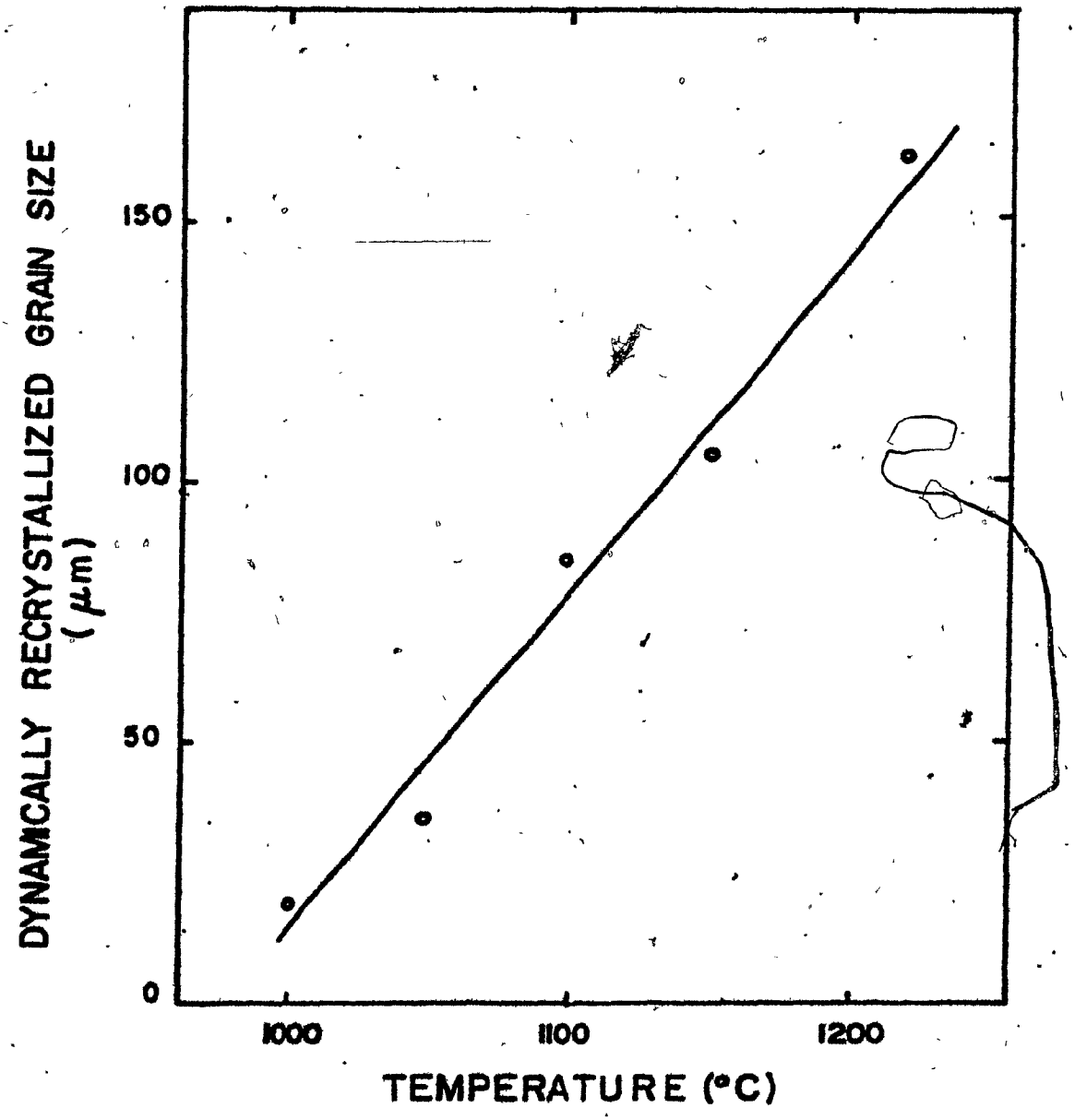

FIGURE 4.37 Dependence of the dynamically recrystallized grain size on the temperature of deformation for Waspaloy.

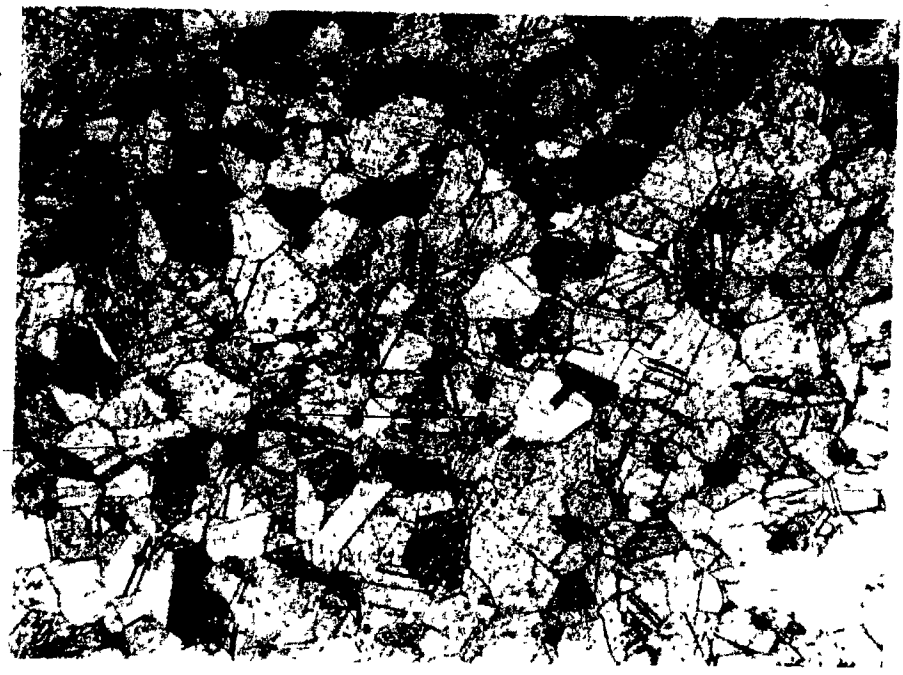

(a)

(b)

FIGURE 4.38 Microstructure of Waspaloy deformed to a strain of 0.1 [illegible]. (a) Deformed at 1100°C at $1.9 \times 10^{-3} s^{-1}$, quenched after holding for 2100 s; (b) deformed at 1150°C at $5.6 \times 10^{-3} s^{-1}$, quenched after holding for 2400 s.

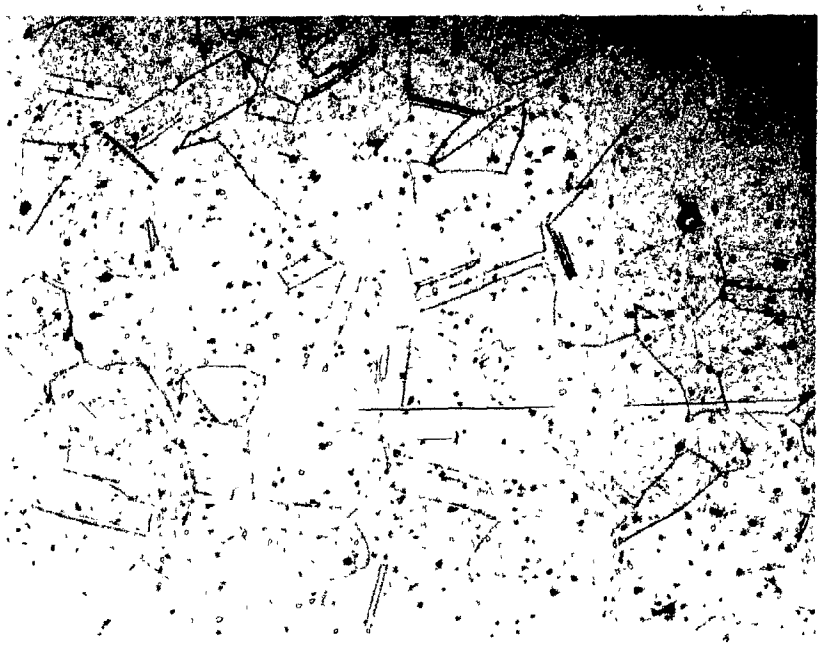

(a)

(b)

FIGURE 4.39 Microstructure of Inconel 718, aged at 1120°C for 30 minutes, quenched, no deformation. (a) X75; (b) X900.

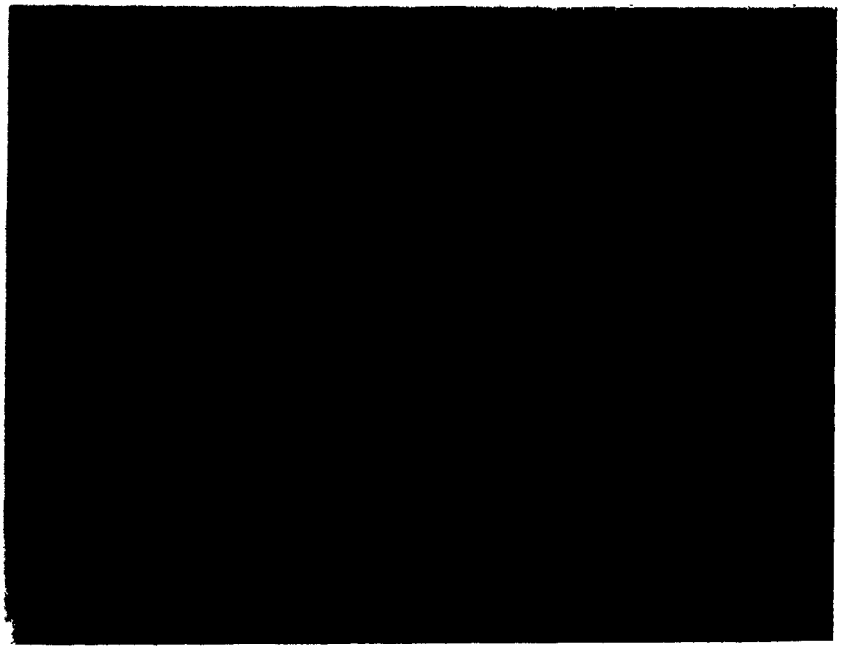

(a)

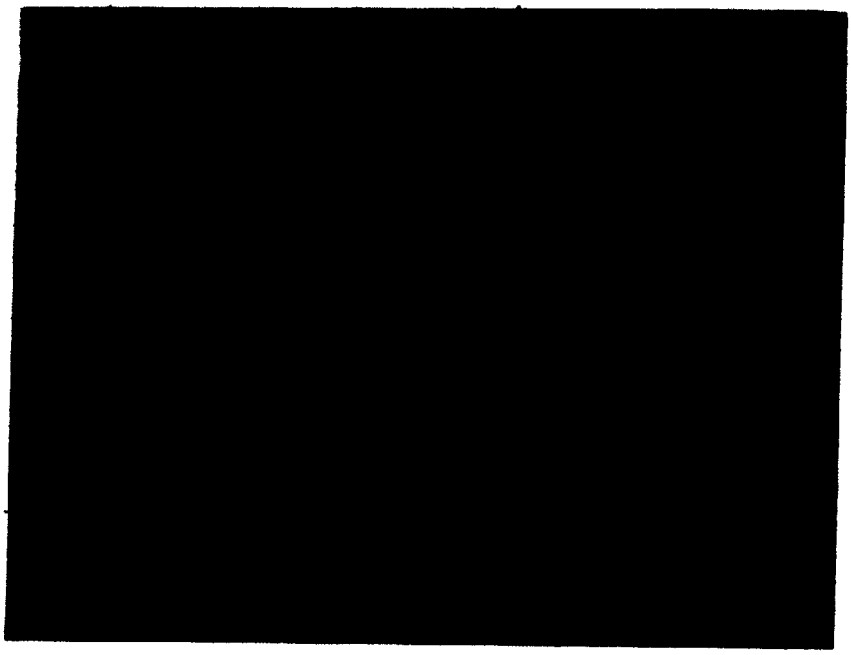

(b)

FIGURE 4.40 Microstructure of Inconel 718 deformed to a strain of 0.7 at $5.6 \times 10^{-3} s^{-1}$ X75. (a) 925°C; (b) 975°C.

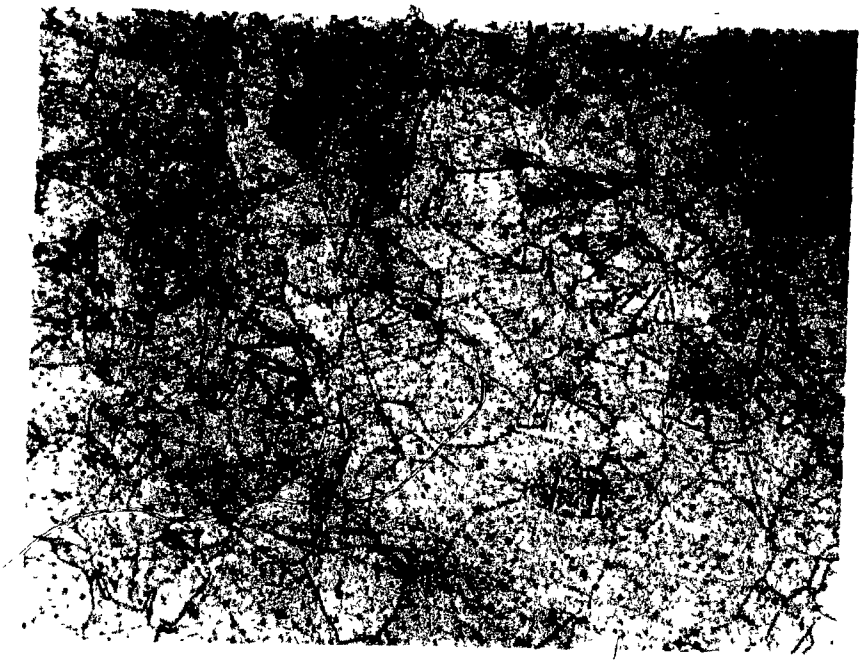

(a)

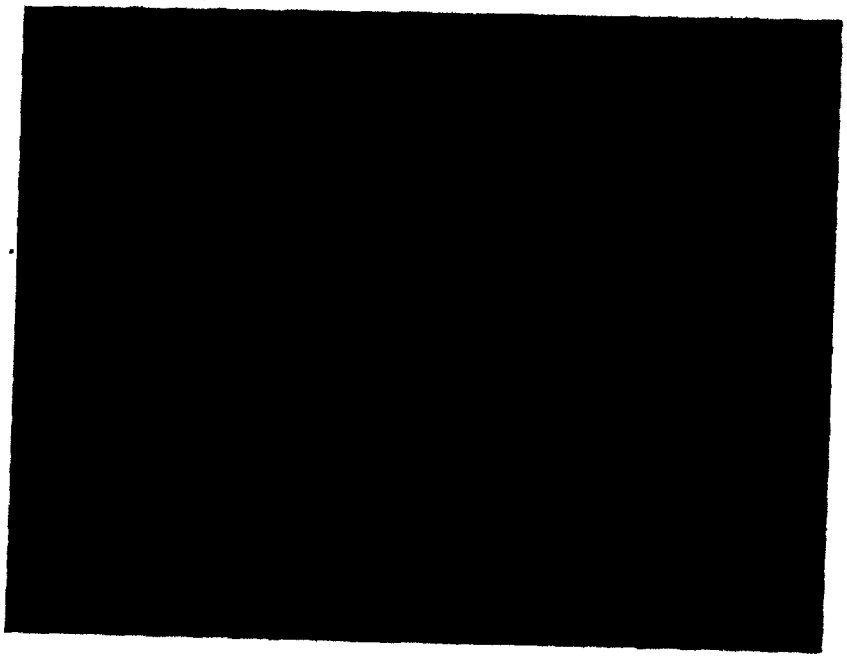

(b)

FIGURE 4.41 Microstructure of Inconel 718 deformed at 1030°C at $5.6 \times 10^{-3} s^{-1}$ X75. (a) strain 0.08; (b) strain 0.7.

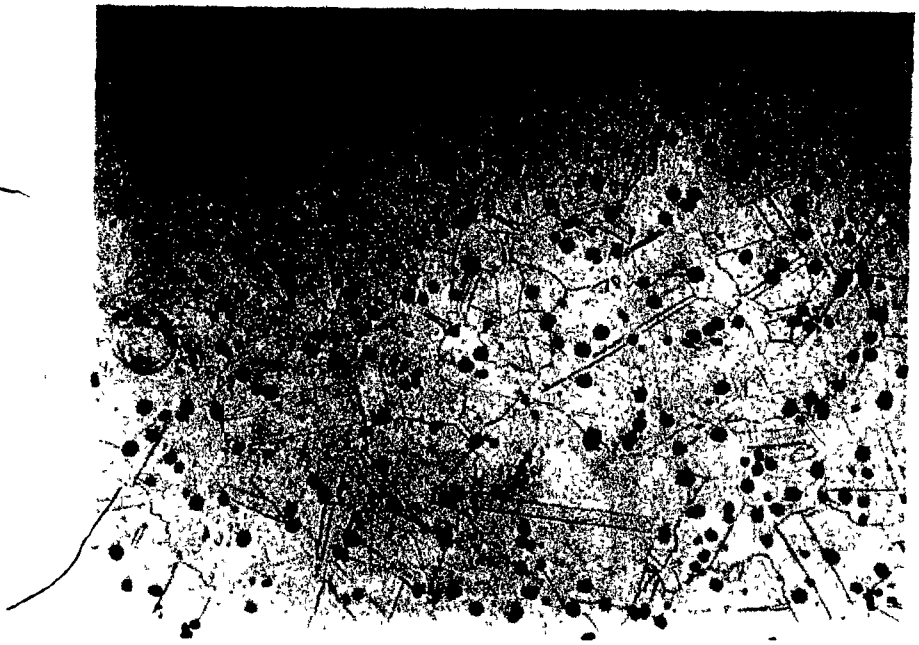

(a)

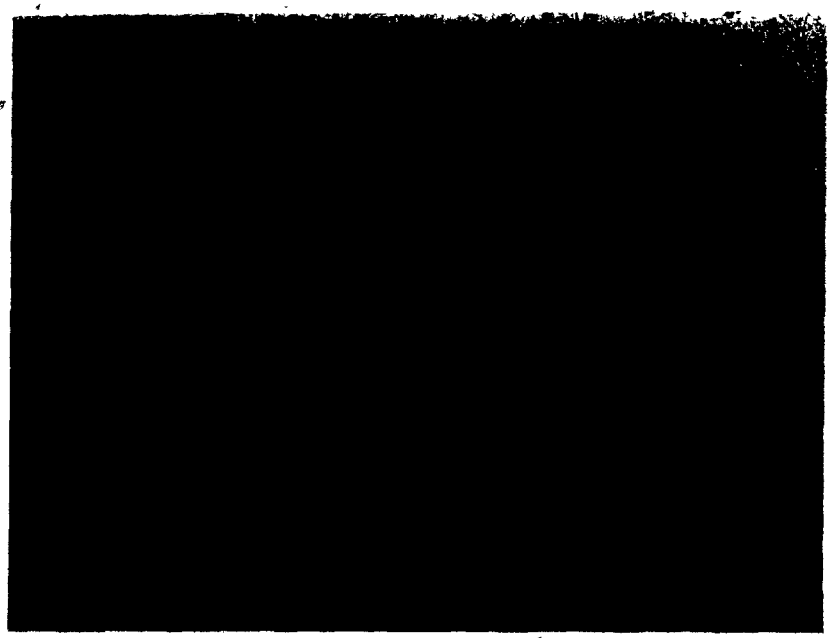

(b)

FIGURE 4.42 Microstructure of Inconel 718 deformed at 1090°C at $1.9 \times 10^{-2} s^{-1}$ X75. (a) strain 0.08; (b) strain 0.7.

CHAPTER 5

DISCUSSION

5.1 Softening Mechanisms Operating During and After the High Temperature Deformation of Waspaloy

During the tests run at 950°C, the flow curves indicated that the amount of flow softening increases with increasing strain rate. When the high value of the flow stress at the higher strain rates is taken into consideration, in combination with the relatively low thermal conductivity of Waspaloy, the observed flow softening can be attributed mainly to adiabatic heating. A rough calculation of the increase in temperature due to adiabatic heating was carried out for the strain rate of $3.8 \times 10^{-1} s^{-1}$.* This leads to a value of 60°C for the increase in test temperature after a strain of 0.7. Considering that this quantity is overestimated due to the simplifications made during the calculation, and adding it to the test temperature, the predicted stress value is in rough agreement with the interpolated experimental value for 990°C. The very small amount of softening at the lower strain rates, on the other hand, sug-

---

* The assumptions made for this calculation were: i) that there is no conduction of heat between the tools and the sample; ii) that no radiation or convection losses occur; and iii) that all the mechanical work is converted into heat. Under these conditions, the increase in temperature ΔT is given by:

$$\Delta T = (1/\rho c) \int \sigma d\varepsilon \qquad (5.2)$$

where ρ is the density (8.138×10^3 Kg/m^3 for Waspaloy) and c is the specific heat at 950°C (7.113×10^2 J/Kg °K).

gests that only dynamic recovery is operating under these conditions. The metallographic results confirm that no dynamic recrystallization is taking place. The grain size remains basically unchanged and the grains and twins become distorted, Figs. 4.24 to 4.29. Pores begin to be seen at around 0.4 strain at some grain boundaries, and at 0.7 deformation, they can be more generally observed, indicating that the ductility at 950°C is likely to be poor. Since nickel-base alloys are designed to be very stable at high temperatures, it is not surprising that when the prior annealing time is raised from 15 to 180 minutes, neither the flow stress nor the structure changes significantly. As noted earlier, a more detailed examination of the microstructures, via transmission electron microscopy, would be necessary to detect any possible changes in γ' size and distribution.

At 1000°C, flow softening begins to be more apparent at lower strain rates, and new recrystallized grains can be seen at the grain boundaries by the time a strain of 0.4 is attained. The original grains, Figs. 4.30 to 4.32, frequently present irregular (serrated) boundaries, showing evidence of localized bulging. This indicates that the new small grains are dynamically recrystallized. After 0.7 deformation, a larger proportion of these new grains is evident. At 1050°C (Fig. 4.33), it is apparent that an almost completely new recrystallized structure has replaced the original structure. At 1100°C, the shape of the flow curve for a strain of $1.9 \times 10^{-3} s^{-1}$ suggests that dynamic recrystallization is taking place. The metallography exhibits

a recrystallized structure, which proves that dynamic recrystallization is the softening mechanism operating under these conditions. A further increase in temperature simply leads to an increase in the dynamically recrystallized grain size.

These observations are in agreement with those presented by Fulop (64), with the exception that he detected partial dynamic recrystallization at 954°C, whereas no recrystallization was apparent at 950°C in the present experiments. It should be pointed out, however, that he utilized a strain rate of 1.0 s^{-1} and an equivalent strain of 1.0 in torsion. Consequently, bearing in mind the greater work done in his material, as well as the adiabatic heating referred to above, it is possible that his actual deformation temperature was considerably higher than 954°C.

After deformation at 1100°C and 1150°C, static recovery and static recrystallization are the softening mechanisms operating (Figs. 4.19 and 4.20). The observation that static recovery is completed after 30 s at 1100°C and after 4 s at 1150°C leads to an estimate for the activation energy for recovery in this material of 330 KJ/mole. This value is in the same range as those for self-diffusion in nickel (276 KJ/mole (51,92)) and for high temperature deformation in pure nickel (297 KJ/mole (51,93)). Static recrystallization starts after 15 and 60 s, respectively, for 1150°C and 1100°C, and is completed after 600 s and 2000 s. By means of a simple calculation, a value of 430 KJ/mole was found for this activation energy, based on the times

for 50% recrystallization. The recrystallization value is in the range of published results for the activation energy for high temperature creep in Nimonic 80A (343 KJ/mole at 650°C, 522 KJ/mole at 860°C (94)) and Nimonic 90 (364 KJ/mole at 670°C, 510 KJ/mole at 860°C (94)), as well as that for the activation energy for hot working of a Ni-20% Fe alloy (393 KJ/mole (51)).

5.2 The Flow Curves and Micrographs for Inconel 718

The shapes of the flow curves for Inconel 718 were basically similar to those for Waspaloy with the exception that yield drops were more often detected. At 925°C, the lowest test temperature used, the flow softening apparent in Fig. 4.10 can also be attributed to adiabatic heating, since it occurs only at the higher strain rates. This conclusion is again confirmed by the metallography, which shows no evidence for dynamic recrystallization, Fig. 4.39a. At 975°C, partial dynamic recrystallization takes place, with small new grains present at the original grain boundaries. At 1030°C, the percentage of these new dynamically recrystallized grains has increased and at 1090°C, dynamic recrystallization is complete throughout the specimen.

5.3 The Yield Point Phenomenon

No data have yet appeared in the literature on the occurrence of yield drops in the nickel-base superalloys at temperatures above 800°C. However, both yield drops and serrated yielding have been reported in various materials (including nickel-base alloys) tested in the range 0-800°C (95-98). Several hypotheses have been suggested to explain these effects:

i) The locking of dislocations by interstitial or substitutional elements (Cottrell and Bilby 1949 (99)).

ii) The Suzuki locking of partial dislocations by the segregation of solutes or precipitates to stacking faults (Suzuki 1963 (100)).

iii) The short-range order locking of dislocations by the formation of short-range ordered regions in their vicinities. (If in an avalanche of dislocations this order is rapidly destroyed, a drop in flow stress (i.e. a yield point) will result (Fisher 1954 (101), Rose and Glover 1966 (102)).

iv) The electronic locking of dislocations by the interaction between the electrical charge of a solute atom and an edge dislocation (Cottrell et al. 1953 (103), Sugiyama 1966 (104)).

v) Precipitation on dislocations (Kelly and Nicholson 1963 (34)).

For nickel-base systems, the appearance of yield points and serrated yielding in the interval from 200-800°C has been attributed to carbide or γ' precipitation on dislocations or stacking faults. However, no proof has so far appeared to confirm that these processes are indeed operating (95). Short-range ordering has also been cited as a possible mechanism leading to a yield point effect, but neither the elements

involved nor the precise mode of locking has been unequivocally described. Choubey and Jonas (105), testing Zircaloy-2 in the temperature range 800-1000°C, reported the presence of yield points. They attributed them to the slow dissolution of the Fe and Cr-rich second phase particles at high temperatures and a subsequent increase in the concentration of Fe and Cr in the β phase when the α phase formed during cooling. The migration of these solutes to dislocations in the β phase and the formation of ordered regions next to the dislocations was thought to produce the locking, and therefore, the yield drop.

5.3.1 Yield Point Effects in Waspaloy

Yield drops occurred while testing Waspaloy in the interval from 1050 to 1150°C. Their appearance, however, did not seem to change the flow stresses for the remaining parts of the curves. For the 1200°C solution heat treatment, they appeared only at a strain rate of $9.3 \times 10^{-2} s^{-1}$ (when testing between 1050 and 1150°C). By decreasing the solution heat treatment temperature to 1150°C, the yield drop was detected at a strain rate of $5.6 \times 10^{-3} s^{-1}$ (for a test temperature of 1100°C). By contrast, no change in behaviour was noted for a test temperature of 1000°C, which is, of course, below the γ-γ' solvus.

During the interrupted tests, yield drops were displayed after 40 s and 180 s respectively for test temperatures of 1150°C and 1100°C. The magnitude of these yield drops

increased to a peak RYD and then decreased with increasing holding time. From Figs. 4.19 and 4.20 it seems that the yield drop appears when the test specimen is almost completely recrystallized. These observations suggest that the yield point in Waspaloy can be attributed to short-range ordering effects. This hypothesis is supported by the observation that a decrease in the heat treatment temperature increases the magnitude of the yield drop. The lower heating temperature, in turn, promotes the formation of a higher number of short-range ordered regions (high heating temperatures promote disordering). It is likely that the γ' forming elements Co, Al and Ti are involved in the short-range ordering patterns, since at temperatures below the γ/γ' solvus, the availability of these elements is much reduced and no yield drops are detected.

5.3.2 Yield Drop Effects in Inconel 718

From the aging kinetic study of the yield drop summarized in Fig. 4.21, activation energies were calculated from the dependence of the time to the peak yield on 1/T. For the primary peaks, a value of 230 (± 30) KJ/mole was found and for the secondary peaks (occurring at 1090°C and estimated at 1030°C), the activation energy was found to be 400 (± 50) KJ/mole. The first value is in the same range as those for the diffusion of aluminum [18], cobalt, chromium, iron, molybdenum and vanadium in nickel (92) (activation energy values for Mn, Si, Nb, Ta and Ti, which are also present in Inconel 718, are lacking in the literature). The higher value for the secondary peak may be

due to heavy elements such as Nb and Ta, as well as to combinations of more than one element or defect, in several possible patterns. These observations suggest that the yield drop in the range 925-1090°C in Inconel 718 is linked first to the presence of elements such as aluminum, cobalt, chromium, iron and vanadium, which may be responsible for the primary peaks, and secondarily to the presence of elements such as niobium and tantalum, or to combinations of more than one element or defect, which may in turn be responsible for the secondary peaks. The fact that yield drops do occur at 925°C, which is below or around the γ'' solvus temperature, suggests that the γ'' forming elements (i.e. Nb, Al and Ti) do not play an important role in the occurrence of the yield drop in Inconel 718, in sharp contrast to the role of the γ' forming elements in Waspaloy.

Because of the complexity of the constitution of Inconel 718, further studies are clearly necessary to determine the precise elements and kinds of locking mechanism involved. Among the possible mechanisms are: i) short-range ordering of the elements cited above; ii) locking of dislocations by carbides, or by γ' and γ'' precipitates. One method of determining the operative elements would be to produce experimental alloys in which the composition is varied with respect to individual elements, taken singly, until the yield point disappears during compression tests, such as the ones described above.

5.4 The Temperature Dependence of the Flow Stress

As shown in Fig. 4.15, deviations from the normal or ideal curve were observed for Waspaloy in the temperature range 1050-1150°C. This temperature interval coincides with that for the occurrence of yield drops. Another fact to bear in mind is that the $\gamma-\gamma'$ solvus temperature is somewhere between 1015-1050°C. Thus, the strengthening mechanisms contributing to the flow stress are different above and below the $\gamma-\gamma'$ solvus. Well above the $\gamma-\gamma'$ solvus (1150-1220°C), strengthening comes from heavy, slow diffusing, elements such as Mo and W, and from the presence of some MC type carbides. Just above the $\gamma-\gamma'$ solvus (1050-1150°C), short-range ordering and solid solution strengthening are the ruling mechanisms, and below the $\gamma-\gamma'$ solvus, order hardening predominates as the strengthening mechanism.

From what has been written above, it seems likely that an interaction between these effects and processes is responsible for the deviations on the σ vs. T curves. When testing well above the $\gamma-\gamma'$ solvus, the temperature is so high that short-range ordering is negligible; as the temperature decreases, the amount of short-range ordering of the γ' forming elements increases. This seems likely to be responsible for the occurrence of the yield drops and, in a parallel manner, for the 'bumps' on the σ vs. T curves. When the γ' actually precipitates, there is a basic change in the strengthening mechanism, and since the elements which were producing the short-range order have now precipitated as γ', no yield drops appear in this lower temperature range.

In the case of the Inconel 718, the situation is different. On the one hand, no deviations from the normal σ vs. T curve were observed; on the other, yield points occurred <u>throughout</u> the range of temperatures tested. Here the main strengthening phase is γ'' ($Ni_3(Nb,Al,Ti)$), and the principal contribution of the γ'' is by means of <u>coherency</u> hardening, instead of by <u>order</u> hardening as in the case of the γ'. Thus, the mechanism responsible for the yield drops, in contrast to the case of Waspaloy, is unlikely to be the short-range ordering of the γ'' forming elements. This is because the occurrence of γ'' precipitation does not affect either the σ vs. T curve or the presence of the yield points.

In Fig. 5.1, the strengthening mechanisms operating in Waspaloy and Inconel 718, in the range of temperatures utilized, are summarized. At very high temperatures, as indicated in the literature review, strengthening comes from solid solution hardening via heavy elements such as Mo, Ta, Nb or W. By decreasing the temperature, the number of short-range ordered regions is increased, and consequently, so is the importance of short-range order as a strengthening mechanism. When γ' or γ'' precipitates, the importance of short-range ordering decreases, giving place to order hardening (for the case of Waspaloy) or coherency hardening (for the case of Inconel 718) as the main mechanism. (Note that Fig. 5.1 is schematic, and is not intended to indicate the quantitative importance of each strengthening mechanism.)

In Figs. 5.2 and 5.3, data from the present research are combined with data from the suppliers (88), and the σ vs. T curves for the temperature interval 25-1220°C (Waspaloy) and 25-1090°C (Inconel 718) are displayed. It is of interest that, in the Waspaloy, a second 'hump' (in addition to the one described above for 1100°C) is seen from 600°C to 800°C. This deviation is not described or explained in the brochure (88) from which the data were extracted. It could, however, be due to serrated yielding, i.e. the occurrence of dynamic strain aging, which has been reported in the literature (95,98) for other nickel-base superalloys in the temperature interval 450-800°C.

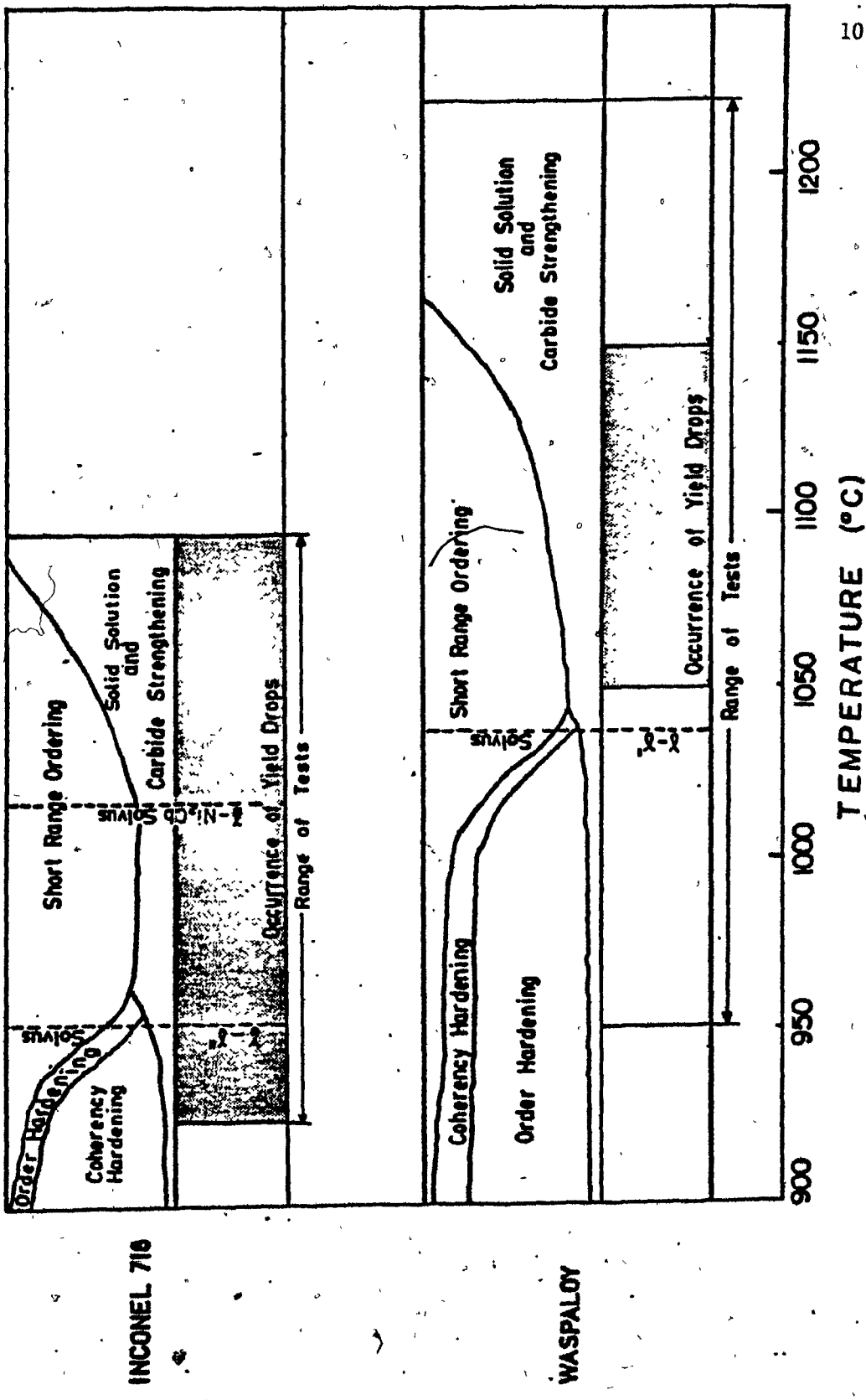

FIGURE 5.1 High temperature strengthening mechanisms in Waspaloy and Inconel 718.

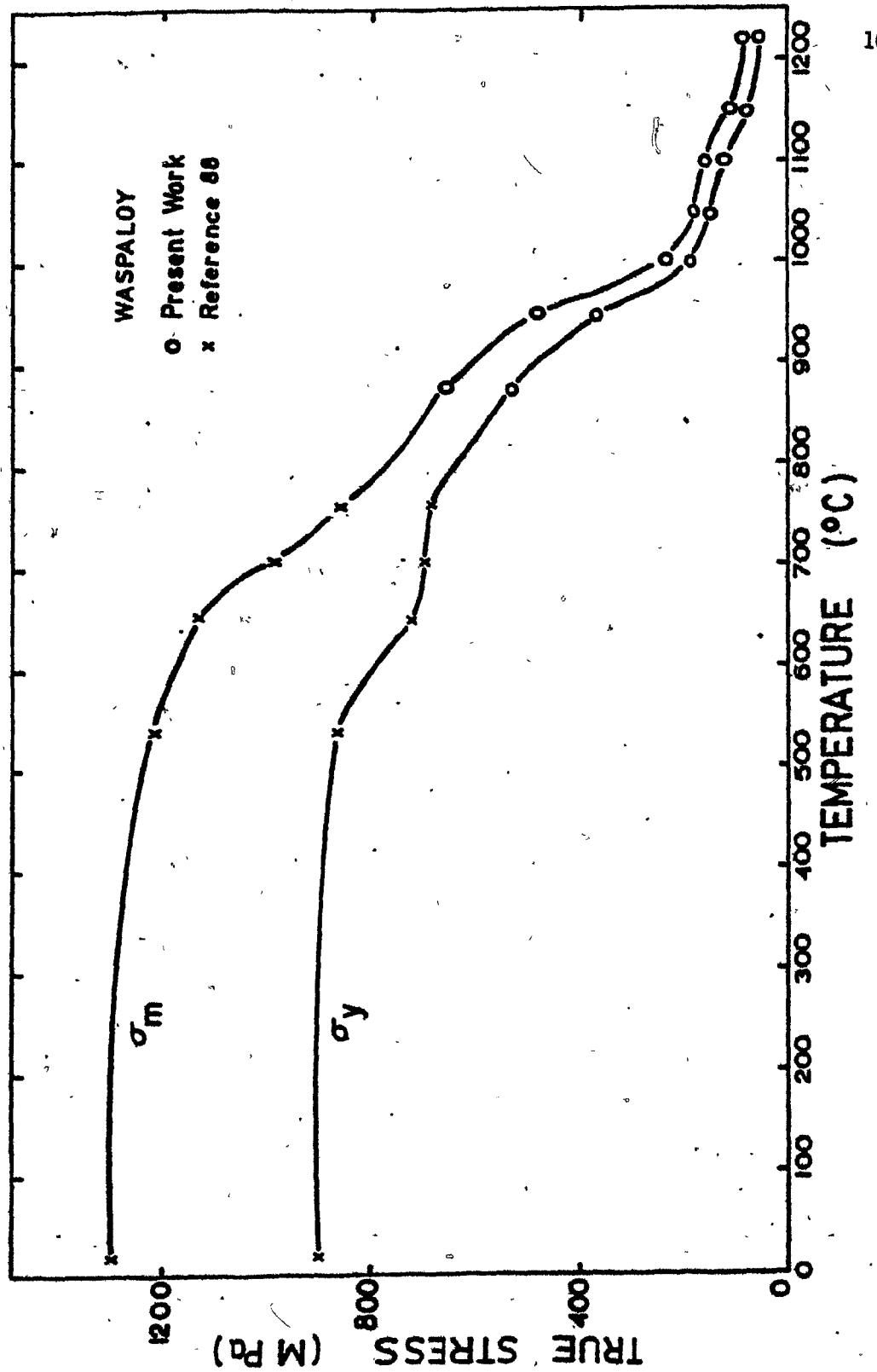

FIGURE 5.2 Temperature dependence of the flow stress for Waspaloy from 25°C to 1220°C. Compression tests (present work), tension tests (ref. 88).

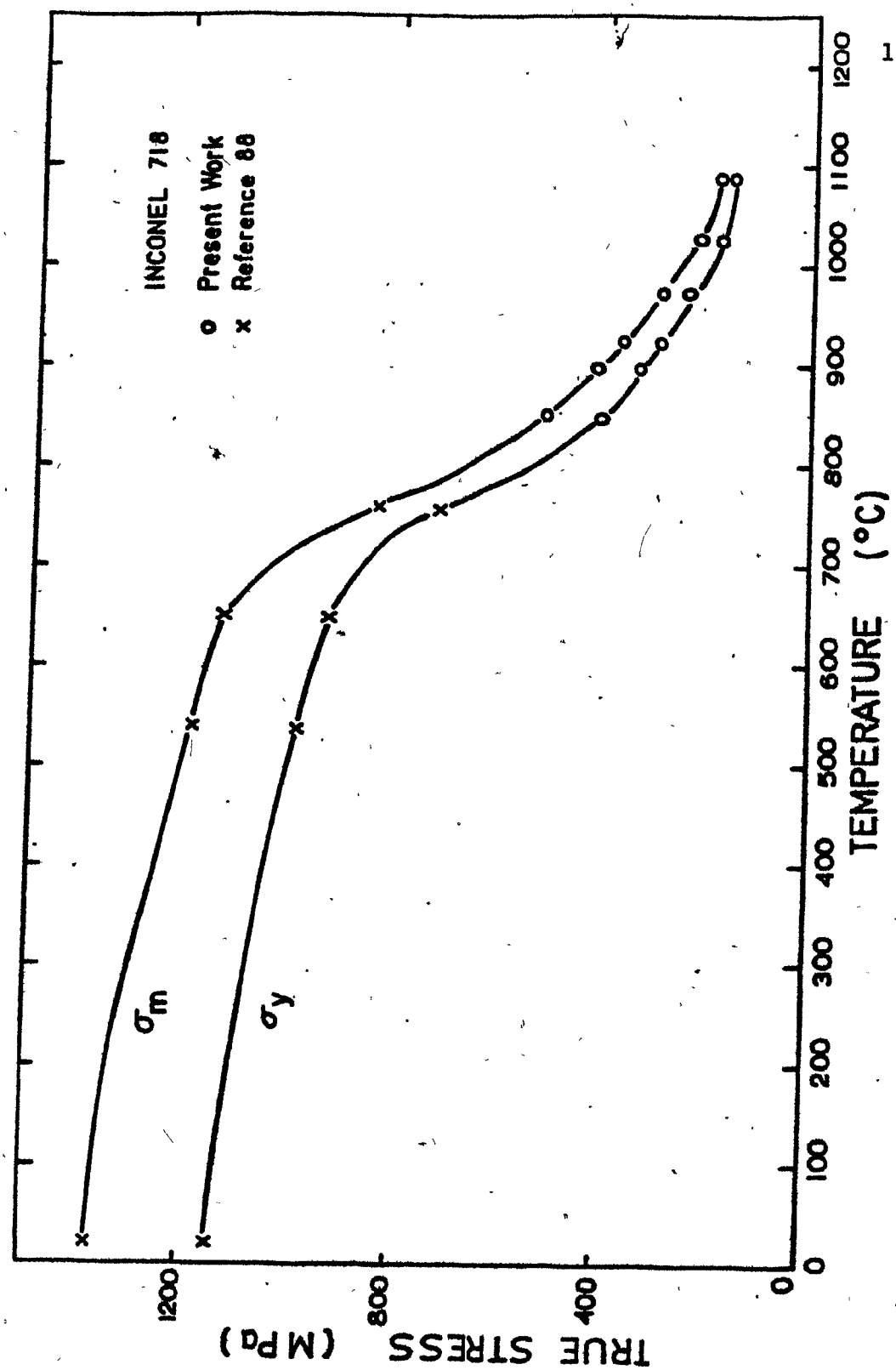

FIGURE 5.3 Temperature dependence of the flow stress for Inconel 718 from 25oC to 1090°C. Compression tests (present work), tension tests (ref. 88).

CHAPTER 6

CONCLUSIONS

The present investigation involved the softening behaviour of Waspaloy and Inconel 718 during and after deformation. It was carried out by means of continuous and interrupted compression testing in the temperature range from 925°C to 1220°C and at strain rates between $5.0 \times 10^{-4} s^{-1}$ and $3.8 \times 10^{-1} s^{-1}$. Another series of experiments was carried out on Waspaloy at the single temperature of 950°C at strain rates of $5.0 \times 10^{-4} s^{-1}$ and $3.8 \times 10^{-1} s^{-1}$, to investigate the effects of annealing time on the hot deformation behaviour. A third series of experiments was performed on Inconel 718 to determine the kinetics of aging as related to yield point effects. All the samples were quenched, polished, etched, and examined metallographically. The following general conclusions were drawn:

1) The flow stress in both materials is strain rate and temperature dependent, and increases with increasing strain rate and decreasing temperature. An increase in the strain rate at the lower temperatures results in flow softening due to adiabatic heating. The amount of work hardening in these materials is generally very small compared to the yield strength, and the peak stress for most conditions is not clearly defined. When it is defined, a tendency towards an increase in peak strain with decrease in temperature or increase

in strain rate is observed.

2) At 950°C for Waspaloy, and 925°C for Inconel 718, dynamic recovery is the softening mechanism occurring during deformation. For these temperatures, the appearance of pores on the micrographs indicates that, under these conditions, ductility is likely to be poor. From 1000°C to 1220°C at strain rates between $5.0 \times 10^{-4} s^{-1}$ and $9.3 \times 10^{-2} s^{-1}$ for Waspaloy, and from 975°C to 1090°C at strain rates between $9.3 \times 10^{-4} s^{-1}$ and $9.3 \times 10^{-2} s^{-1}$ for Inconel 718, dynamic recrystallization is observed after 0.4 strain. Increasing the annealing time before the tests at 950°C for Waspaloy, from 15 to 180 minutes, did not change the flow stress or the structure observed with the aid of an optical microscope, due to the stability of Waspaloy at this temperature.

3) The results of the interrupted tests indicate that, after hot working, static softening in Waspaloy proceeds by the sequential operation of static recovery and static recrystallization.

4) Yield drops occurred while testing Waspaloy and Inconel 718 from 1050°C to 1150°C and 925°C to 1090°C, respectively. The appearance of these discontinuous curves is attributed to short-range ordering. For the case of the Waspaloy, the Y'

forming elements Co, Al and Ti are considered to be responsible for the ordering. For the case of Inconel 718, no conclusive evidence was found which could identify the element or elements responsible for the ordering. It is believed that unlike the case for Waspaloy, the γ'' forming elements do not play an important role. The elements which could possibly be responsible for the ordering, in this case, are Cr, V, Al, Fe and Co.

5) The deviations in the stress-temperature curve for Waspaloy are also attributed to the short-range ordering of the γ' forming elements. When the temperature is decreased from 1220°C, short-range ordering gradually becomes significant, and the deviations begin to appear. When the γ' actually precipitates, the stress-temperature curve returns to its normal form since short-range ordering is no longer important and does not cause any further yield points.

REFERENCES

1. C.D. Desforges: "Source Book on Materials for Elevated Temperature Applications", ed. by ASM (1979), 1.

2. R.E. Reed-Hill: "Physical Metallurgy Principles", van Nostrand Publishing, New York, 2nd ed. (1973), 236.

3. C. Hammond and J. Nutting: Met. Sci., 11 (1977), 474.

4. N.S. Stoloff: "The Superalloys", ed. by C.T. Sims and W.C. Hagel, Wiley & Sons, New York (1972), 79.

5. R.F. Decker: "Source Book on Materials for Elevated Temperatures Applications", ed. by ASM (1979), 275.

6. R.F. Decker and C.T. Sims: "The Superalloys", ed. by C.T. Sims and W.C. Hagel, Wiley & Sons, New York (1972), 33.

7. N.F. Mott and F.R.N. Nabarro: "Report on the Conference on Strength of Solids", Physical Society (1948), 1.

8. B.E.P. Beeston, I.L. Dillamore and R.E. Smallman: Met. Sci., 2 (1968), 12.

9. B.E.P. Beeston and L.K. France: J. Inst. Met., 96 (1968), 105.

10. R.M.N. Pelloux and N.J. Grant: Trans. Met. Soc. AIME, 218 (1960), 232.

11. R.L. Fleisher: Acta Met., 11 (1963), 203.

12. R.L. Fleisher: "The Strengthening of Metals", ed. by D. Peckner, Reinhold Publishing Co. (1967), 93.

13. R. Nordheim and N.J. Grant: J. Inst. Met., 82 (1954), 440.

14. P.A. Flinn: Acta Met., 6 (1958), 631.

15. P.S. Kotval: Trans. Met. Soc. AIME, 242 (1968), 1764.

16. D.F. Paulonis, J.M. Oblak and D.S. Duvall: Trans ASM, 62 (1969), 611.

17. J.W. Cahn: Acta Met., 9 (1961), 795.

18. A.J. Ardell and R.B. Nicholson: Acta Met., 14 (1966), 1295.

19. H.F. Merrick: "Precipitation Processes in Solids", ed. by K.C. Russell and H.I. Aaronson, TMS-AIME (1978), 161.

20. V.A. Phillips: Acta Met., 14 (1966), 1533.

21. H. Gleiter and E. Hornbogen: Mat. Sci. Eng., 2 (1968), 285.

22. J.M. Oblak, W.A. Owczarski and B.H. Kear: Acta Met., 19 (1971), 355.

23. L.M. Brown and R.K. Ham: "Strengthening Methods in Crystals", ed. by A. Kelly and R.B. Nicholson, Wiley & Sons (1971), 9.

24. D.H. Kirkwood: Acta Met., 18 (1970), 563.

25. W.O. Gentry and M.E. Fine: Acta Met., 20 (1972), 181.

26. C.L. Corey, B.Z. Rosenblum, and G.M. Cmeeve: Acta Met., 21 (1973), 837.

27. R.G. Faulkner and B. Ralph: Acta Met., 20 (1970), 703.

28. V.A. Phillips: Phil. Mag., 16 (1967), 103.

29. R.G. Davies and N.S. Stoloff: Trans. Met. Soc. AIME, 233 (1965), 711.

30. H. Gleiter and E. Hornbogen: Phys. Stat. Sol., 12 (1965), 251.

31. V. Gerold and H. Haberkorn: Phys. Stat. Sol., 16 (1966), 675.

32. D. Raynor and J.M. Silcock: Met. Sci., 4 (1970), 121.

33. S.M. Copley and B.H. Kear: Trans. Met. Soc. AIME, 239 (1967), 984.

34. A. Kelly and R.B. Nicholson: Prog. Mat. Sci., 10 (1963), 149.

35. P. Beardmore, R.G. Davies and T.L. Johnson: Trans. Met. Soc. AIME, 245 (1969), 1537.

36. M.C. Chaturvedi, D.J. Lloyd and D.W. Chung: Met. Sci., 11 (1976), 373.

37. G. Meyer: Diploma Thesis, Erlangen (1979).

38. R. Heider: Diploma Thesis, Erlangen (1979).

39. A. Melander and P.A. Persson: Met. Sci., 12 (1978), 391.

40. E.J. Lee and A.J. Ardell: ICSMA 5, 1 (1979), 633.

41. A.J. Ardell: Met. Sci., 14 (1980), 221.

42. V. Munjal and A.J. Ardell: Acta Met., 23 (1975), 513.

43. J.M. Oblak, D.F. Paulonis and D.S. Duvall: Met. Trans., 5 (1974), 143.

44. R.F. Decker and J.R. Mihalisin: Trans. ASM, 62 (1969), 481.

45. A. Melander: ICSMA 4, 1 (1976), 234.

46. J.P. Stroup and L.A. Pugliese: Met. Prog., 93 (1968), 96.

47. R.F. Decker and J.W. Freeman: University of Michigan, private communication.

48. R.T. Holt and W. Wallace: Int. Met. Rev., 21 (1976), 1.

49. H.J. McQueen and J.J. Jonas: "Plastic Deformation of Materials", ed. by R.J. Arsenault, Academic Press (1975), 393.

50. J.J. Jonas: ICSMA 4, 3 (1976), 976.

51. J.J. Jonas, C.M. Sellars and W.J. McG. Tegart: Met. Rev., 14 (1969), 1.

52. H.J. McQueen and S. Bergerson: Met. Sci., 6 (1972), 25.

53. R.A.P. Djaic and J.J. Jonas: J.I.S.I., 210 (1972), 256.

54. G. Glover and C.M. Sellars: Met. Trans., 14 (1973), 765.

55. A. LeBon, J. Rofes-Vernis, C. Rossard: Met. Sci., 9 (1975), 36.

56. M.J. Luton and W.J. McG. Tegart: Met. Sci., 3 (1969), 142.

57. M.J. Luton and C.M. Sellars: Acta Met., 17 (1969), 1033.

58. J.P. Sah, G.J. Richardson and C.M. Sellars: Met. Sci., 8 (1974), 325.

59. E. Shapiro and G.E. Dieter: Met. Trans., 2 (1971), 1385.

60. E. Shapiro and G.E. Dieter: Met. Trans., 1 (1970), 1711.

61. C. Rossard: ICSMA 3, 2 (1973), 175.

62. F. Haessner: "Recrystallization of Metallic Materials", ed. by F. Haessner, Dr. Riederer-Verlag, Stuttgart, 2nd ed. (1978), 1.

63. S. Fulop and H.J. McQueen: 2nd Int. Conf. on Superalloys, Seven Springs, PA. (1972).

64. S. Fulop: M. Eng. Thesis, Concordia University, Montreal (1976).

65. R.E. Bailey: 2nd Int. Conf. on Superalloys, Seven Springs, PA (1972).

66. R.S. Cremisio and H.J. McQueen: 2nd Int. Conf. on Superalloys, Seven Springs, PA (1972).

67. B. Weiss, G.E. Grotke and R. Sticker: Weld. Res. Supplement, 35 (1970), 471.

68. R.E. Bailey: Met. Eng. Quarterly, 15 (1975), 43.

69. A.E. Marsh and G. Oakes: Int. Hot Working Conf., Sheffield (1979).

70. J-P.A. Immarigeon, W. Wallace and G. Van Drunen: DME/NAE Bulletin No. 1 (1977).

71. M. Dahlen and L. Winberg: Acta Met., 28 (1980), 41.

72. H.J. McQueen and J.J. Jonas: "Metal Forming: Interrelation between Theory and Practice", ed. by A.L. Hoffmanner, Plenum Publishing Co., NY (1971), 393.

73. G.E. Dieter: "Mechanical Metallurgy", McGraw Hill Book Co., 2nd ed. (1976), 544.

74. W.J. McG. Tegart: "Elements of Mechanical Metallurgy", MacMillan, NY, 1966.

75. G.T. van Rooyen and W.A. Backofen: Int. J. Mech. Sci., 1 (1960), 1.

76. G.W. Pearsall and W.A. Backofen: Trans ASM, 85 (1963), 68.

77. A.L. Hoffmanner: AFML, TR 69-174 (1969).

78. J.J. Jonas and M.J. Luton: "Advances in Deformation Processing", ed. by J.J. Burke and Volker Weiss, Plenum Publishing Co., NY (1978), 215.

79. S.L. Semiatin and G.D. Lahoti: submitted to Met. Trans. (1980).

80. A.S. Rizkalla, M.Eng. Thesis, McGill University, Montreal (1977).

81. K.C. Kadien: M.Eng. Thesis, McGill University, Montreal (1977).

82. I. Weiss: Ph.D. Thesis, McGill University, Montreal (1978).

83. M.J. Luton, J-P. A. Immarigeon and J.J. Jonas: J. Phys. E. Sci. Inst., 7 (1974), 862.

84. B. Heritier: Ph.D. Thesis, McGill University, Montreal (1976).

85. R.A. Petkovic-Luton: Ph.D. Thesis, McGill University, Montreal (1975).

86. J-P.A. Immarigeon: Ph.D. Thesis, McGill University, Montreal (1974).

87. W.H. Couts, Jr.: "The Superalloys", ed. by C.T. Sims and W.C. Hagel, Wiley & Sons, New York (1972), 451.

88. Special Metals Corporation Brochures on Waspaloy and Inconel 718 (1979).

89. R.A.P. Djaic and J.J. Jonas: Met. Trans., 4 (1973), 621.

90. R.A. Petkovic, M.J. Luton and J.J. Jonas: Can. Met. Quart., 14 (1975), 1.

91. C. G'sell and J.J. Jonas: submitted to J. Mat. Sci., Oct. (1980).

92. "Handbook of Chemistry and Physics", ed. by R.C. Weast, CRC Press, Florida (1979), F66.

93. C.M. Sellars and W.J. McG. Tegart: Mem. Sci. Revue Metall., 63 (1966), 731.

94. J. Helsop: J. Inst. Met., 91 (1962), 28.

95. E.O. Hall: "Yield Point Phenomena in Metals and Alloys", Plenum Press, New York (1970), 201.

96. P. Haasen and A. Kelly: Acta Met., 5 (1957), 192.

97. L.Y. Popov and V.F. Sukhovarov: Phys. of Met. and Metalog., 17 (1964), 428.

98. R.A. Mulford and U.F. Kocks: Acta Met., 27 (1979), 1125.

99. A.H. Cottrell and B.A. Bilby: Proc. Phys. Soc., A62 (1949), 49.

100. H. Suzuki: N.P.L. Symposium, No. 15, 'Relation between structure and mechanical properties of metals', 517.

101. J.C. Fisher: Acta Met., 2 (1954), 9.

102. K.S.B. Rose and S.G. Glover: Acta Met., 14 (1966), 1505.

103. A.H. Cottrell, S.C. Hunter and F.R.N. Nabarro: Phil. Mag., 44 (1953), 1064.

104. A. Sugiyama, J. Phys. Soc. Japan, 21 (1966), 1873.

105. R. Choubey and J.J. Jonas: submitted to Met. Sci. (1980).